

Summer 2006

# Design and development of triangular, spiral, and fractal antennas for radio frequency identification tags

Jeevan K. Vemagiri  
*Louisiana Tech University*

Follow this and additional works at: <https://digitalcommons.latech.edu/dissertations>



Part of the [Electrical and Computer Engineering Commons](#)

---

## Recommended Citation

Vemagiri, Jeevan K., "" (2006). *Dissertation*. 570.  
<https://digitalcommons.latech.edu/dissertations/570>

This Dissertation is brought to you for free and open access by the Graduate School at Louisiana Tech Digital Commons. It has been accepted for inclusion in Doctoral Dissertations by an authorized administrator of Louisiana Tech Digital Commons. For more information, please contact [digitalcommons@latech.edu](mailto:digitalcommons@latech.edu).

DESIGN AND DEVELOPMENT OF TRIANGULAR, SPIRAL, AND FRACTAL  
ANTENNAS FOR RADIO FREQUENCY IDENTIFICATION TAGS

by

Jeevan K. Vemagiri, M.S

A Dissertation Presented in Partial Fulfillment  
of the Requirements for the Degree  
Doctor of Philosophy  
Engineering

COLLEGE OF ENGINEERING  
LOUISIANA TECH UNIVERSITY

August 2006

UMI Number: 3259726

### INFORMATION TO USERS

The quality of this reproduction is dependent upon the quality of the copy submitted. Broken or indistinct print, colored or poor quality illustrations and photographs, print bleed-through, substandard margins, and improper alignment can adversely affect reproduction.

In the unlikely event that the author did not send a complete manuscript and there are missing pages, these will be noted. Also, if unauthorized copyright material had to be removed, a note will indicate the deletion.

**UMI**<sup>®</sup>

---

UMI Microform 3259726

Copyright 2007 by ProQuest Information and Learning Company.

All rights reserved. This microform edition is protected against unauthorized copying under Title 17, United States Code.

ProQuest Information and Learning Company  
300 North Zeeb Road  
P.O. Box 1346  
Ann Arbor, MI 48106-1346

LOUISIANA TECH UNIVERSITY

THE GRADUATE SCHOOL

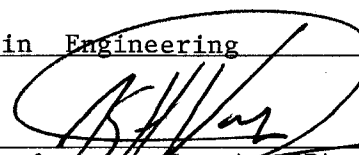
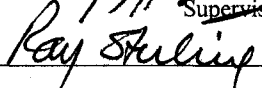
July 13, 2006

Date

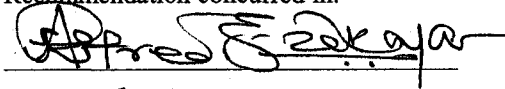
We hereby recommend that the dissertation prepared under our supervision by Jeevan K. Vemagiri

entitled DESIGN AND DEVELOPMENT OF TRIANGULAR, SPIRAL, AND FRACTAL ANTENNAS FOR RADIO FREQUENCY IDENTIFICATION TAGS

be accepted in partial fulfillment of the requirements for the Degree of Doctor of Philosophy in Engineering

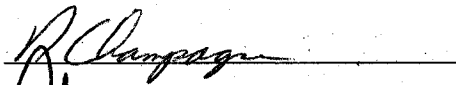
  
\_\_\_\_\_  
Supervisor of Dissertation Research  
  
\_\_\_\_\_  
Head of Department  
Engineering  
\_\_\_\_\_  
Department

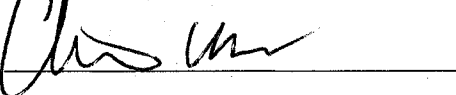
Recommendation concurred in:

  
\_\_\_\_\_

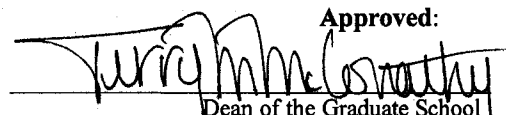
  
\_\_\_\_\_

Advisory Committee

  
\_\_\_\_\_

  
\_\_\_\_\_

Approved:  
  
\_\_\_\_\_  
Director of Graduate Studies

Approved:  
  
\_\_\_\_\_  
Dean of the Graduate School

  
\_\_\_\_\_  
Dean of the College

## ABSTRACT

This dissertation reports on the design and development of three compact, non-meandered microstrip patch antennas for ultra high frequency (UHF) radio frequency identification (RFID) applications. The monopole antennas considered in this work are an inset-fed triangular antenna, one arm Archimedes spiral antenna and a Half-Sierpinski fractal antenna. These antennas with small length to width ratios ( $< 2/1$ ), can be the preferred choice, in the tagging of small size consumer end products, over the ubiquitous meandered dipole antenna (length/ width  $> 5/1$ ), which is often the antenna of choice, due to its high gain for UHF RFID applications. The lengths and widths of all three antennas are less than 5.5 cm. Earlier reports of planar antennas for RFID applications in the UHF range have lengths larger than 9 cm on one side or are developed on a rigid substrate. All three antennas have a surface area of about 30 cm<sup>2</sup> and are designed for a flexible polyimide substrate. The new antennas satisfy the requirement of a voltage standing wave ratio (VSWR)  $< 2$  and exhibit a gain close to or greater than 0 dBi at the operation frequency of 915 MHz. All three antennas have a return-loss less than -10 dB at 915 MHz and a -10 dB bandwidth greater than 12 MHz. While the triangular and spiral antennas display peak gains of over 2 dBi, the fractal antenna has a gain close to 0 dBi (-0.64 dBi). The effect of ground geometry on the radiation performance of the antennas has been analyzed using ANSOFT Designer software. Slots, aligned to the top patch were

introduced in the antenna ground plane to increase the gain of the antennas. The fabricated and tested antennas were then employed in the transmission-delay-line-based passive radio-frequency identification tag. The location of the antenna with respect to the transmission line on the tag was found to affect the radiation pattern of the antenna. A circular disc monopole antenna having a gain of 8.88 dBi and having a -10 dB bandwidth greater than 300 MHz was employed to transmit and receive the interrogating and back-scattered signals, respectively. The generation of bits, employing On-Off Keying (OOK) modulation technique was successfully demonstrated. The tag, fabricated with the triangular antenna is found to perform the best.

APPROVAL FOR SCHOLARLY DISSEMINATION

The author grants to the Prescott Memorial Library of Louisiana Tech University the right to reproduce, by appropriate methods, upon request, any or all portions of this Dissertation. It is understood that "proper request" consists of the agreement, on the part of the requesting party, that said reproduction is for his personal use and that subsequent reproduction will not occur without written approval of the author of this Dissertation. Further, any portions of the Dissertation used in books, papers, and other works must be appropriately referenced to this Dissertation.

Finally, the author of this Dissertation reserves the right to publish freely, in the literature, at any time, any or all portions of this Dissertation.

Author V. J. [Signature]

Date 07/26/2006

## TABLE OF CONTENTS

ABSTRACT.....	iii
TABLE OF CONTENTS.....	iv
LIST OF TABLES.....	x
LIST OF FIGURES .....	xi
ACKNOWLEDGMENTS .....	xvii
CHAPTER 1 INRODUCTION.....	1
1.1 Definition of RFID.....	2
1.1.1 History.....	2
1.1.2 Present Applications .....	3
1.1.3 Projected Applications.....	4
1.1.4 Classification.....	5
1.1.4.1 Active, passive and semi-passive tags.....	5
1.1.4.2 Chip-based and chip-less tags .....	6
1.1.4.3 Low-frequency and ultra high-frequency tags .....	6
1.1.4.4 Re-writable and read only tags.....	7
1.2 RFID Components .....	7
1.2.1 Integrated Circuit/Chip .....	7
1.2.2 Sensor.....	7
1.2.3 Antenna.....	8

1.2.3.1 Physical requirements .....	8
1.2.3.2 Electrical requirements.....	9
1.3 Antennas for RFIDs .....	9
1.3.1 Present RFID Antenna Designs .....	9
1.3.2 Scope for Design Improvement .....	11
1.4 Research Objectives and Considerations .....	11
1.5 Organization of Dissertation .....	15
<b>CHAPTER 2 ANTENNAS FOR PASSIVE RFID SYSTEMS .....</b>	<b>16</b>
2.1 Antenna Theory .....	20
2.1.1 Antenna Input Impedance and Efficiency.....	22
2.1.2 Electromagnetic Fields Produced by the Antenna .....	25
2.1.3 Radiation Pattern.....	26
2.1.4 Antenna Directivity, Gain and Equivalent Isotropically Radiated Power .....	27
2.1.5 Antenna Polarization.....	28
2.2 Triangular, Spiral and Fractal Antennas .....	28
2.2.1 Triangular Antenna .....	28
2.2.2 Spiral Antenna .....	30
2.2.3 Fractal Antenna.....	31
2.3 Simulation Analysis.....	33
2.3.1 Simulation Models.....	33
2.3.2 Simulation Setup.....	37
2.3.2.1 Layout preparation .....	38
2.3.2.2 Incorporation of the excitation features.....	40

2.3.2.3 Defining of boundaries.....	41
2.3.2.4 Analysis set-up .....	42
2.3.3 Design Considerations .....	44
2.3.3.1 Size change.....	45
2.3.3.2 Shape change.....	45
2.3.3.3 Slit introduction.....	46
2.3.3.4 Slot introduction.....	47
2.3.3.5 Stub introduction.....	48
2.3.3.6 Short introduction.....	50
2.3.3.7 Antenna skewing .....	51
2.3.4 Triangular Patch Antenna .....	51
2.3.4.1 Design.....	52
2.3.4.2 Tuning .....	55
2.3.4.3 Gain improvement.....	65
2.3.5 Spiral Patch Antenna.....	59
2.3.5.1 Design.....	61
2.3.5.2 Tuning .....	64
2.3.5.3 Gain improvement.....	65
2.3.6 Half-Sierpinski Fractal Antenna .....	69
2.3.6.1 Design.....	71
2.3.6.2 Tuning .....	72
2.3.6.3 Gain improvement.....	75
2.4 Comparison of Antennas.....	77

CHAPTER 3 FABRICATION AND CHARACTERIZATION .....	79
3.1 Fabrication of Antennas .....	79
3.1.1 Photolithography .....	80
3.1.1.1 Mask preparation .....	80
3.1.1.2 Lithography process .....	81
3.1.2 Low Cost Patterning Method .....	83
3.1.2.1 Mask preparation .....	83
3.1.2.2 Patterning method .....	83
3.2 Characterization of Antennas .....	86
3.2.1 VSWR Measurement .....	87
3.2.1.1 Sample preparation .....	87
3.2.1.2 Network analyzer calibration .....	87
3.2.1.3 Measurement procedure .....	88
3.2.1.4 Results and discussion .....	89
3.2.2 Radiation Pattern Measurement .....	90
3.2.2.1 Sample preparation .....	90
3.2.2.2 Experimental set-up .....	91
3.2.2.3 Results and discussion .....	92
CHAPTER 4 ANTENNA INTEGRATION IN DELAY BASED RFID SYSTEM .....	95
4.1 Simulated Integrated System .....	95
4.1.1 Transmission Line Influence on the Antenna Radiation Pattern .....	96

4.1.2 Line Grounding Influence on the Antenna Radiation Pattern .....	97
4.1.3 Transmission Line Layout Influence on the Antenna Radiation Pattern .....	99
4.2 Modulation Scheme .....	100
4.3 Fabrication of Integrated System .....	101
4.4 Characterization of Integrated System.....	102
4.4.1 Pulse Spreading Effect .....	104
4.4.2 Design, Fabrication and Testing of a Circular Disc Monopole Antenna .....	105
4.4.3 System Testing .....	110
4.4.3.1 System with triangular patch.....	112
4.4.3.2 System with spiral patch .....	113
4.4.3.3 System with Half-Sierpinski patch.....	114
CHAPTER 5 CONCLUSIONS AND FUTURE RECOMMENDATIONS .....	115
5.1 Conclusions.....	115
5.2 Preliminary Results for Antenna Temperature Sensor .....	118
APPENDIX .....	123
REFERENCES .....	128

## LIST OF TABLES

Table 1.1	Antenna requirements, requirement basis, limitations and Adopted approaches .....	14
Table 2.1	Calculated slot edge location values with respect to the corresponding triangular antenna's outermost edges .....	58
Table 2.2	Widths of the segments of the single arm spiral antenna .....	63
Table 2.3	Widths of the segments of the higher gain single arm spiral antenna.....	66
Table 2.4	Calculated slot edge location values with respect to the corresponding spiral antenna's outermost edges.....	68
Table 2.5	"The Seven S" Microstrip Antenna Design tool .....	76
Table 2.6	Comparison of the triangular, spiral and fractal antenna with other antennas (italicized) .....	78
Table 3.1	Solution composition for low-build and high-build copper .....	86
Table 4.1	Obtained values of VSWR and gain for different values of ground plane width and ground-plane gap.....	108
Table 4.2	Values of the gain of CDM antenna as a function of the dimensions of CDM .....	109
Table 4.3	Comparison table of the older and the improved versions of the Circular Disc Monopole.....	109
Table 5.1	Magnitude of measured signal with respect to the temperature sensed by the tag .....	122

## LIST OF FIGURES

Figure 1.1	Aperture-coupled patch antenna.....	10
Figure 2.1	Schematic of LC delay circuit tapped before 1 <sup>st</sup> LC pair and after 2 <sup>nd</sup> LC pair to generate 1010 code.....	18
Figure 2.2	Schematic of transmission line based delay scheme.....	20
Figure 2.3	Cross-section of the antenna substrate with $\epsilon_{r1} = \epsilon_{r3} = 3.3$ , $\epsilon_{r2} = 3.5$ ; $\delta_1 = \delta_3 = 0.027$ , $\delta_2 = 0.008$ .....	22
Figure 2.4	Equivalent circuit of the transmitting antenna .....	23
Figure 2.5	Electric far-field of the transmitting antenna .....	25
Figure 2.6	Normalized (power) radiation pattern .....	27
Figure 2.7	Triangular patch antenna with (a) horizontal slits (b) with tuning stub for integration with the system (c) cross-section on the dielectric substrate.....	29
Figure 2.8	Triangular patch antenna with slotted ground plane .....	29
Figure 2.9	Spiral patch antenna with (a) varying widths (b) with tuning stub for integration with the system (c) cross-section on the dielectric substrate.....	30
Figure 2.10	Simulation layout of large (a) spiral patch antenna and (b) spiral patch antenna with slotted ground plane.....	31
Figure 2.11	The Sierpinski monopole .....	31
Figure 2.12	Half-Sierpinski fractal antenna with (a) varying feed section widths and tuning stub for integration with the system and (b) cross-section on the dielectric substrate .....	32
Figure 2.13	Half-Sierpinski patch antenna with slotted ground plane .....	33

Figure 2.14	Cross-section of the microstrip antenna and the charge distribution in the antenna .....	34
Figure 2.15	Schematic of microstrip cavity with electric field distribution for the $TM_{100}$ mode .....	35
Figure 2.16	Stack up option window to build layers in Ansoft Designer.....	38
Figure 2.17	Simulation layout of the antenna substrate cross-section.....	40
Figure 2.18	Simulation layout of cross-section showing a 2-d surface defined as lumped-port to simulate excitation.....	41
Figure 2.19	Simulation layout of the radiation boundary surrounding the antenna.....	42
Figure 2.20	Analysis window for specific analysis .....	43
Figure 2.21	Parametric sweep analysis window .....	44
Figure 2.22	Simulation layout of rectangular elements (a) before union and (b) after union .....	46
Figure 2.23	Simulation layout of triangular patch antenna (a) before boolean subtraction and (b) after boolean subtraction .....	47
Figure 2.24	Simulation layout of ground plane of the antenna, (a) unslotted and (b) slotted.....	48
Figure 2.25	Tuning stub calculator .....	49
Figure 2.26	Real and imaginary impedance plots of (a) untuned and (b) tuned antenna .....	49
Figure 2.27	Simulation layout of the tuning stub of the antenna with a ground short.....	50
Figure 2.28	VSWR plots with and without grounded stub.....	50
Figure 2.29	Simulation layout of ground plane (a) before skewing and (b) after skewing in the y-direction .....	51
Figure 2.30	(a) Simulation layout of inset-fed triangular patch antenna (b) VSWR plot for inset-fed triangular patch antenna .....	53
Figure 2.31	(a) Simulation layout and (b) VSWR plot of vertical slit triangular patch antenna .....	53

Figure 2.32	(a) Simulation layout and (b) VSWR plot of horizontal slit triangular patch antenna .....	54
Figure 2.33	Radiation pattern of the horizontal slit triangular antenna .....	54
Figure 2.34	(a) Simulation layout and (b) radiation pattern of patched Ground inset-fed triangular patch antenna .....	55
Figure 2.35	(a) VSWR plot and (b) real and imaginary impedance plots of untuned triangular patch antenna .....	56
Figure 2.36	(a) VSWR plot and (b) real and imaginary impedance plots of tuned triangular patch antenna .....	56
Figure 2.37	(a) Simulation layout and (b) radiation pattern of tuned triangular patch antenna .....	57
Figure 2.38	(a) Patch and (b) ground layouts of inset-fed triangular antenna with $H = 5.54$ cm, $L = 5.34$ cm, $F_1 = 2.33$ cm $I_w = 0.15$ cm, $I_1 = 1.07$ cm, $G_1 = 6.09$ cm, $G_w = 5.19$ cm .....	58
Figure 2.39	(a) VSWR plot and (b) radiation pattern plot of the triangular patch antenna .....	59
Figure 2.40	(a) Simulation layout, (b) VSWR plot) and (c) radiation pattern of uniform width spiral antenna .....	62
Figure 2.41	Radiation pattern of uniform width spiral antenna.....	62
Figure 2.42	Spiral arm of different segments .....	63
Figure 2.43	(a) VSWR versus Frequency plot and (b) radiation pattern of the spiral antenna .....	64
Figure 2.44	(a) VSWR plot and (b) real and imaginary impedance plots of spiral patch antenna.....	64
Figure 2.45	(a) Layout and (b) gain of tuned spiral patch antenna.....	66
Figure 2.46	Large spiral arm with different segments.....	66
Figure 2.47	(a) VSWR versus Frequency plot and (b) radiation pattern of the high-gain spiral antenna .....	67

Figure 2.48	(a) Patch and (b) ground layouts of spiral antenna with widths of the spiral arms (inward from outermost) 0.1 cm, 0.8 cm, 0.2 cm, 0.8 cm, 0.8 cm, 0.2 cm, 0.7 cm, 0.8 cm and 0.8 cm; $L=5.0$ cm, $G_f=5.4$ cm, $G_w = 5.7$ cm.....	68
Figure 2.49	a) VSWR versus Frequency plot and (b) radiation pattern plot of the spiral patch antenna .....	68
Figure 2.50	Several stages in the construction of the sierpinski gasket-fractal .....	70
Figure 2.51	Half-Sierpinski fractal (a) layout and (b) VSWR-Frequency plot.....	71
Figure 2.52	Half-Sierpinski fractal (a) layout and (b) VSWR-Frequency plot.....	71
Figure 2.53	Feed-width (a) simulation layout (a) cross-section having three partitions of widths $w_1, w_2$ and $w_3$ .....	72
Figure 2.54	(a) Simulation layout, (b) VSWR plot and (c) radiation pattern of the fractal antenna .....	73
Figure 2.55	(a) VSWR plot, (b) real and imaginary impedance plots of untuned Half-Sierpinski patch antenna .....	73
Figure 2.56	(a) VSWR plot and (b) gain of tuned Half-sierpinski fractal patch antenna.....	74
Figure 2.57	(a) Layout and (b) VSWR vs Frequency plot of tuned Half-Sierpinski fractal antenna.....	74
Figure 2.58	(a) Patch and (b) ground layouts of Half-Sierpinski fractal antenna with $H = 5.7$ cm, $L = 3.3$ cm, $w_1 = 0.25$ cm, $w_2 = 0.35$ cm, $w_3=0.15$ cm, $w_4 = 0.35$ cm, $w_5 = 0.15$ cm .....	75
Figure 2.59	(a) VSWR plot and (b) radiation pattern plot of the Half-Sierpinski fractal antenna.....	76
Figure 2.60	VSWR versus frequency plots of (a) Triangular, (b) spiral and (c) fractal antennas .....	77
Figure 3.1	Cross-section of the antenna substrate with $\epsilon_{r1} = \epsilon_{r3} = 3.3$ , $\epsilon_{r2} = 3.5$ ; $\delta_1 = \delta_3 = 0.027$ , $\delta_2 = 0.008$ .....	81
Figure 3.2	Cross-section of the printed polyimide .....	84

Figure 3.3	Optical Images of the top and ground layers of (a) Triangular antenna (b) Spiral antenna and (c) Half-Sierpinski fractal antenna .....	86
Figure 3.4	Network Analyzer employed for measurement of the VSWR of the antennas.....	87
Figure 3.5	VSWR versus Frequency plot for three different antennas.....	89
Figure 3.6	Simulation and experimental VSWR plots of (a) triangular (b) spiral and (c) Half-Sierpinski fractal antennas .....	90
Figure 3.7	Test site used for antenna radiation pattern measurement.....	91
Figure 3.8	(a) Transmitting and (b) receiving junctions .....	91
Figure 3.9	Radiation plots of triangular antenna in (a) XZ-plane and (b) YZ-plane.....	93
Figure 3.10	Radiation plots of spiral antenna in (a) XZ-plane and (b) YZ-plane.....	93
Figure 3.11	Radiation plots of Half-Sierpinski Fractal antenna in (a) XZ-plane and (b) YZ-plane.....	94
Figure 4.1	(a) 3 dimensional radiation plot and (b) radiation pattern of gain ( $\phi=0$ , $\theta=0$ i.e. normal to the plane of the antenna) for the half-Sierpinski fractal antenna .....	96
Figure 4.2	(a) 3 dimensional radiation plot and (b) radiation pattern of gain ( $\phi=0$ , $\theta=0$ i.e. normal to the plane of the antenna) of The open-ended transmission line .....	96
Figure 4.3	(a) 3 dimensional radiation plot and (b) radiation pattern of the integrated seirpinski fractal.....	97
Figure 4.4	Effect of ground location at a distance of (a)0.25" (b) 2.5" (c) 5" and (d) 7.5" from the feed-junction .....	98
Figure 4.5	Effect of antenna location at the (a) corner and (b) middle of the Transmission line.....	99
Figure 4.6	Optical picture of the (a) Pulse-Generator and (b) the RF switch.....	100

Figure 4.7	Schematic of meandered transmission line.....	101
Figure 4.8	Pictures of fabricated (a) triangular (b) spiral and (c) Half-Sierpinski fractal tags.....	102
Figure 4.9	Optical picture of anechoic housing for tag testing .....	103
Figure 4.10	Effect of anechoic housing.....	104
Figure 4.11	Schematic of experimental set-up .....	104
Figure 4.12	Experiment set-up for tag characterization .....	105
Figure 4.13	Pulse spreading through (a) Yagi and (b) Circular Disc Monopole antennas .....	106
Figure 4.14	(a) Simulation layout and cross-section of the Circular Disc Monopole.....	106
Figure 4.15	Simulation layout of the (a) 2.7 cm radii microstrip fed CDM (b) enlarged view of gap between ground point and the feed location .....	107
Figure 4.16	Simulation layout of (a) old and (b) new versions of Disc Monopole.....	108
Figure 4.17	(a) Picture and (b) return loss plot of Circular Disc Monopole.....	110
Figure 4.18	Measurement set-up for determining back-scattered power.....	110
Figure 4.19	Antenna return loss measured in anechoic chamber with RFID tag present.....	111
Figure 4.20	Signals with and without tag.....	112
Figure 4.21	5 nsec and 10 nsec delay deliverable triangular antenna RFID tag .....	113
Figure 4.22	5 nsec and 10 nsec delay deliverable spiral antenna RFID tag .....	113
Figure 5.1	(a) Effect due to proximity of human skin on the resonant Frequency and (b) correction of the error through scaling .....	117
Figure 5.2	Loss tangent plots at different temperatures .....	118

Figure 5.3	VSWR versus frequency plot of antenna with temperature sensitive material (a) over the antenna, (b) over the polyimide as the substrate, for the antenna.....	120
Figure 5.4	Polyimide with (a) a differential deposited PPGE and DCH in two coatings (b) a uniform deposited PPGE and DCH in two coatings and (c) a single coating of PPGE and minute quantity of DCH.....	120
Figure 5.5	Variation of resonant frequency when subject to temperature .....	122

## **ACKNOWLEDGEMENTS**

I thank my advisor, Dr. Kody Varahramyan for his guidance of my work. His insight and discussions have paved a way, for a good presentation of the subject researched on. I thank my advisory committee members Dr. Rastko Selmic, Dr. Nathan Champagne, Dr. Alfred Gunasekaran and Dr. Chester Wilson for their patient review of my work. I acknowledge the invaluable assistance received from Mr. Tom Emory in the laboratory work. I thank Dr. Mangilal Agarwal and Ms. Deeba Balachandran for their helpful technical discussions. I also thank the staff of the Institute for Micromanufacturing, including Mr John McDonald, Mr. Scott Williams, Mr. Dee Tatum and Ms. Deborah Wood, for their help in the lab-work. Last but not the least, it was great working with wonderful and encouraging project members Mr. Sudhir Shrestha, Mr. Aravind Chamarti, Ms. Sireesha Ramisetti, Mr. Wajid Ali Mohammad and Mr. Ujwal Kumar Dandgey.

## **CHAPTER 1**

### **INTRODUCTION**

Radio Frequency Identification (RFID) is a method which involves the sending of a radio frequency (1 Hz to  $10^{12}$  Hz) query signal from a remote reader to a tag or transponder and receiving the back-scattered or returned back modulated signal back from the tag. The tag is attached to an object with the information of the object either in a re-writable or un-writable form on the tag. The reader then decodes the signal received, and sends the information of the object to a central processing unit. This unit might be receiving information from nearby readers, placed at other locations communicating with nearby tags. Thus we have a communication system by which items, located at different corners of a retail-store or a warehouse, can be tracked and identified. Based on the modulation scheme employed by the ID generation circuit on the tag, such a data collection system is unobtrusive in nature primarily due to its large reading/tracking distance and high efficiency in managing large quantities of information.

The antennas used in such a system, the antenna on the tag and the antenna on the reader employed for signal/power transfer, constitute the back-bone of the system. The antennas determine the amount of power transferred from the reader to the tag and back from the tag to the reader. Though there aren't any constraints on the physical parameters on the reader antenna, such as being planar or small in size, these

constraints do apply in the design of the antenna that is to be integrated on the tag. In fact, the sizing down of the tag is limited by the size of the antenna, the largest component on the tag. This work details the design of planar, small size and compact antennas for use in the tag, their integration with the other components on the tag, and the realization and performance of a radio frequency identification system.

### **1.1 Definition of RFID**

RFID is a contactless method for data transfer in object identification. The three components of an RFID system are as follows [1]:

1. An electronic data carrying device called a transponder, or a tag that is attached to the item to be identified.
2. A reader or a scanner that communicates with the tag by using radio frequency signals.
3. A central processing system that contains information on the identified item and distributes information to other data processing systems.

RFID is a wireless communication system because the scanner communicates with the tag by using electromagnetic waves at radio frequencies. Several factors affect the communication range, or the distance at which the reader unit identifies the tag. Some examples are the frequency used for identification, the gain, orientation and polarization of both the reader and transponder antennas and the placement of the tag on the object to be identified.

#### **1.1.1 History**

The basic principle of RFID was first applied in World War II when the British employed coded radar signals, which would activate the transponder in the aircraft and

return an identifiable code in a scheme, called the Identification: Friend or Foe (IFF), to distinguish friendly planes from those of the enemies [2]. The first documented report on communication by means of reflected signal was first made by Harry Stockman [3]. In his 1948 paper titled, "Communication by Means of Reflected Power" he explains, "It is believed that the reflected-power communication method may yield one or more of the following characteristics: high directivity, automatic pinpointing in spite of atmospheric bending, elimination of interference fading, simple voice-transmitter design without tubes and circuits and power supplies, increased security, and simplified means for identification and navigation." The simplicity of the technology, though outlined very early by Stockman, was not harnessed until recently with the world-wide re-birth of RFID technology. In the 70's, Los Alamos Research Laboratory developed RFID tagging of nuclear equipment and personnel tracking [4]. RFID technology was sought after in cattle stock monitoring and tracking through railroad applications after trying and failing in the effort to use bar-code technology. An earlier report of the use of RFID technology was in the year 1980 for the application of detecting avalanche victims [5].

### **1.1.2 Present Applications**

RFID has applications in various areas, such as retail item management, electronic toll collection, asset identification, access control, animal tracking and vehicle security [5]. "Talking prescriptions" or tags that transmit information that is subsequently transformed into an audio form, are given to visually impaired veterans where he/she just needs to scan the prescription tag with the reader for the reader to speak the name of the drug, instructions, warnings etc [6]. Low frequency (13.56 MHz) RFID tags can be implanted in pets which can be returned to their owners, if lost. Beer kegs are tagged with

RFID. The books in a library have 13.56 MHz RFID tags on them. Pallet tracking, airline baggage tracking and apparel item tracking is done through RFID's. High frequency tags are used in identification badges which can be placed at greater distances than the conventional magnetic swipe card for authenticating the holder [6]. The American Express has announced that their Blue credit card has a high frequency (2.4 GHz) RFID tag embedded in it. RFID's are used for electronic toll collection at toll booths. RFID transponders are being embedded into tires to monitor tire pressure [6]. Smart key or Smart start options are being integrated into their car designs by Toyota in their 2006 and 2007 models for the car door to be opened with the key inside the driver's pocket or purse [6]. RFID chips are now being implanted in humans for secure access purposes. Combined with sensors to monitor body functions, the device manufactured by Digital Angel could monitor patients [7]. In October 2004, the Federal Drug Administration (FDA) has approved the implanting of chips in humans. Such a chip can give useful medical information about the person, assist with medical care and prevent errors. RFID is presently gaining popularity and acceptance in the public and private sectors of the world of commercial enterprise.

### **1.1.3 Projected Applications**

RFIDs may never completely eliminate less expensive bar-code technology though it has many significant advantages over the old method. RFID is being proposed to replace the cashier with an automatic system that requires no barcode scanning. An organization called GS1, is working on international standards for the use of RFID and the Electronic Product Code (EPC) in the identification of any item in the supply chain for companies in any industry, anywhere in the world. The use of RFID to prevent mix-ups between sperm and ova in In-vitro fertilization (IVF) clinics is being considered [7].

A few countries have considered embedding RFID chips into passports. Such RFID enabled passports uniquely identify their holder and also other personal information. The RFID passport is shielded against skimming. For successful interrogation of a reader, a few characters (PIN) have to be input to the reader. Moreover, the data is encrypted to prevent any fraudulent schemes. A few states in the US are considering implementation of RFID's in licenses to help perform look-ups faster for the police and government officials [8]. Incorporation of RFID in retail store management may completely eliminate the cashier and allow checking out by automatic scanning and billing of the products bought through RFID interrogation. Another use of RFID is for traffic positioning systems, in which a RFID RBS (Road Beacons) is embedded in the pavement and communicates with the in-vehicle unit which also translates the traffic lights into voice. Such a system complements the satellite positioning system in places such as tunnels and indoors [8]. These are just a few of the many innovative applications in which Radio Frequency Identification has been employed.

#### **1.1.4 Classification**

The classification of RFID can be done based on four factors, (i) Active, Passive and Semi-Passive, (ii) Chip-based and Chip-less, (iii) Low frequency and Ultra High Frequency tags and (iv) Re-writable tags or Read only tags.

##### **1.1.4.1 Active, passive and semi-passive tags**

The tag is called an active tag if an on-board battery exists on the tag for its performance. The active tag has its own on-board signal source, the circuit derives its power from the battery and does not need an external transceiver for operation. However, the active tag is also capable of processing information from the transceiver. The read distance of such as tag is greater than a passive or semi-passive tag. A passive tag does

not have an on-board battery and derives its power from the incident radio frequency energy, storing the incident energy as dc energy and re-using it for circuit performance. Another category of passive tags simply work on a back-scatter principle where the incident wave is modulated by the on-board circuit and is reflected back to the reader [1]. The read-distances of passive tags are smaller than an active tag and a semi-passive tag. A semi-passive tag has a battery but without its own signal source and works in a reader-tag system like the passive tag. The semi-passive tag has a greater reading distance than the passive tag and lesser reading distance than the active tag.

#### **1.1.4.2 Chip-based and chip-less tags**

A chip-based tag is one in which an IC chip of specific impedance and functions is integrated with the antenna. Most of the commercial RFID tags are of this type where the designer need not worry about standards to be followed as all standards are satisfied by the chip itself. On the other hand, a chip-less tag, as discussed later in Chapter 2, is one in which the IC is replaced by the designer's own modulation circuit which is capable of transposing the code onto the signal. In this design, the designer has to take caution to match the output impedance of the circuit with the output impedance of the antenna or any additional functional elements, such as a circulator or an isolator, that the designer desires to place on the tag.

#### **1.1.4.3 Low-frequency and ultra high-frequency tags**

This categorization is based on the operation frequency of the tag. Low-frequency tags, operate at 13.56 MHz tag by inductive coupling [9]. An inductor-capacitor circuit is designed to resonate at the desired frequency. The reading distance of the low-frequency tag is confined to a few cm or inches. Ultra high-frequency tags (915 MHz) operate with tags having antennas operating in the near field radiating mode, and are capable of

receiving and sending the signal from and to the reader at distances of a few feet up to a few metres, depending on the gain of and the power transmitted through the antenna.

#### **1.1.4.4 Re-writable tags and read-only tags**

Re-writable tags are those in which the data can be erased and written-back by a reader. A few chip-based tags are re-writable and offer flexibility and the re-use of tags. Read-only tags are low cost, use-once-and-throw-away tags, which are also the main focus of commercial firms. Data is either hard-coded on the IC or the modulation circuit is designed to give a fixed code.

## **1.2 RFID Components**

### **1.2.1 Integrated Circuit**

One of the main components of RFID is the integrated circuit which is responsible for transposing of information onto the signal. For the case of a chip, usually silicon based, a fixed amount of data bits are available to be written to or read from. The data to be written on the chip can be written by a reader or at the time of the manufacture of the chip. In the case of a circuit, the circuit is designed to give a fixed identification code each time the tag is interrogated by the reader. The IC is available with a definite output impedance, such as 50 ohms [10] and is integrated with the rest of the circuit having the same output impedance.

### **1.2.2 Sensor**

A sensor gives additional functionality to the RFID tag, in that it senses the analyte to be measured or sensed i.e. temperature, pressure, humidity, etc. and gives its response in either an on/off switch form or an analyte specific signature transposed onto the carrier [11]. The sensor integrated with the RFID tag, termed RFID sensor, is capable

of identification/tracking as well as sensing applications. A very useful application is in the transportation of perishable drugs/pharmaceuticals wherein the drugs, are tracked over their origin/route of travel as well as to determine if they have been subject to extremes of temperature en-route before reaching the point of sale. Another example is with a pressure sensor [12] integrated with the RFID. In this case, the RFID sensor attached to a pallet carrying fragile items can inform the end-consumer if the products have been tampered with while in-transit or during transfer of goods from the warehouse.

### **1.2.3 Antenna**

The antenna is the most important part of the RFID tag, especially for the case of a passive RFID tag wherein the power received is dependent upon the gain and the impedance match of the antenna to the rest of the circuit. The gain of the antenna determines the reading distance of the tag. The polarization and radiation pattern of the antenna is to be taken into account before the placement of the tag on the object. The antenna that is used for an RFID tag is a microstrip antenna. A microstrip antenna is a conductive trace on a metallized dielectric substrate.

#### **1.2.3.1 Physical requirements**

The antenna for an RFID tag needs to be planar so that the tag is conformal with the surface of the object it is attached to. Thus, a microstrip antenna is the obvious solution. The small size of the antenna allows the tag size to be smaller and thus the tag can be attached to smaller objects. Meander designs are usually incorporated to decrease the size of the antenna. Typical meander dipole antenna dimensions for RFID applications in the 915 MHz range is of the order of 13 cm x 2 cm [9]. The common designs that have been adopted for planar antennas are the planar dipole microstrip

meander antenna, the slot antenna [13] (having slots in the ground plane, which are responsible for radiation) and the patch antenna.

### **1.2.3.2 Electrical requirements**

The antenna for an RFID tag needs to have high gain. Gain is a characteristic of the antenna to concentrate the radiated power in one-direction rather than transmitting in all directions uniformly. The antenna which transmits the power uniformly in all directions is called an isotropic antenna. A high gain antenna can receive and transmit the signal at greater distances from the source and the receiver respectively. However, most of the times it is preferred that the gain be omni-directional so that the tag would be more or less insensitive to the location of the reader.

## **1.3 Antennas for RFIDs**

### **1.3.1 Present RFID Antenna Designs**

A wide variety of antennas have been considered for RFID applications. The most important requirements for the antenna are a high gain and a small size. Hence, the first step in searching for a desirable antenna is the meander dipole antenna. A genetic algorithm, capable of evaluating different permutations of arm lengths, is employed to optimize the lengths of the arms of the meander antenna [14]. The other antenna that is considered is the Planar Inverted F-antenna (PIFA) which, in the form of an inverted-F allows the antenna size to be small. Another category of antennas that are usually considered are the slot antennas where the shape of the slots in the ground plane affects the radiation pattern of the antenna. A 2.45 GHz RFID application includes a transponder design containing an antenna, a rectifier, a Manchester encoder (RFID chip) and a backscattering circuit using a bipolar transistor [15]. Another design includes a dipole

antenna whose impedance can be matched easily by varying the geometric parameters. The dipole ends of the antenna are open for adjustment, especially for the input reactance of the antenna [16]. Along the same lines, a slot antenna is designed for RFID applications, wherein the dimensions of the slot can be varied to vary the ratio of the first and the second excitation frequencies, thus giving an option to tune the same antenna for different applications [17]. An efficient design of an antenna for RFID includes the incorporation of electromagnetic band structures (EBG) in the ground plane of the antenna [18]. These EBG structures forbid the propagation of electromagnetic wave at a certain frequency [19]. When EBG structures are used with microstrip patch antennas, they suppress the excitation of surface waves and substrate modes and therefore offer a solution to enhance the radiation properties in the vicinity of metal, which could be a very possible scenario for RFID application where the RFID tag is very close to a metallic surface. Another antenna design for RFID is the aperture coupled microstrip patch antenna (Fig. 1.1) [20].

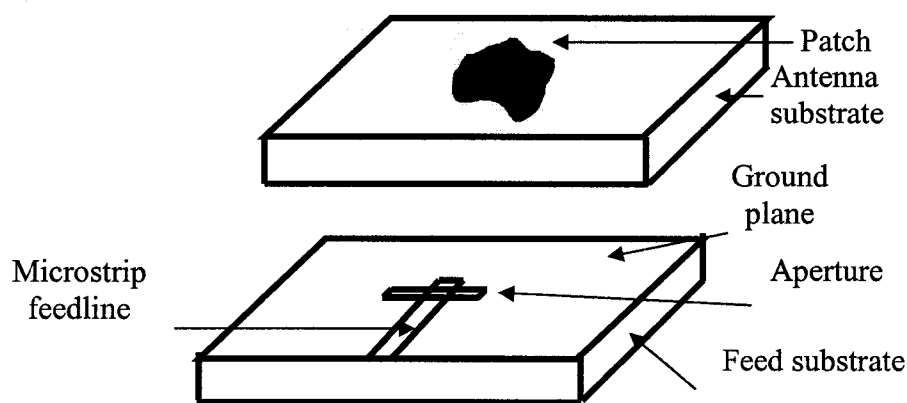


Fig. 1.1. Aperture-coupled patch antenna.

An interesting antenna design for RFID applications is designing one as a meandering text [21] and keeping it hidden behind the text on the object.

### **1.3.2 Scope for Design Improvement**

While all the antennas considered until now have a high gain, most of the antennas still are large in size (greater than  $6 \text{ cm}^2$ ) and pose practical difficulty in integration of the antenna onto tags which need to be attached onto small objects, like those in a retail store. Since RFID technology is being widely adopted these days as the platform for wireless identification and tracking in logistics, supply chain management and various other applications, there is a need for a suitable antenna for integration into the passive wireless sensor system. While a high gain antenna is certainly preferred, a few RFID applications may need the radiation pattern to be more omni-directional than directional [22]. Work has been done on different classes of antennas, namely triangular fed patch antennas, spiral antennas and fractal antennas, to evaluate their radiation performance. Also, since the tag is a flexible substrate, the antenna needs to be designed on a flexible dielectric. The objective of this research work is to develop a small size, narrow-band triangular patch, wide-band spiral antenna and multi-band half-sierpinski antenna for a flexible polyimide platform.

### **1.4 Research Objectives and Considerations**

The objective of this research is to study a variety of microstrip patch antennas which are electrically small (the length of the antenna  $< \lambda/2$ , where  $\lambda$  is the wavelength), light weight and low-profile in nature. One advantage of such a structure is that they could be used in movable systems having space constraints. The antenna needs to be designed for operation at 915 MHz. The usual polarization pattern of such a microstrip

patch antenna is linear. However, for application in movable systems, circular polarization is preferred. Hence, the antenna design procedure to be followed should take into consideration the requirement of a circularly polarized radiation pattern.

Extensive research is being carried out to miniaturize the antenna for various applications. Many approaches [23-29] have been adopted to realize electrically small antennas. Among these many approaches only a few have a more or less conformal nature. A corrugated circular microstrip patch antenna has been fabricated by Lee et al., [23] in which a reduction of 8.0% in patch diameter has been attained. The size reduction was attributed to the shortened current length in comparison to a circular microstrip patch antenna. Use of high-dielectric substrates is another method for reducing the size of the antenna [24]. In a frequency-reduction scheme for a spiral slot antenna, Wang et. al. [25] have obtained a reduction in size by about 20%. The radius of the circular microstrip line and spiral spot for a 1.58 GHz antenna was 3.1cm. By loading the same antenna with a circular capacitive stub, the resonant frequency was brought down to 1.28 GHz. Modification of shape by introducing diametrically opposed perturbation segments (of the inset type) on the boundary of a circular patch was found to reduce the size of the antenna [26]. Another example of a shape-modified reduction in size is a patch antenna without a regular geometric shape having six radiating slots [27]. A novel antenna miniaturization technique is the use of fractal geometry [28]. Fractal geometry involves a recursive generating methodology that results in contours with infinitely intricate fine structures. These contours are able to add more electrical length in small volume. Meander antennas form a dominant class of antennas which contribute to a reduction in the size of antennas [29]. In this work, techniques for miniaturization were considered

and compared for design of a 915 MHz antenna to be used in a passive wireless application.

An antenna having circular polarization (CP) is useful as a mobile communication antenna [30]. A spiral antenna is a CP radiator and is a candidate for such applications. Spiral antennas have been extensively used due to their characteristic of broad bandwidth and circular polarization [31]. The shape of a spiral antenna can be equiangular, Archimedean, logarithmic, or rectangular. Spiral antennas may be configured with a single arm, double arms, or multiple arms. The multiple-arm spiral antenna can provide squinted beams through the variation of the spiral parameters or by using adaptive arrays. An eccentric spiral antenna can be used for beam steering as well by adjusting its eccentricity constants [32]. The spiral radiators can be implemented as wires, printed strips, or slots [33 - 34]. In order to reduce the size of a spiral antenna, a square or square zigzag shape may be used instead of a circular shape, but at the cost of a reduction in gain. Different configurations of the spiral antenna could be investigated to explore the radiation effect. One such configuration is the Archimedean spiral, with a zigzag shape to the outer turn of the broadband spiral antenna [35]. The Archimedean spiral for a flexible substrate was investigated in this work.

The effect of ground plane geometry and thickness of the dielectric substrate on a microstrip-patch antenna radiation is very dominant. Various ground plane geometries, that have been investigated, are mainly directed at modifying the radiation and decreasing spurious radiations [36-44]. Different ground plane configurations were investigated to observe the effect on radiation and the ground plane configuration was optimized for integration with the wireless sensor system. The types of antennas that have been studied for incorporation in the passive wireless sensor system are as follows:

- (i) Triangular patch antenna
- (ii) Spiral patch antenna
- (iii) Fractal geometry antenna

The objective of the research is to explore a wide variety of antennas with respect to band-width, single-resonant frequency/multi-resonant frequency types and design them to be small and having a high-gain by following the ground modification approach. Such designed antennas are then integrated with an integrated circuit capable of generating a code and the performance of the entire system is tested. Table 1.1 summarizes the antenna requirements, the requirements basis, the limitations faced and the approach adopted for this work.

Table 1.1 Antenna requirements, requirement basis, limitations and adopted approaches.

Feature	Requirement	Requirement basis	Limitation	Adopted Approach
Size	Small and compact	Tagging of small-size objects	The effective antenna length for 915 MHz is 16 cm. A lower length implies lower gain.	Choice of triangular, spiral & fractal antennas
Rigid or Flexible	Flexible	Tagging of individual low-cost items.	Flexible substrate requires very thin dielectric substrates. Thinner the dielectric, lesser the antenna gain.	Use of 127 $\mu$ m thick polyimide dielectric.
VSWR	< 2.0 over a sufficient bandwidth	To allow for greater than 90% power transfer.	Very narrow band-width can pose deviation from expected performance due to fabrication discrepancies.	Modification of feed-width, length and antenna shape
Gain	Greater than 0 dBi	To allow for greater reading distances.	Stacking of substrates, thicker dielectric, antenna arrays are undesirable.	Introduction of slots in the ground plane.

### **1.5 Organization of Dissertation**

This dissertation is divided into seven chapters. The first chapter contains the introduction and the second chapter is a discussion on the various microstrip antennas. The fabrication and characterization of these antennas is discussed in the third chapter. Testing of the antennas integrated with the system is detailed in the fourth chapter. The fifth chapter is the concluding chapter with a few remarks given on the employment of the RFID tag and an example of an RFID sensor with temperature sensing capability.

## CHAPTER 2

### ANTENNAS FOR PASSIVE RFID SYSTEMS

The generation of the “identification (ID) code” is done by various modulation schemes, such as amplitude shift keying (ASK), phase shift keying (PSK), frequency shift keying (FSK), Pulse Width Modulation (PWM), On-Off Keying (OOK), etc. All of the above modulation schemes involve the modulation of the incoming signal either in amplitude, phase or frequency or use an active component, such as a transistor or a filter to accomplish such a modulation. An entirely new way of generating ID through a delay-line has recently been proposed in two different delay schemes: the LC based delay scheme [45] and the transmission line based delay scheme [46], which is employed for integration of antennas in this work. While in the first scheme, the delay is brought about by either using lumped inductive and capacitive components, in the second, the delay is brought about by using the intrinsic inductance and capacitance of a transmission line. Both schemes are suitable for a passive RFID design, as they do not require any active components which require power. The performance of such passive RFID sensors is largely dependent on the integrated antenna.

The RFID transponder or tag can be upgraded as an RFID sensor when a sensing element or material is placed as a switch at some location on the transmission line. Such a switch is closed when the non-conducting sensing element senses the variant, such as

temperature, pressure or humidity and becomes conductive thus closing the path for the current to flow and the code to be transmitted from the tag. Such a sensing scheme is both simple and basic in that only the absence or presence of the variant is detected. Hence the sensing is only qualitative and not quantitative. A further simplified RFID sensor model is the antenna acting as the sensing element. The antenna is designed to resonate on a temperature/pressure/humidity sensitive dielectric (switch ON) for a particular ambient condition and not to resonate (switch OFF) in all other conditions of ambient. The design could also include the deposition of an ambient sensitive superstrate over the antenna layer. In all these designs, the antenna is acting both as a sensing and signal transmitting/receiving device. Such an antenna design for a combined sensing application needs to have an optimized bandwidth because a large bandwidth would deprive the antenna of its sensing capability and too narrow a bandwidth would make the antenna sensitive to other effects, such as fabrication discrepancies.

Another component used in the tag besides the antenna, the id generation circuit and the sensor, is the circulator that allows the use of a single antenna for both transmission and reception purposes in an RFID communication scheme. A circulator is a ferrite based three-terminal device. The current is circulated in this device either in a clock-wise or anti clock-wise direction and either in a 1-2-3 or 1-3-2 direction. When the circulator is designed for the current to flow in a 1-2-3 mode, the signal fed at terminal 1 is available at terminal 2 and there is no signal at terminal 3. The same is for the case with the signal fed at 2. The signal is available at terminal 3 and not at 1 and for the signal fed at 3, the signal is available at terminal 1 and not at terminal 2.

Let us briefly discuss the two delay schemes before we discuss the role and the design of the antenna for a passive RFID system. The two delay line based ID generation schemes that will be discussed now are the (i) LC based Delay Scheme and (ii) Transmission Line based Delay Scheme.

(i) LC based delay scheme [45]: Lumped inductor and capacitor elements are capable of delaying an electromagnetic current of any frequency. The magnitudes of the inductor and the capacitor can be designed to give a precise delay at a particular frequency. A meander line design with optimized line width and line gap is employed for an inductor and conductive trace over a grounded dielectric is employed as a capacitor to realize the lumped inductor and capacitor. The schematic of the LC based Delay Scheme is shown in Fig. 2.1.

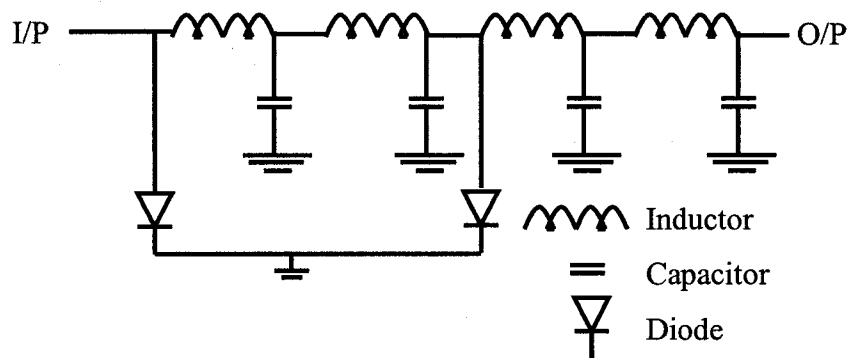


Fig. 2.1 Schematic of LC delay circuit tapped before the 1<sup>st</sup> LC pair and after the 2<sup>nd</sup> LC pair to generate 1010 code.

The incoming modulated signal from the external transceiver is passed through a array of LC elements connected in series. For a 915 MHz signal, the inductor and capacitor components are designed to give a total delay of  $T/4$ , where  $T$  is the time period of the interrogating signal and  $T$  equals 1.1 nsec. Thus, the signal at the end of one LC

section is delayed by  $T/4$  with respect to the incoming signal. Likewise the signal at the end of two LC sections is delayed by  $T/2$  and the delay at the end of three LC sections is delayed by  $3T/4$  nsec with respect to the incoming signal. Tapping the signal at the desired points and adding it to the incoming signal results in the formation of the id desired.

(ii) Transmission line based delay scheme [46]: The circuit level representation of a transmission line reveals a similar arrangement of inductor and capacitor elements as in the LC delay based scheme. Here, in this case, the magnitudes of the inductance and capacitance are dependent on the width of the transmission lines and the thickness and permittivity of the dielectric. A precise delay is obtained for a specific length of the transmission line. The schematic of the transmission based delay scheme is shown in Fig. 2.2. In the transmission line system, the delay is obtained by passing the signal through a lengthier microstrip line and then adding it to the direct signal. The delay caused by 1 inch of microstrip line for a 50-ohm input impedance system is 0.13 nsec and the width of the transmission line is  $406.25 \mu\text{m}$ . A meander design is chosen for the transmission line to decrease the area occupied by the lengthier microstrip line. The gap between the lines of the meander is optimized to minimize the cross-coupling effect between closely spaced lines. Such a design of the Transmission Line is simpler than the earlier LC delay based scheme as it does not include the integration of a diode, an extra component in the circuit and avoids the impedance matching issues associated with the integration. However the transmission line based circuit is larger in size for the realization of the required delay, which is 10 nsec. The circulator routes the receiving and the transmission signals in the proper direction and ensures the flow of current in one direction.  $I_1$  and  $I_2$  are the currents in the shorter and the longer transmission lines respectively. The current

is tapped at the proper location on the longer transmission lines and added to the signal by means of isolators, which ensures a single direction for the current when placed at different locations.

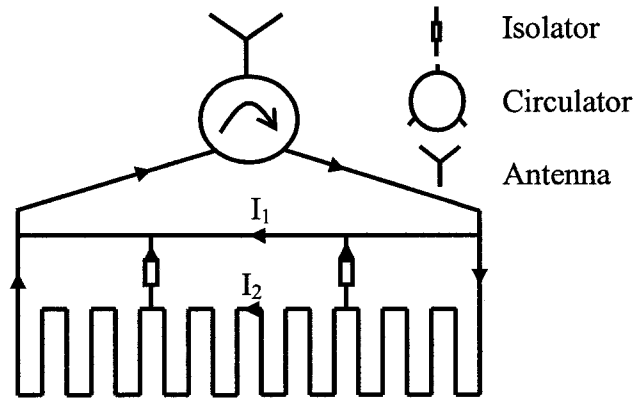


Fig. 2.2 Schematic of transmission line based delay scheme.

## 2.1 Antenna Theory

The amount of power captured by the tag depends on the impedance matching of the antenna. The impedance matching of the antenna at a particular frequency is known from the Voltage Standing Wave Ratio (VSWR), which will be explained in depth in a subsequent section. A VSWR=1 implies zero power reflected back into the air and a VSWR of  $\infty$  implies all the power reflected back into the air. An efficient antenna design aims for a VSWR  $< 2$  at the frequency of operation, which when translated into percentage is 88.9% of the power received. Another important parameter is the gain of the antenna which determines the reading distance of the tag relative to the reader. The antennas for delay based RFID systems should be small in size and their gain greater than 2.15 dBi, the maximum gain of a typical half-wave dipole antenna. “dBi” is the gain of the antenna over an isotropic antenna. An isotropic antenna is one which transmits equally in all directions. A high gain antenna implies more power in a particular

direction. Higher gain implies lesser omni-directionality. Though higher gain allows for a greater reading distance, omni-directionality is preferred for the reading of the tags in different orientations to the fixed reader antenna.

An increase of gain can be accomplished by employing an array of antennas or by the stacking of substrates [47]. Both methods increase the size of the tag and make the fabrication of the tag complex. An array of antenna needs splitter circuits to feed the antennas in sequence, thus making the feeding mechanism complex. Stacking of substrates would make the fabrication of the tag more complex due to issues like the alignment of the top and bottom copper patterns and the loss of the overall flexibility of the tag. In this work, the microstrip line fed antennas were designed and developed on a single polyimide substrate with dielectric constant of 3.5 and loss-tangent of 0.008. The antennas were designed to resonate at 915 MHz and to have a matching impedance of 50 ohms. All the antennas developed were built on a Kapton polyimide dielectric substrate, sandwiched between thin layers of adhesive (for the promotion of adhesion between the dielectric and copper films) and copper. The parameters  $\epsilon$  and  $\delta$  represent the dielectric constant and the loss tangent of the given material, respectively. Fig. 2.3 illustrates the cross-section of the substrate for which the antennas, in this work have been designed.

The major considerations in choosing an antenna for a passive RFID system are:

1. The type of antenna
2. Its impedance
3. RF performance when applied to the object
4. RF performance when the object has other structures around it.

The goal of antenna design, besides making it a high gain and high efficiency transducer (converting a guided wave propagating in a transmission line to an electromagnetic wave

propagating in an unbounded medium) is to meet the performance requirements for the intended applications. The basic antenna parameters [47] are discussed in the following section.

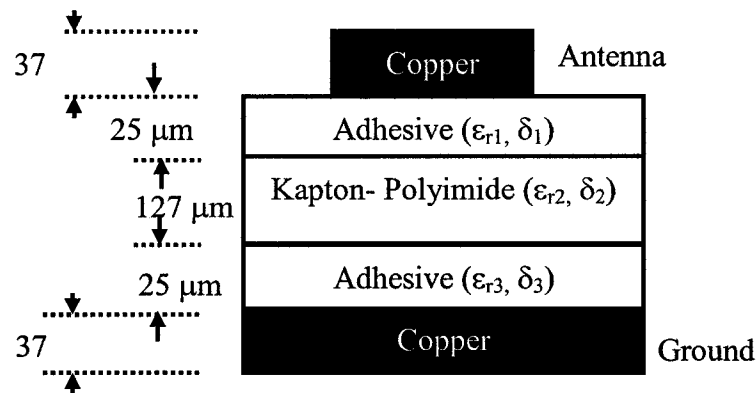


Fig. 2.3 Cross-section of the antenna substrate with  $\epsilon_{r1} = \epsilon_{r3} = 3.3$ ,  $\epsilon_{r2} = 3.5$ ;  $\delta_1 = \delta_3 = 0.027$ ,  $\delta_2 = 0.008$ .

### **2.1.1 Antenna Input Impedance and Efficiency**

An antenna is a device for radiating electromagnetic energy in the transmitting mode. A key parameter of the antenna is its input impedance,  $Z_A$ . It equals the ratio of the voltage  $V_A$  to the current  $I_A$  at its input terminals. The equivalent circuit of the transmitting antenna is shown in Fig. 2.4.  $R_S$  is the source resistance,  $X_S$  is the source reactance, antenna resistance,  $R_A = R_R + R_D$ , where  $R_R$  is the antenna radiation resistance and  $R_D$  is the antenna loss resistance.  $X_A$  is the antenna reactance.  $Z_A$  is the input impedance.

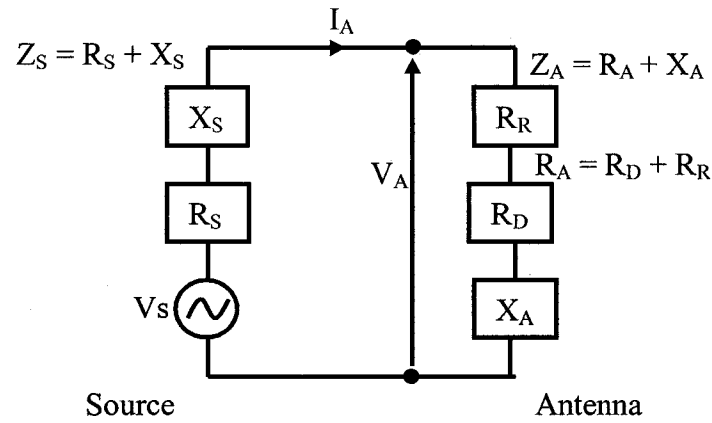


Fig. 2.4 Equivalent circuit of the transmitting antenna [47].

If the antenna is driven by a source  $V_s$  with impedance  $Z_s$ , then the voltage and the current at the antenna terminals are

$$V_A = \frac{V_s Z_A}{Z_s + Z_A}, \quad (2.1)$$

and

$$I_A = \frac{V_s}{Z_s + Z_A}. \quad (2.2)$$

The time-average power absorbed by the antenna terminals,  $P_A$  is

$$P_A = \frac{1}{2} \operatorname{Re} [V_A I_A^*] = \frac{|V_s|^2 R_A}{2 |Z_s + Z_A|^2}. \quad (2.3)$$

The total power radiated by the antenna, expressed as a fraction of  $P_A$  is  $P_R = e P_A$ , where  $e$  is the antenna efficiency. The difference between  $P_A$  and  $P_R$  is the power  $P_D$  dissipated by the antenna, where

$$P_D = P_A - P_R = (1-e) P_A \quad (2.4)$$

The time-average power absorbed by the antenna terminals,  $P_A$ , the total power radiated by the antenna,  $P_R$ , and the power dissipated by the antenna,  $P_D$  can be expressed in terms of the antenna input current,  $I_A$ , as follows:

$$\begin{aligned}
P_A &= \frac{1}{2} R_A |I_A|^2, \\
P_R &= \frac{1}{2} R_R |I_A|^2, \\
P_D &= \frac{1}{2} R_D |I_A|^2.
\end{aligned}
\tag{2.5}$$

The antenna efficiency can be expressed as:

$$e = \frac{R_R}{R_A} = \frac{R_R}{R_R + R_D}.
\tag{2.6}$$

The impedance of the antenna must match that of the transmission line to avoid reflections. The matching is measured by VSWR or the Voltage Standing Wave Ratio (S). VSWR provides a measure of the mismatch between the load impedance and the transmission line's characteristic impedance. VSWR (S) is mathematically expressed in terms of the voltage reflection coefficient ( $\Gamma$ ),

$$S = \frac{1 + |\Gamma|}{1 - |\Gamma|},
\tag{2.7}$$

The Voltage reflection coefficient ( $\Gamma$ ) is mathematically expressed as the ratio of the amplitude of the reflected voltage wave to the amplitude of the incident voltage wave at the load. This matching between the antenna load and the transmission line's characteristic impedance can be achieved by varying the feed length and width or the feed position.

In a passive RFID scheme, the antenna is required to have good matching which determines the amount of power captured by the antenna. In a delay based RFID scheme, good impedance matching becomes more important with the requirement that the amplitudes of the tapped delayed signals be large for an identifiable code output.

### 2.1.2 Electromagnetic Fields Produced by the Antenna

At a far distance from the antenna, the antenna electric field can be expressed as [76]

$$\mathbf{E}(\mathbf{r}) = \frac{e^{-jkr}}{r} [\mathbf{FF}_\phi(\mathbf{k}) \hat{\phi} + \mathbf{FF}_\theta(\mathbf{k}) \hat{\theta}] \quad (2.8)$$

where  $k = 2\pi/\lambda$  is the freespace wave number,  $\lambda = c/f$  represents the free-space wavelength,  $\hat{\theta}$  and  $\hat{\phi}$  are unit vectors in  $\theta$  and  $\phi$  directions, and  $\mathbf{FF}_\theta$ ,  $\mathbf{FF}_\phi$  are the field components in the  $xz$  and  $xy$  planes, respectively.  $c = 3 \times 10^8$  m/s is the freespace speed of light and  $f$  is the frequency of operation.  $\mathbf{k} = \hat{x} \sin\theta \cos\phi + \hat{y} \sin\theta \sin\phi + \hat{z} \cos\theta$  is a unit vector that points from the antenna toward the observer and  $\hat{x}$ ,  $\hat{y}$  and  $\hat{z}$  are unit vectors in the  $x$ ,  $y$  and  $z$  directions. At any distance from the antenna the electric field propagates radially away from the antenna and attenuates as  $1/r$  because of spherical spreading. The electric field has no  $r$ -directed component and the field can be fully characterized in terms of its  $\phi$  and  $\theta$  components. Fig. 2.5 depicts the far-field vector components of the transmitting antenna.

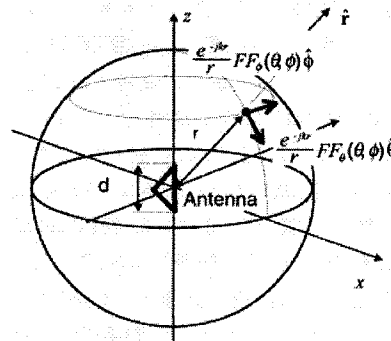


Fig. 2.5 Electric far-field vector components of the transmitting antenna [47].

At a far distance the electric field radiated by the antenna locally behaves as a plane wave. The antenna's magnetic field can then be expressed as

$$\mathbf{H}(\mathbf{r}) = \frac{1}{\eta} \frac{e^{-jkr}}{r} [\mathbf{F}\mathbf{F}_\phi(\mathbf{k})\hat{\phi} - \mathbf{F}\mathbf{F}_\theta(\mathbf{k})\hat{\theta}] \quad (2.9)$$

where  $\eta = (\mu_0/\epsilon_0)^{1/2}$  is the free-space wave impedance, and  $\mu_0$  and  $\epsilon_0$  the free-space permeability and permittivity respectively. The Poynting vector  $\mathbf{S}(\mathbf{r}) = [\mathbf{E}(\mathbf{r}) \times \mathbf{H}(\mathbf{r})^*]/2$  characterizes the power flow associated with the electromagnetic field. Substituting Equations (2.8) and (2.9), we have,

$$\mathbf{S}(\mathbf{r}) = \frac{1}{2\eta r^2} [\mathbf{F}\mathbf{F}_\phi(\mathbf{k})^2 + \mathbf{F}\mathbf{F}_\theta(\mathbf{k})^2] \hat{\mathbf{r}} \quad (2.10)$$

The radiation intensity  $U(\mathbf{k})$  of the antenna is

$$\begin{aligned} U(\mathbf{k}) &= r^2 |\mathbf{S}(\mathbf{r})| \\ &= \frac{1}{2\eta} [\mathbf{F}\mathbf{F}_\phi(\mathbf{k})^2 + \mathbf{F}\mathbf{F}_\theta(\mathbf{k})^2] \hat{\mathbf{r}} \end{aligned} \quad (2.11)$$

It is preferred for our application that the antennas not have a very narrow beam-width as it would lead to severe directional problems.

### **2.1.3 Radiation Pattern**

The electric and magnetic fields are characterized by Equations (2.8) and (2.9) respectively. These equations fully specify the radiation field of an antenna. The radiation pattern of an antenna (Fig. 2.6) is the graphical representation of the radiation of an antenna and could include information on the energy distribution, phase, and polarization of the radiated fields. The region of strong radiation is termed as the antenna's "main beam."

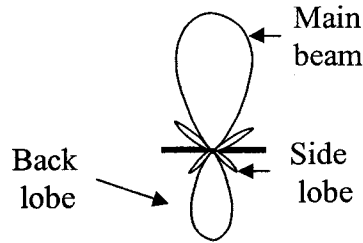


Fig. 2.6 Normalized (power) radiation pattern.

#### **2.1.4 Antenna Directivity, Gain & Equivalent Isotropically Radiated Power**

The directivity ( $D$ ) is a measure of the antenna's ability to concentrate the radiated power in a particular direction. By definition, the radiation intensity of the hypothetical radiator equals  $U_{ave}$ , the average radiation intensity of the antenna being characterized. For a circular symmetric antenna, the smaller the diameter of the antenna, the greater the beam-width. For a rectangular patch antenna, the smaller the width, the greater the beam-width.

$$D(k) = \frac{U(k)}{U_{ave}} = \frac{4\pi U(k)}{P_R} \quad (2.12)$$

The gain of the antenna is defined as

$$G(k) = \frac{4\pi U(k)}{P_A} \quad (2.13)$$

The maximum gain is denoted as

$$G = G(k)_{max} = \frac{4\pi U_{max}}{P_A} \quad (2.14)$$

The equivalent isotropically radiated power (EIRP) is the total power that would be radiated by a hypothetical antenna with radiation intensity equal to the maximum

radiation intensity of the antenna being characterized [47]. Since the total radiated power equals  $4\pi$  times the radiation intensity for an isotropic antenna, we have

$$\text{EIRP} = 4\pi U_{\max} = GP_A = eDP_A = DP_R \quad (2.15)$$

### **2.1.5 Antenna Polarization**

The antenna to be designed is to possess a required polarization feature. This is important, because in the receiving mode, only that component of the wave whose electric field is parallel to that of the antenna polarization state, is absorbed. The methods in which circular polarization (CP) could be achieved for various antennas are as follows:

- (i) Rectangular patch: CP possible with single feed.
- (ii) Square patch: CP possible with single feed using center slot, truncated corners, etc.
- (iii) Disk: CP possible with single feed using center slot, etc.
- (iv) Ellipse: CP possible with single feed
- (v) Pentagon: CP possible with single feed

## **2.2 Triangular, Spiral, and Fractal Antennas**

### **2.2.1. Triangular Antenna**

The microstrip triangular patch finds a large number of applications in the design of many useful MIC components, such as resonators, circulators and filters. Triangular patches have been investigated both theoretically and experimentally [48-49]. They are found to provide characteristics similar to those of rectangular patches, but with a smaller size. In the present work, an inset-fed triangular patch antenna, with a side length = 5.6 cm, has been developed on a 127  $\mu\text{m}$  thick polyimide substrate. The location of the feed-point determines the impedance matching of the antenna. To improve the impedance matching of the antenna, horizontal slits are introduced on the sides of the antenna, as

shown in Fig. 2.7 (a). The antenna thus designed is for a substrate of size  $6\text{ cm}^2$  and impedance matched to 50 ohms. This antenna can be readily integrated with an RFID chip ( $<0.5\text{ cm}^2$  area) for the realization of an RFID tag. For integration of the triangular patch antenna with the transmission line, further tuning is required for matching the antenna to 50 ohms. Fig. 2.7(b) shows the triangular patch antenna with a tuning stub added. In order to increase the gain of the triangular patch antenna, the ground plane of the antenna is modified. Fig. 2.8 shows the triangular patch antenna on a patched ground.

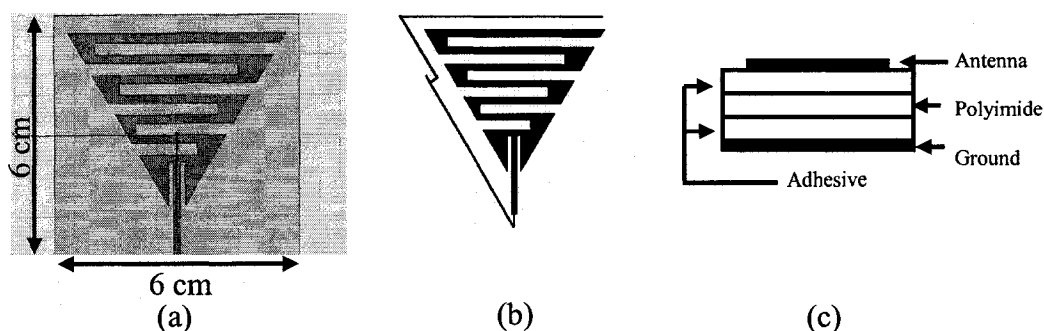


Fig. 2.7 Triangular patch antenna (a) with horizontal slits; (b) with tuning stub for integration with the system, and (c) cross-section on the dielectric substrate.

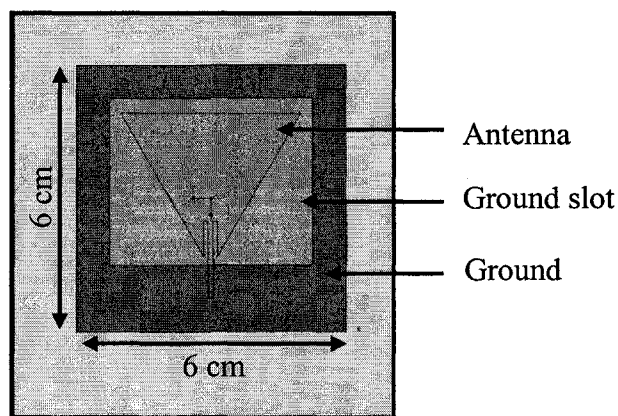


Fig. 2.8 Triangular patch antenna with slotted ground plane.

### 2.2.2 Spiral Antenna

A spiral antenna is a radiation element that radiates a circularly polarized (CP) wave over a wide frequency bandwidth. The spiral is often backed by a conducting plane to change the inherently bi-directional beam to be unidirectional. The radiation pattern has been qualitatively and quantitatively investigated [50]. It is seen, that as the distance between the spiral and the conducting plane decreases, the capability of the antenna to form a CP radiation beam deteriorates. The spiral antenna that is considered here is a single arm, eleven segment Archimedes spiral antenna (Fig. 2.9). The minimum width of the spiral arm is 2 mm and the maximum width is 8mm. The widths of the eleven segments are varied within this range, and for a particular width-combination, the impedance of the antenna is found to match to 50 ohms. The antenna thus designed is for

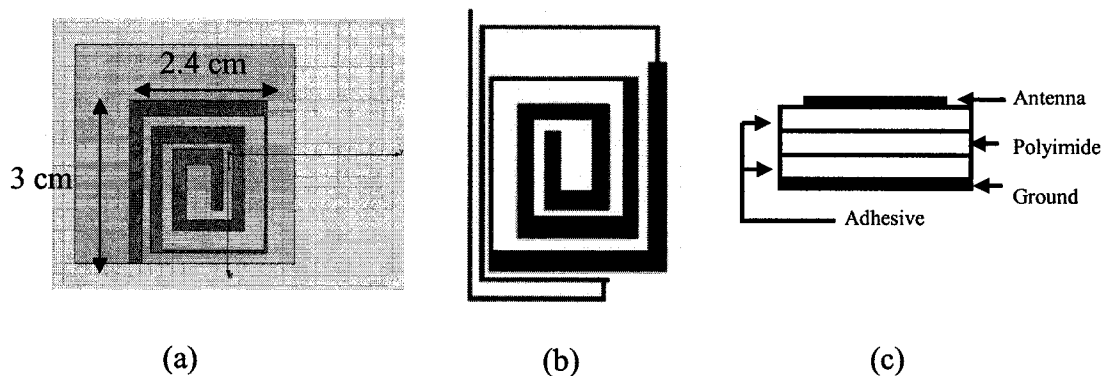


Fig. 2.9 Spiral patch antenna (a) with varying widths (b) with tuning stub for integration with the system (c) cross-section on the dielectric substrate.

a substrate of size  $6 \text{ cm}^2$  and impedance matched to 50 ohms. This antenna can be readily integrated with an RFID chip ( $<0.5 \text{ cm}^2$  area) for the realization of the RFID tag. For integration of the spiral patch antenna with our own developed ID circuit which is a transmission line, further tuning is to be required for matching the antenna to 50 ohms. Fig. 2.9 (b) shows the spiral patch antenna with a tuning stub added to it. Fig. 2.9 (c)

reveals the cross-section of the substrate platform for which the spiral antenna is designed. In order to increase the gain of the spiral patch antenna, the size of the antenna is increased (Fig. 2.10 (a)). In order to still increase the gain of the spiral antenna, the ground plane of the antenna is modified. The spiral patch antenna on the slotted ground plane is shown in Fig. 2.10 (b).

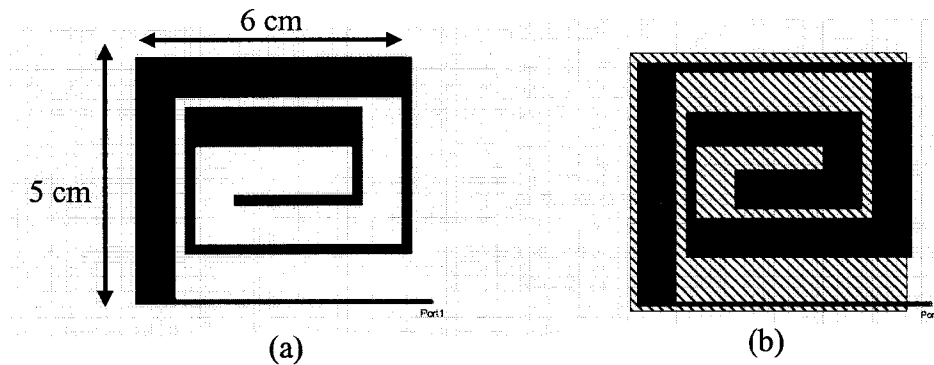


Fig. 2.10 Simulation layout of large (a) spiral patch antenna and (b) spiral patch antenna with slotted ground plane.

### 2.2.3 Fractal Antenna

The fractal antenna considered in this work is the Half-Sierpinski antenna, which is derived from the Sierpinski gasket and is known for its multi-band properties. The Sierpinski gasket is named after the Polish mathematician Sierpinski. He described some of the main properties of this fractal shape in the year 1916 [51-52]. The original gasket (Fig. 2.11) is constructed by subtracting a central inverted triangle from a main triangle.

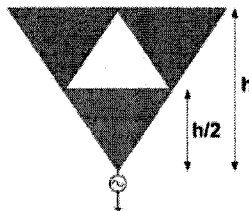


Fig. 2.11 The Sierpinski monopole.

After the subtraction, three equal triangles remain on the structure, each one's height being half of the height of the original one. One can iterate the same subtraction procedure on the remaining triangles and if the iteration is carried out an infinite number of times, the ideal fractal Sierpinski gasket is obtained. In such an ideal structure, each of its three main parts is exactly equal to the whole object, but scaled by a factor of two and so is each of the three gaskets that compose any of those parts [53].

A half-Sierpinski antenna (Fig. 2.11) is chosen so as to decrease the size of the antenna and, at the same time, retain the multi-band property in order to accommodate other technologies running at other frequencies. The impedance of the antenna is matched according to the following procedure. The feed of the antenna is partitioned into three sections (Fig. 2.12).

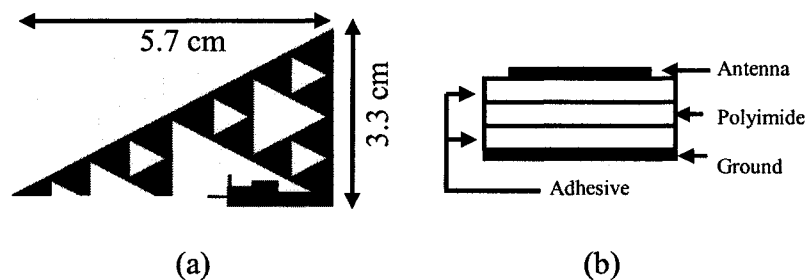


Fig. 2.12 Half-Sierpinski fractal antenna (a) with varying feed section widths and tuning stub for integration with the system, and (b) cross-section on the dielectric substrate.

For different widths of these sections, the fractal antenna is found to possess a different impedance. The widths of the section are varied and a particular combination of the widths is found to make the impedance of the antenna 50 ohms. Fig. 2.12 (a) shows the feed of the antenna having different widths. For integration of the half-sierpinski fractal patch antenna with the transmission line, further tuning is accomplished by introducing a stub for matching the antenna to 50 ohms. Fig. 2.12 (a) shows the fractal patch antenna

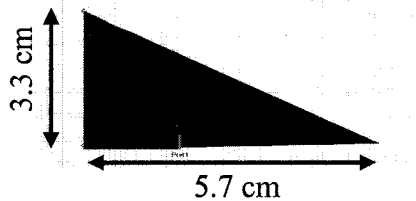


Fig. 2.13 Half-Sierpinski patch antenna with slotted ground plane.

with a tuning stub added to it. To increase the gain of the fractal patch antenna, the ground plane of the antenna is modified. Fig. 2.13 shows the half-sierpinski fractal patch antenna on a patched ground.

### **2.3 Simulation Analysis**

Extensive simulation work is performed to obtain the required VSWR and gain for all the designed antennas. Ansoft Designer [54] and Ansoft High Frequency Structure Simulator (HFSS) [55] have been employed as the simulation tools. Both simulation tools are utilized in the designing of the antenna.

#### **2.3.1 Simulation Models**

The model that was employed herein is the cavity model. In this model, the interior region of the patch is modeled as a cavity bounded by electric walls on the top and bottom, and a magnetic wall all along the periphery. The interior and exterior fields are solved for, using the inhomogeneous wave equation [56] and the boundary conditions on the walls and the top and bottom conductors. A microstrip antenna, in its simplest configuration, consists of a radiating metallic patch on one side of a dielectric substrate with a ground plane on the other side. Radiation from a microstrip antenna can be determined from the field distribution between the patch metallization and the ground plane. In other words, radiation can be described in terms of the surface current

distribution on the patch metallization. Let us now consider a microstrip patch antenna that has been connected to a microwave source. The energization of the patch will establish a charge distribution on the upper and lower surfaces of the patch as well as on the surface of the ground plane, as can be seen in Fig. 2.14. The patch, being half-wave long at the dominant mode, causes negative and positive charges to be present on the edges of the patch [56].

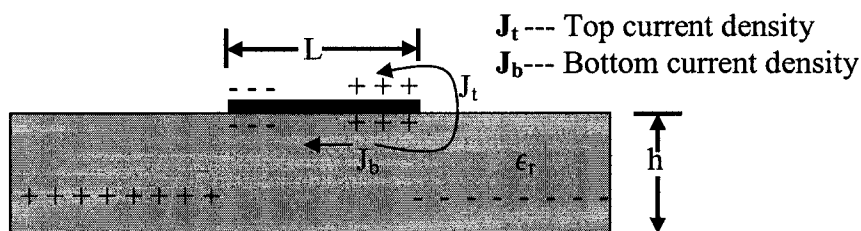


Fig. 2.14 Cross-section of the microstrip antenna and the charge distribution in the antenna.

The repulsive forces between like charges on the bottom surface of the patch tend to push some charges from the bottom surface, around its edges, and on to its top surface. This movement of charges creates corresponding current densities  $J_b$  and  $J_t$  at the bottom and top surfaces of the patch. Since the ratio  $h/W$  is very small for most microstrip antennas, the attractive force between the charges dominates and most of the charge concentration and the current flow remain underneath the patch. A small amount of current flowing around the edges of the patch to its top surface gives rise to a weak magnetic field tangential to the edges. Hence, a simple approximation can be made that the tangential magnetic field is zero by keeping magnetic walls all around the periphery of the patch. This assumption has greater validity for thin substrates with high  $\epsilon_r$ . With the substrate

being very thin compared to the wavelength ( $h \ll \lambda$ ), the field variations along the height can be considered to be constant and the electric field normal to the patch surface.

The four sidewalls of the cavity (Fig. 2.15) represent four narrow apertures or slots through which radiation takes place. Using the Huygens' field equivalence principle,

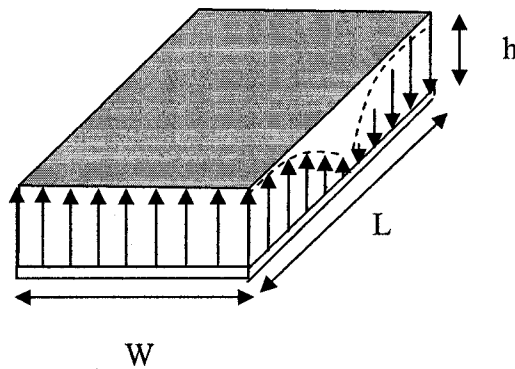


Fig. 2.15 Schematic of microstrip cavity with electric field distribution for the  $TM_{100}$  mode.

The microstrip patch can be represented by an equivalent current density  $\mathbf{J}_t$  at the top surface which accounts for the presence of patch metallization. The equivalent current densities across the four side slots are  $\mathbf{J}_s$  and  $\mathbf{M}_s$  corresponding to the magnetic and electric field  $\mathbf{H}_a$  and  $\mathbf{E}_a$  respectively. The equivalent currents are given as follows:

$$\mathbf{J}_s = \hat{\mathbf{n}} \times \mathbf{H}_a \quad (2.16)$$

$$\mathbf{M}_s = -\hat{\mathbf{n}} \times \mathbf{E}_a \quad (2.17)$$

$\mathbf{J}_t$  is much smaller than  $\mathbf{J}_b$  for thin substrates and hence can be set to zero. Likewise, the tangential magnetic fields along the patch edges and the corresponding current density  $\mathbf{J}_s$  are set to zero. Hence the only nonzero current density is the equivalent magnetic current

density  $\mathbf{M}_s$  along the periphery of the patch. Due to the ground plane, the equivalent current density is doubled [56]. The new current density is then given by

$$\mathbf{M}_s = -2\hat{\mathbf{n}} \times \mathbf{E}_a . \quad (2.18)$$

Antenna analysis is carried out for many reasons. A few of them are:

- (i) To reduce the number of costly cut-and-try cycles by aiding the design process.
- (ii) To ascertain the advantages as well as limitations of the antenna by carrying out parametric studies.
- (iii) To provide an understanding of the operating principles that could be useful for a new design, for modifications to an existing design, and for the development of new antenna configurations.

The analysis of microstrip antennas is complicated due to the presence of dielectric inhomogeneity, inhomogeneous boundary conditions, narrow frequency band characteristics, and a wide variety of feed, patch shape, and substrate configurations [56]. A balance is reached between the complexity of the method and the accuracy of the solution by compromising one or more of the features listed above. A model is said to be a good model if the model:

- (i) can be used to calculate all impedance and radiation characteristics of the antenna under discussion.
- (ii) can bring in results accurate enough for the intended purpose.
- (iii) is as simple as possible, while providing the proposed accuracy for the impedance and radiation properties.
- (iv) lends itself to interpretation in terms of known physical phenomena [56].

The microstrip antenna characteristics are determined by many elaborate techniques. All these techniques can be broadly classified into two categories: the analytical techniques and full-wave methods. Full-wave methods are numerical based and are more accurate, being based on Sommerfeld-type integral equations and the solution of Maxwell's equations in the time domain.

The analytical techniques are as follows:

- (i) The transmission line model
- (ii) Generalized transmission line model
- (iii) Cavity model and
- (iv) Multiport network model.

The prominent full-wave methods are as follows:

- (i) Integral equation analysis in the spectral domain,
- (ii) Integral equation analysis in the space domain and
- (iii) The Finite-Difference Time-Domain approach.

In the following section of this chapter we shall explore the method of moment, which is the Integral Equation analysis in the spectral domain employed by Ansoft Designer and the Finite Element method employed by Ansoft HFSS. The features of these full-wave methods are explained in the appendix.

### **2.3.2 Simulation Setup**

The simulation setup for Ansoft Designer and Ansoft HFSS are quite different. The Ansoft Designer is a two-dimensional electromagnetic analysis tool and Ansoft HFSS is a three-dimensional electromagnetic analysis tool. The four steps for obtaining the simulation response of a given microstrip antenna are as follows:

- (i) Preparation of the layout of the substrate and the antenna layers

- (ii) Incorporation of the excitation features
- (iii) Defining of boundaries and
- (iv) Setting up the analysis

### 2.3.2.1 Layout preparation

Initially, the layout of the substrate and antenna layers is prepared. Preparation of the substrate and the antenna layers is quite different in Ansoft Designer and Ansoft HFSS. Let us discuss the layout preparation for both of the softwares.

(i) Ansoft Designer: The Stack-up option is available in Ansoft designer to define the substrate layers, their properties, their thickness and the order in which they are stacked below the antenna. The antenna is defined as the “signal layer” and the ground layer is defined as the “metallized signal” layer. Fig. 2.16 reveals the stack-up window wherein the properties and the thicknesses of the layers can be defined. To create the

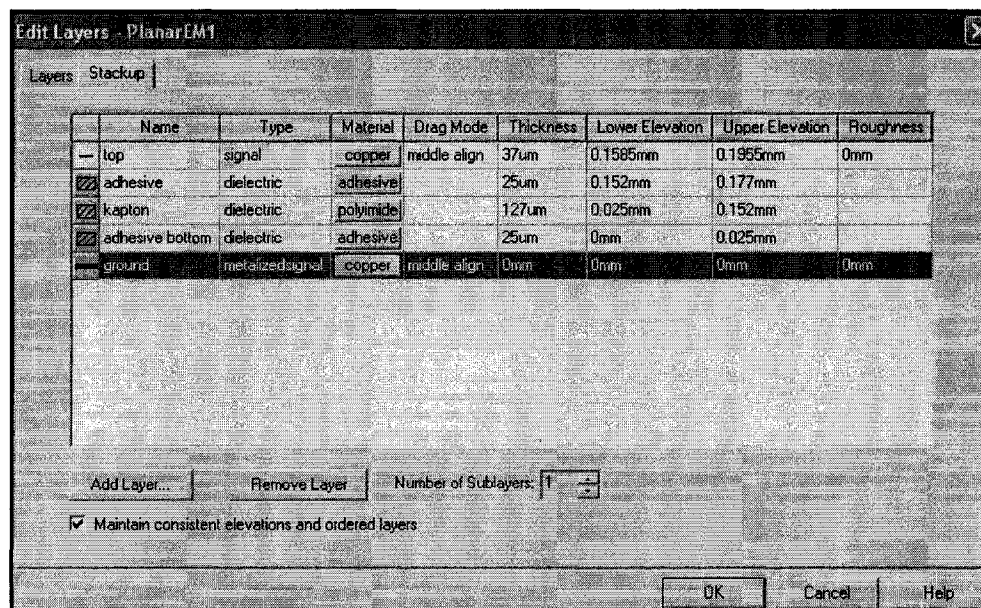


Fig. 2.16 Stack up option window to build layers in Ansoft Designer.

shape or modify the shape of a particular layer, this layer is selected as the active layer before creating or modifying the shape. It is to be noted that in Ansoft Designer, the substrate and the ground layers are assumed to be infinite or the finite substrate effects are approximated as being absent. Creation of any shape, with ground layer as the active layer, implies a slot in that layer of the specific shape created. For example to create a rectangular slot in the ground plane, the ground plane is selected as the active layer and a rectangle is drawn. Finally to create the antenna shape, the signal-layer is selected and the shape of the antenna is drawn, using the available shapes in the library, and the shape is modified using Boolean addition and subtraction.

(ii) Ansoft HFSS: The three-dimensional layout space is initially opened using the simulation route. Using the 2-dimensional and 3-dimensional objects already available in the library the substrate and the antenna layers are created. The three-dimensional objects are created either by directly importing them from the library, or by creating a 2-dimensional object and then sweeping the 2-dimensional object in the z-direction. It is to be noted, that since the thickness of the antenna layer has little effect on the impedance matching and the radiation properties of the antenna, defining the antenna layer as a 2-dimensional object would decrease the number of nodes and therefore, the magnitude of the simulation task assigned to the processor. Boolean addition, subtraction, sizing and scaling can be employed to modify the shape and size of the antenna and the substrate layers. Fig. 2.17 shows the cross-section of the different layers which comprise the substrate for the antenna.

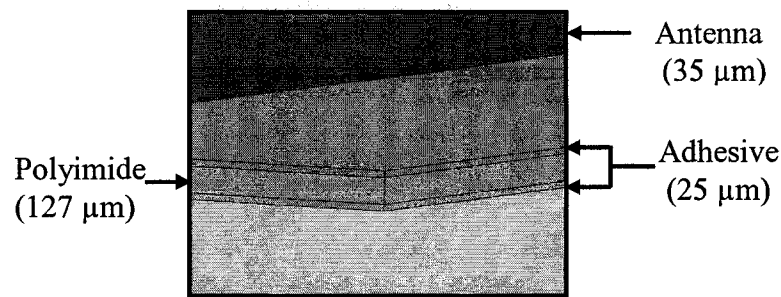


Fig. 2.17 Simulation layout of the antenna substrate cross-section.

### 2.3.2.2 Incorporation of excitation features

In order to obtain the simulation response of the antenna, excitation has to be defined on the antenna. The way excitation is defined in Ansoft Designer and Ansoft HFSS is different. Let us discuss the two procedures:

(i) Ansoft Designer: Setting up the excitation is simple in the Ansoft Designer. After creating the layout of the antenna, which is a 2-dimensional object, an edge to which excitation is to be given is selected. The selected edge is then defined for excitation. This is the edge through which the antenna is fed. The current and voltage magnitudes can be defined in the port parameters window. It is to be defined that any change of these magnitudes will not affect the impedance matching values or the gains or the radiation pattern of the antenna.

(ii) Ansoft HFSS: Setting up the excitation in HFSS involves the defining of one surface as the lumped port. The complex impedance  $Z_s$  defined for a lumped port serves as the reference impedance of the S-matrix on the lumped port. The impedance  $Z_s$  has the characteristics of a wave impedance; it is used to determine the strength of a source, such as the modal voltage and modal current  $I$ , through complex power normalization (the magnitude of the complex power is normalized to 1). In either case, one would get an

identical S-matrix by solving a problem using a complex impedance for a lumped  $Z_s$  or renormalizing an existing solution to the same complex impedance. A 2-dimensional surface is created whose top touches the antenna layer and the bottom, the ground layer. This layer is then given a lumped port excitation. The magnitude of the impedance matching is then input to the software. While defining the lumped port, the direction of the field is also defined and is dependent on the direction of the current, which is determined by the antenna acting in the transmission or the receiving mode. Since all the antennas designed are reciprocal (same impedance and radiation characteristics) the direction of the field is redundant for determining the radiation performance and the impedance matching conditions of the antenna. Fig. 2.18 shows the lumped port at the edge of the microstrip antenna.

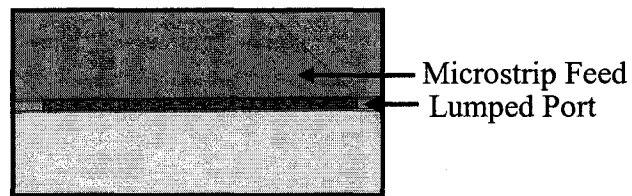


Fig. 2.18 Simulation layout of cross-section, showing a 2-d surface defined as lumped-port to simulate excitation.

### **2.3.2.3 Defining boundaries**

Simulation using Ansoft HFSS requires the boundaries to be defined. Such boundary definitions are not necessary in Ansoft Designer. The 2-d antenna layer and the ground layers created in Ansoft HFSS are defined as perfect E boundaries in order to assign very high conductivity to these layers. Since Ansoft HFSS is based on finite element analysis, a radiation boundary needs to be defined to limit the size of the problem. A radiation boundary is used to simulate an open problem that allows waves to

radiate infinitely far into space. HFSS absorbs the wave radiation boundary, essentially ballooning the boundary infinitely far away from the structure. A radiation surface does not have to be spherical, but it must be exposed to the background, is convex with regard to the radiation source, and located at least a quarter wavelength from the radiating source. In a few cases, the radiation boundary (Fig. 2.19) may be located closer than one-quarter wavelength, such as portions of the radiation boundary where little radiated energy is

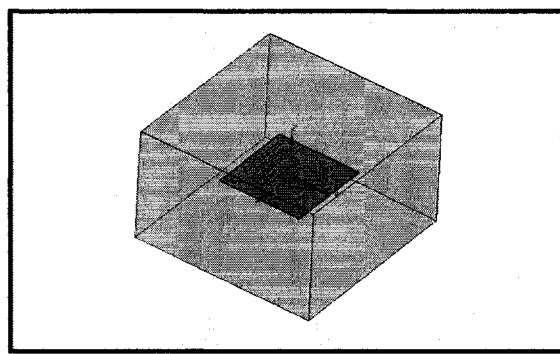


Fig. 2.19 Simulation layout of the radiation boundary surrounding the antenna.

expected. The route for defining the boundary after selecting the object to assign the radiation boundary is HFSS>Boundaries>Assign>Radiation.

#### **2.3.2.4 Analysis set-up**

Setting up the analysis for obtaining the response of the antenna is similar in both Ansoft Designer and Ansoft HFSS. Two different types of analysis can be executed by either software; specific analysis and parametric analysis.

(i) Specific analysis: The analysis is done for specific dimensions of the antenna. The software needs an input for the solution frequency, which is the frequency at which the software does adaptive meshing in order to get accurate results. A frequency sweep is to

be defined for the simulation problem at hand and the number of steps employed in the sweep. Fig. 2.20 reveals the analysis window with the values to be submitted for the simulation.

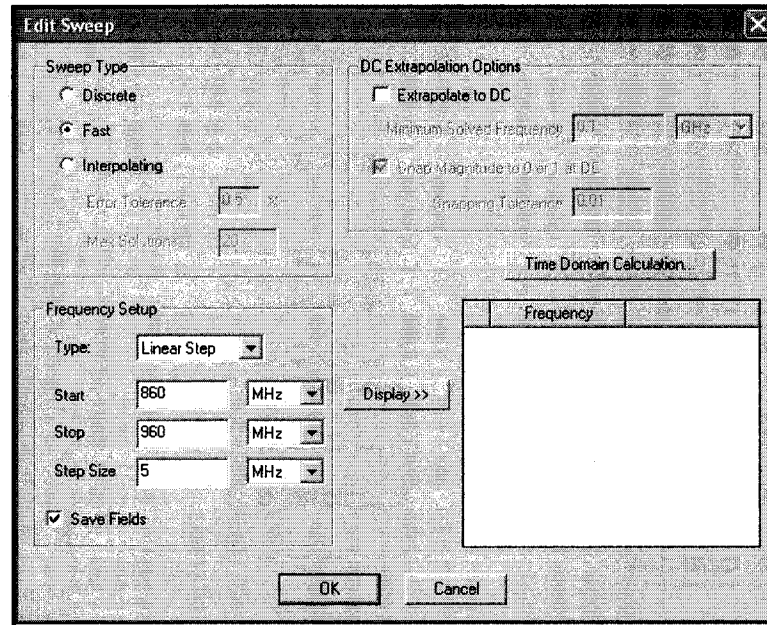


Fig. 2.20 Analysis window for specific analysis.

(ii) Parametric analysis: The parametric analysis is run to obtain the effect of antenna dimensions on the VSWR or the gain of the antenna at the solution frequency. The dimension of the antenna is defined with a user named parameter and the parameter is swept in the range given to obtain the values of VSWR or gain at different values of the parameter. Fig. 2.21 reveals the parametric analysis window. The number of solutions for the parametric analysis is the product of the number of values considered for each parameter. If  $p$  is the number of values considered for a parameter A,  $q$  the number of values for a parameter B and  $r$ , the number of values for the parameter C, the total number of solutions for the parametric sweep are  $p \times q \times r$ .

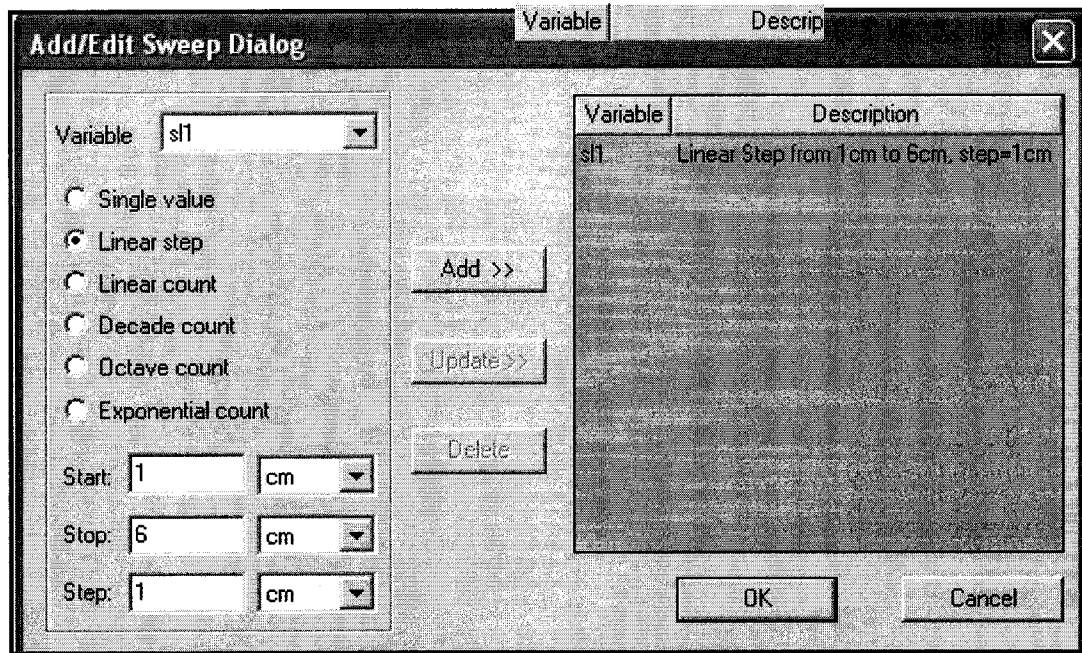


Fig. 2.21 Parametric sweep analysis window.

### 2.3.3 Design Considerations

The antennas have been designed using different techniques. The different techniques can be collectively named using the acronym, the Seven S, namely, size, shape, slit, slot, stub, short and skew. The different techniques are as follows:

- (i) Size change
- (ii) Shape change
- (iii) Slit introduction
- (iv) Slot introduction
- (v) Stub introduction
- (vi) Short introduction
- (vii) Skewing of antenna.

### **2.3.3.1 Size change**

The size of the antenna is scaled in the x and y directions in order to increase or decrease the size of the antenna on the substrate. This procedure was followed in the simulation to determine the size of the antenna where the impedance is matched. This feature is available only in the HFSS simulation package. All the objects in the simulation, i.e. the antenna, polyimide dielectric layer, adhesive layers, lumped excitation port, radiation sphere boundary etc. are selected for scaling. This is to ensure that accurate simulation results are obtained after scaling. This is an important step, because the simulation of the scaled antenna with an unscaled lumped port plane, or the radiation sphere boundary, would give erroneous results. Scaling can also be done in decimal formats and thus, a fine tuning of the antenna can be done using this technique.

### **2.3.3.2 Shape change**

The antenna shape or the ground plane is changed to obtain the required values of the impedance and the gain of the antenna. The different shape change procedures that were followed are as follows:

- (i) Inset feeding method: In order to match the impedance of the antenna, the feed point of the antenna is located not at the edge or the tip of the antenna, but to a distance inside the antenna. This technique was followed to impedance match the triangular patch antenna.
- (ii) Antenna width variation: The width of the antenna is changed to impedance match the antenna. This technique was followed to impedance match the spiral antenna.
- (iii) Feed width change: This relates to the change of the shape of the microstrip antenna at its feed location, where the microstrip feed line joins the microstrip antenna. This is to

match the impedance of the antenna. This technique was followed to impedance match the half-Sierpinski fractal antenna.

The shape can be changed by subtracting and adding 2-dimensional and 3-dimensional objects to the already designed shape. The simulation route for subtraction and addition of shapes is as follows:

Ansoft Designer: Layout >> Merge Polygons >> Union/Subtract

Ansoft HFSS: 3d Modeler >> Boolean >> Unite/Subtract

Two planes or bodies have to be selected before a Boolean addition operation or a subtraction operation is performed. Fig. 2.22 illustrates such a shape change operation in Ansoft HFSS.

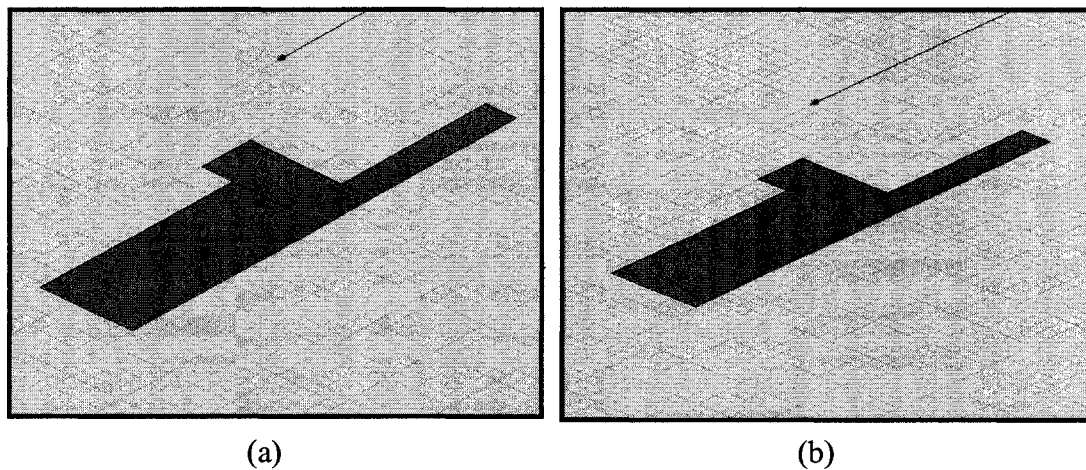


Fig. 2.22 Simulation layout of rectangular elements (a) before union and (b) after union.

### **2.3.3.3 Slit introduction**

A slit is an open gap introduced on the antenna which opens itself towards the edge of the substrate. The slit is obtained by doing a Boolean subtraction with 2-dimensional or 3-dimensional objects. Note that only similar objects (either both of them are 2 dimensional, such as a rectangle and a square or both of them are 3 dimensional,

such as a cube and a sphere) can be Boolean operated. This technique is employed to match the impedance of the triangular patch antenna. The simulation route for subtraction of shapes is as follows:

Ansoft Designer: Layout >> Merge Polygons >> Subtract

Ansoft HFSS: 3d Modeler >> Boolean >> Subtract

Fig. 2.23 shows the formation of a slit by a Boolean subtraction.

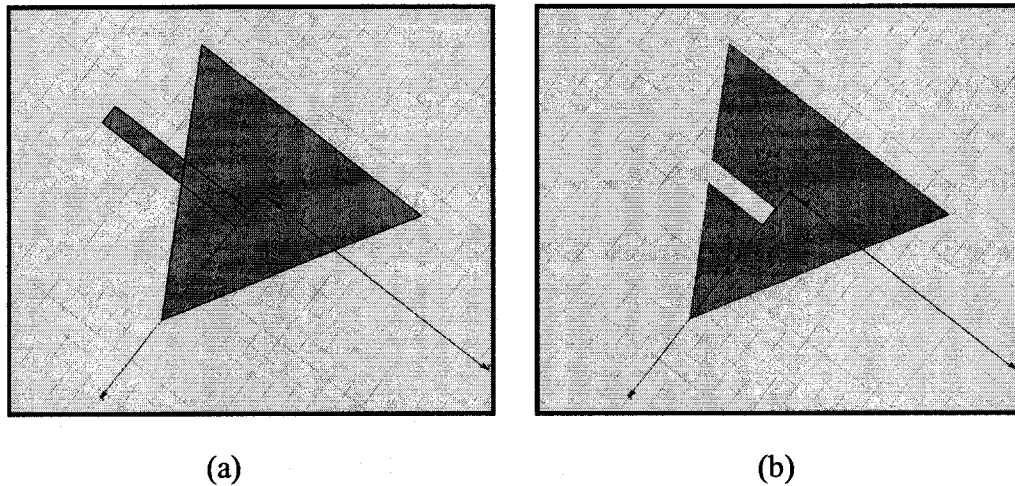


Fig. 2.23 Simulation layout of triangular patch antenna (a) before boolean subtraction and (b) after boolean subtraction.

#### **2.3.3.4 Slot introduction**

A slot is a closed gap introduced on the antenna or on the ground layer. The slot is obtained by doing a Boolean subtraction with 2-dimensional or 3-dimensional objects. Note that only similar objects (either both of them are 2-dimensional, such as a rectangle and a square or both of them are 3-dimensional, such as a cube and a sphere) can be Boolean operated. Slots are created in the ground plane to increase the gain of the antenna. An increase in gain of over 20 dB is observed when slots are introduced in the ground plane. This technique was followed to increase the gain of all the antennas.

The simulation route for subtraction of shapes is as follows:

Ansoft Designer: Layout >> Merge Polygons >> Subtract

Ansoft HFSS: 3d Modeler >> Boolean >> Subtract

Fig. 2.24 reveals the formation of a slot by a Boolean subtraction.

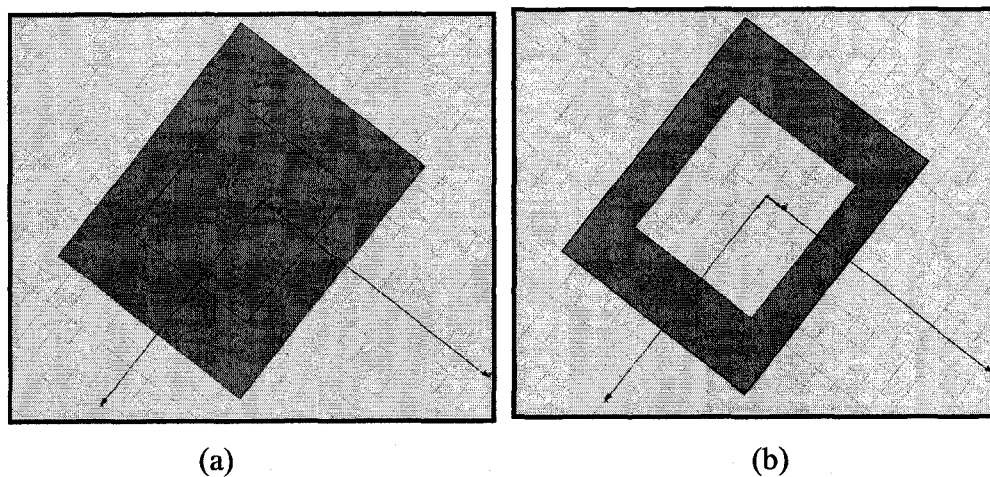


Fig. 2.24 Simulation layout of ground plane of the antenna, (a) unslotted and (b) slotted.

### 2.3.3.5 Stub introduction

A stub is a microstrip line extension added to the microstrip feed-line at a specific distance from the feed junction (the point of intersection of the microstrip line feed and the microstrip antenna). This feature is only available in the Ansoft Designer Simulation software through the Tuning Option tool. The input values for the tool are the reactance to be compensated, and the resistance to be added and the width of the microstrip line, which is determined by the characteristic impedance of the antenna. The distance from the feed junction and the length of the microstrip line extension are the two output values of the tool. The microstrip extension (stub) is to be Boolean added to the microstrip line feed in such a way that the stub is perpendicular to the feed. This technique is employed for integration of all antennas with the delay-based transmission line of the tag.

The route for the tuning tool option is as follows:

Ansoft Designer: Planar EM>>Estimate>>Imp. Match>>Tuning Stub

Fig. 2.25 depicts the tuning tool calculator for determining the tuning stub location and length. Fig. 2.26 shows the real and imaginary impedance values obtained before and after tuning. The imaginary value of the impedance is close to zero after tuning at 915 MHz.

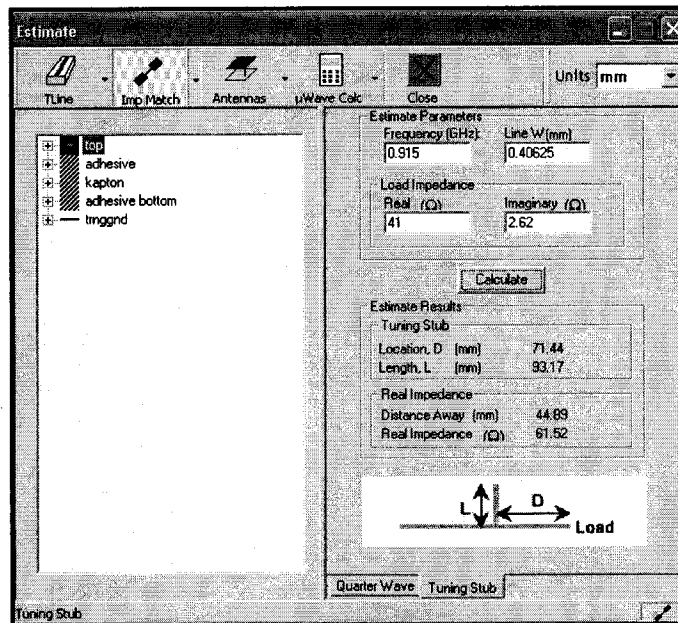


Fig. 2.25 Tuning stub calculator in Ansoft Designer.

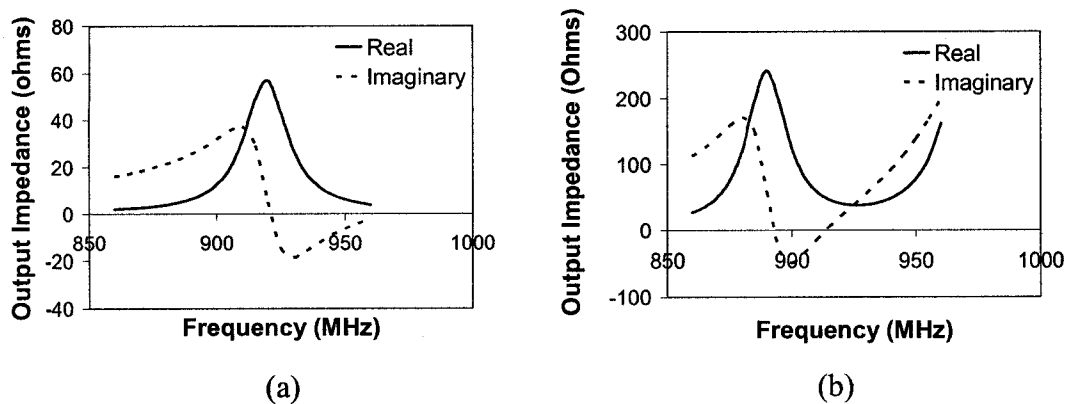


Fig. 2.26 Real and Imaginary impedance plots of (a) untuned and (b) tuned antenna.

### 2.3.3.6 Short introduction

This technique is related to the earlier discussed technique, i.e. introduction of a stub. In some cases, when the length of the stub is too long, a grounding of the stub is employed to decrease the length of the stub and at the same time achieve the required effects of the stub. This method is very useful as it reduces the antenna size due to the inclusion of the stub. This technique is employed for tuning the Half-sierpinski fractal antenna for integration with the system. Fig. 2.27 reveals the location of the ground on the stub. Care should be taken in the experimental procedure to ensure proper grounding of the stub as such an error would have a dominant effect on the impedance matching of the antenna, as shown in Fig. 2.28.

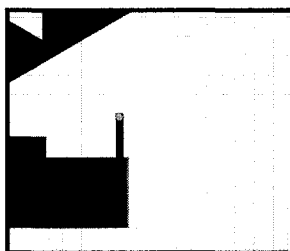


Fig. 2.27 Simulation layout of the tuning stub of the antenna with a ground short.

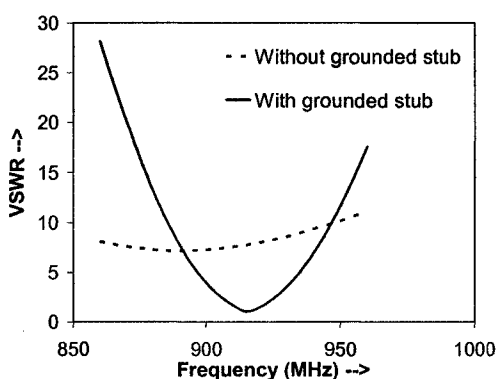


Fig. 2.28 VSWR plot with and without grounded stub.

### 2.3.3.7 Antenna skewing

Skewing of the antenna is a powerful tool to tune the antenna for a specific resonant frequency and to perform impedance matching of the antenna. By skewing we mean scaling the antenna in x- and y-directions using a different scale. This feature is only available in Ansoft HFSS and is used to bring the antenna close to the required resonant frequency. As is the case for increasing the size of the antenna, we have to select all the objects in the simulation layout for performing the skewing operation. Care should be taken to scale the excitation plane and the radiation boundary plane, to avoid erroneous results. Fig. 2.29 reveals the skewing effect on the antenna. The simulation route for the skewing option is as follows. Ansoft HFSS: Edit >>Scale.

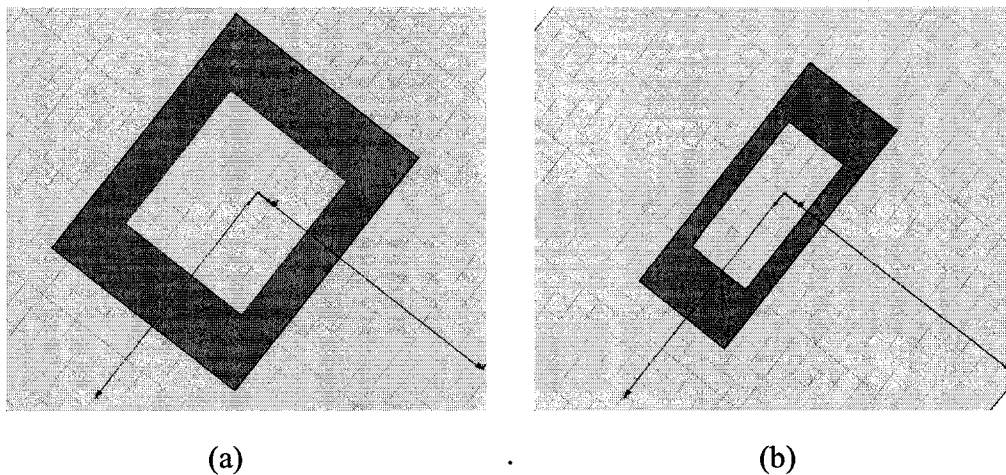


Fig. 2.29 Simulation layout of ground plane (a) before skewing and (b) after skewing in the y-direction.

This technique is performed to increase the gain of the wide-band circular disc monopole, which is used in the system testing of the antenna as a source of the signal

### 2.3.4. Triangular Patch Antenna

Triangular patches are found to provide radiation characteristics similar to those of rectangular patches, but with a smaller size. The size of the antenna can be reduced

further by loading it with a short and/or slot. Being the simplest of the triangular shapes, it comprises an equilateral triangular conductor on a grounded dielectric substrate. The triangular patch antenna is developed first using the Ansoft HFSS simulation method and is then fine-tuned for integration with the system (transmission line and circulator device) using Ansoft Designer.

#### **2.3.4.1 Design**

An inset-fed triangular patch antenna was considered (Fig. 2.30). In order to keep the size of the designed antenna small and the length of the radiating side of the antenna within the limits of an efficient, electrically small antenna with dimensions ( $\lambda/4$  (8 cm) and  $\lambda/10$  (3cm)), the size of the ground plane was kept at 6 cm x 6 cm. A wave-port excitation was given to the microstrip patch antenna. The antenna was designed for a port impedance of 50 ohms. The length of the feed ( $y$ ) and the width of the inset ( $x$ ) were considered as the parameters for a parametric sweep of these two parameters, which are also the usual parameters considered for the impedance matching of the inset-fed microstrip fed antennas. With the given substrate dimension limit of 6 cm, it was not possible to impedance match the antenna. The VSWR value obtained was 760 due to high impedance mismatch (Fig. 2.30). To reduce the VSWR, vertical and horizontal slits were introduced upon the triangular patch antenna. It was observed that the effect of the introduction of slits improved the impedance-matching far better than the inset-fed method. Fig. 2.30 gives the simulation layout and the simulation response using inset-feeding method. Introduction of vertical slits on the triangular patch antenna was found to bring the VSWR to a value of 11.97 from 760 as shown in Fig. 2.31.

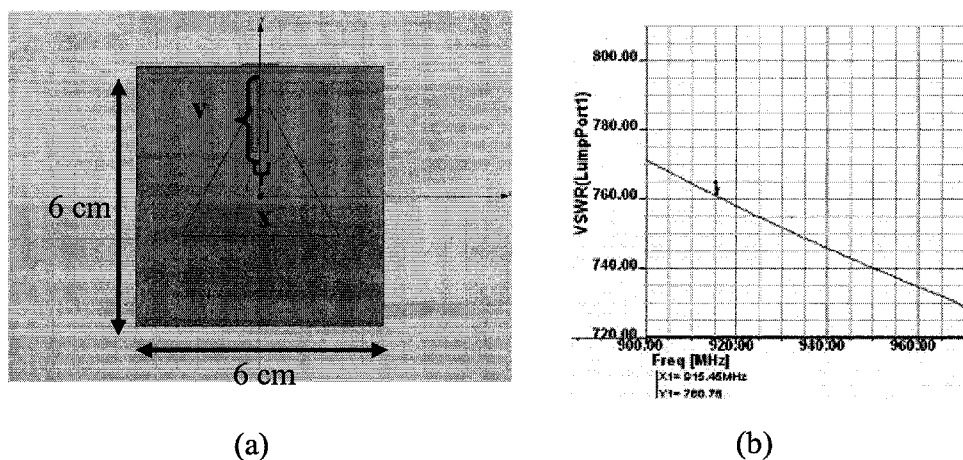


Fig. 2.30 (a) Simulation layout of inset-fed triangular patch antenna, and (b) VSWR plot for inset-fed triangular patch antenna.

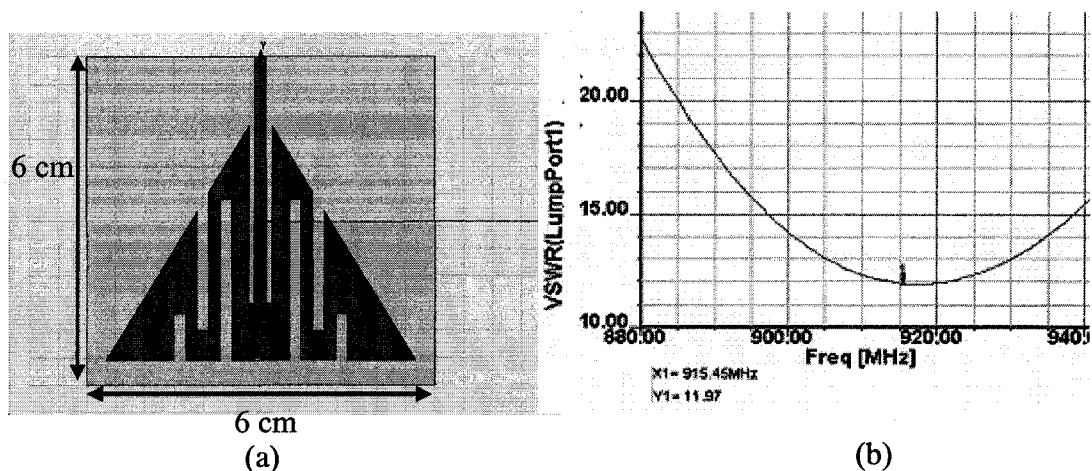


Fig. 2.31 (a) Simulation layout of vertical slit triangular patch antenna, and (b) VSWR plot of vertical slit triangular patch antenna.

However, the introduction of horizontal slots eventually proved to be the best impedance-matching procedure for the triangular patch antenna. The VSWR significantly improved to a very efficient value of 1.53 (Fig. 2.32). The gain of the antenna was found to be -30 dB (Fig. 2.33).

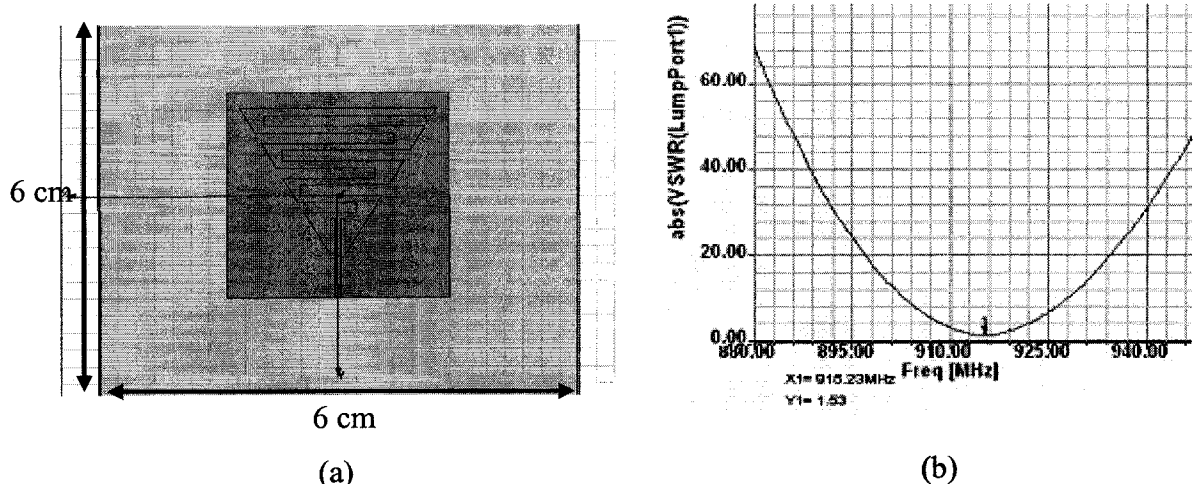


Fig. 2.32 (a) Simulation layout of horizontal slit triangular patch antenna, and (b) VSWR plot of horizontal slit triangular patch antenna.

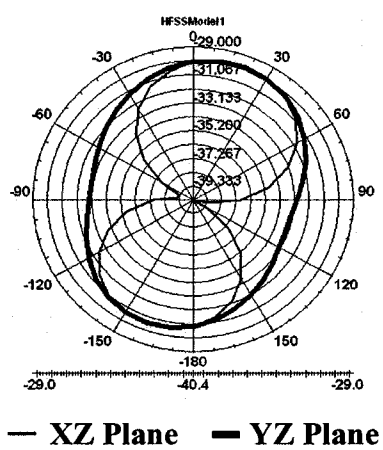


Fig. 2.33 Radiation pattern of the triangular antenna with horizontal slit.

Simulations were carried out to study the effect of ground plane geometry on the gain and the radiation pattern of the inset-fed triangular patch was studied. A 2 cm<sup>2</sup> patch was inserted at each corner of the antenna substrate. A patched ground plane was found to increase the gain of the antenna to -14 dB. Fig. 2.34 shows the increase in gain when a patched ground plane is used.

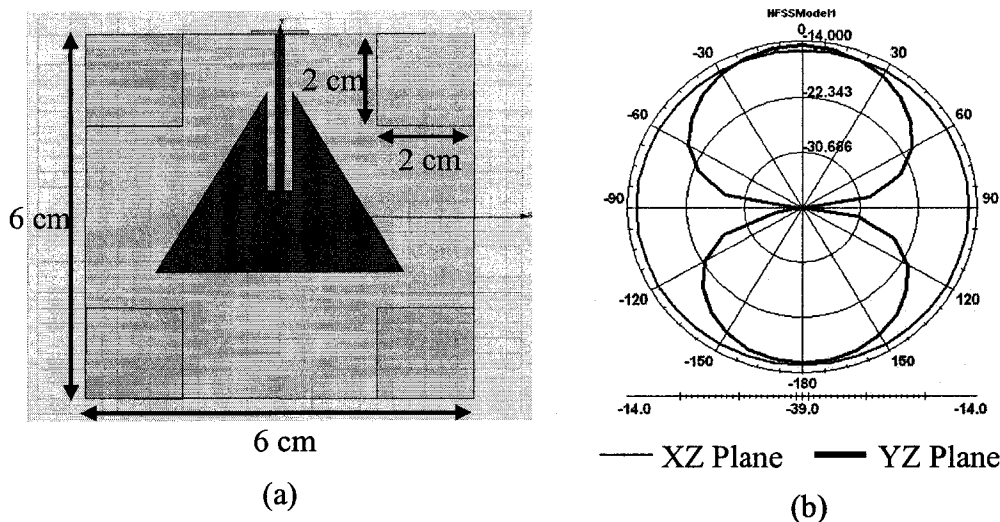


Fig. 2.34 (a) Simulation layout, and (b) radiation pattern of a patched ground, inset-fed triangular patch antenna.

#### 2.3.4.2 Tuning

The layout of the triangular patch antenna, generated using Ansoft HFSS, is imported to the Ansoft Designer in which the antenna analysis is carried out in an infinite substrate environment. This environment is suitable for analysis of the antenna which will be integrated with the transmission line. On performing an analysis of the antenna design imported from HFSS, it was found that there was a slight increase of VSWR, as shown in Fig. 2.35 (a). The plots of real and imaginary impedance can be seen in Fig. 2.35 (b).

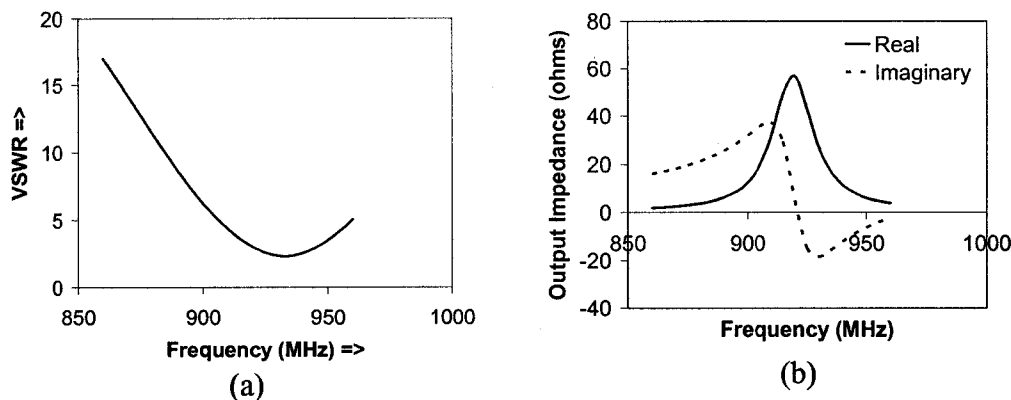


Fig. 2.35 (a) VSWR plot and (b) real and imaginary impedance plots of untuned triangular patch antenna.

Using the tuning tool, the length of the stub and its location (the distance of the stub from the feed point) is determined and is found to be 80 mm and 54 mm, respectively. After adding the stub, the VSWR obtained was found to be 1.13. The real and imaginary impedance plots of the tuned triangular patch antenna are shown in Fig. 2.36. Now, the triangular patch antenna is ready for integration with the system. Fig. 2.37 shows a picture of the tuned triangular patch antenna.

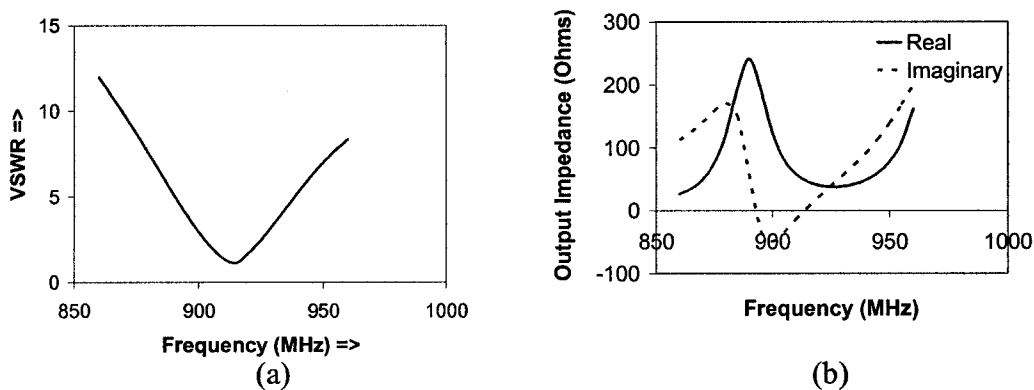


Fig. 2.36 (a) VSWR plot and (b) Real and imaginary impedance plots of tuned triangular patch antenna.

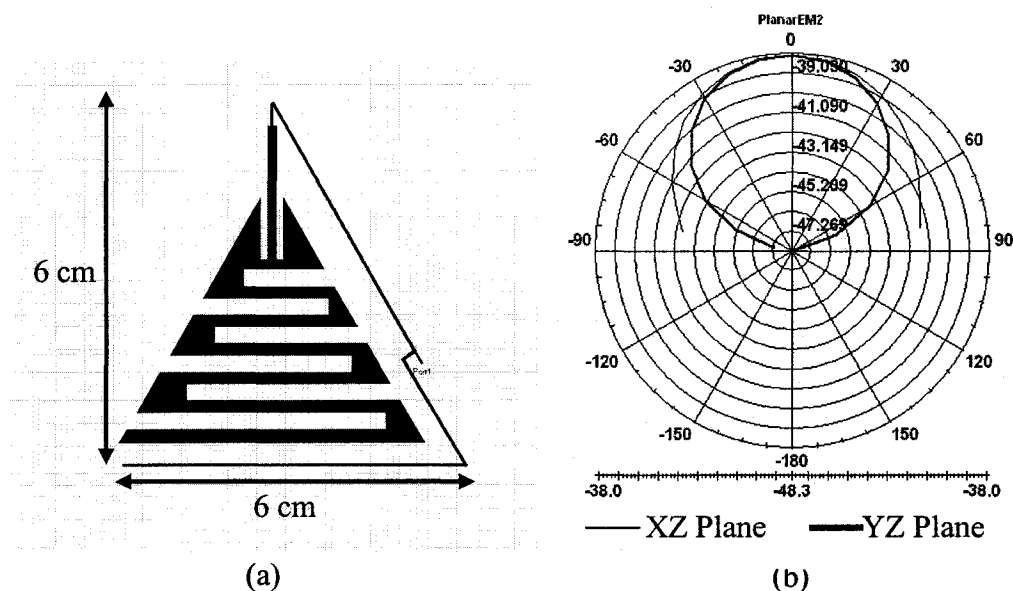


Fig. 2.37 (a) Simulation layout and (b) radiation pattern of tuned triangular patch antenna.

#### 2.3.4.3 Gain improvement

In order to develop the triangular patch antenna for commercial RFID applications, it was necessary to increase the gain of the antenna over 0 dB or over 2.15 dBi. Modification of the ground plane was employed to increase the gain of the triangular patch antenna. Ansoft Designer was used to perform this simulation. A rectangular slot is made in the ground plane of the triangular patch antenna. Slots in the ground plane were introduced according to the following criterion. The openings in the ground should lie directly below the antenna to enhance the effect of the ground slot on the radiation performance and thus contribute to the increase of antenna gain. The length and the width of the ground plane slot are defined as the parameter and a parametric sweep is run to obtain the required values of gain and VSWR. The relative position of the slot in the ground plane is given in Table 2.1.

Table 2.1 Calculated slot edge location values with respect to the corresponding triangular antenna's outermost edges.

Slot location	Distance away from the antenna
Top edge	-19.54 mm*
Bottom edge	16.08 mm
Left side edge	3.65 mm
Right side edge	3.87 mm

\* A negative value implies that the edge of the slot is into the antenna

The layout of the modified triangular patch antenna and the ground layout are shown in Fig. 2.38. After modification, the gain of the triangular patch antenna was found to be 3.35 dBi. The VSWR of the triangular patch antenna is 1.41 which satisfies the impedance matching requirement. The simulated VSWR and radiation patterns in the XZ and the YZ can be seen in Fig. 2.39.

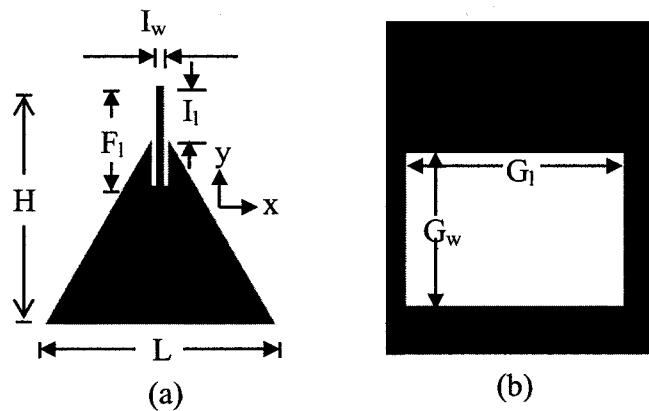


Fig. 2.38 (a) Patch and (b) Ground layouts of inset-fed triangular antenna with  $H= 5.54$  cm,  $L = 5.34$  cm,  $F_1= 2.33$  cm,  $I_w= 0.15$  cm,  $I_1= 1.07$  cm,  $G_1= 6.09$  cm,  $G_w= 5.19$  cm.

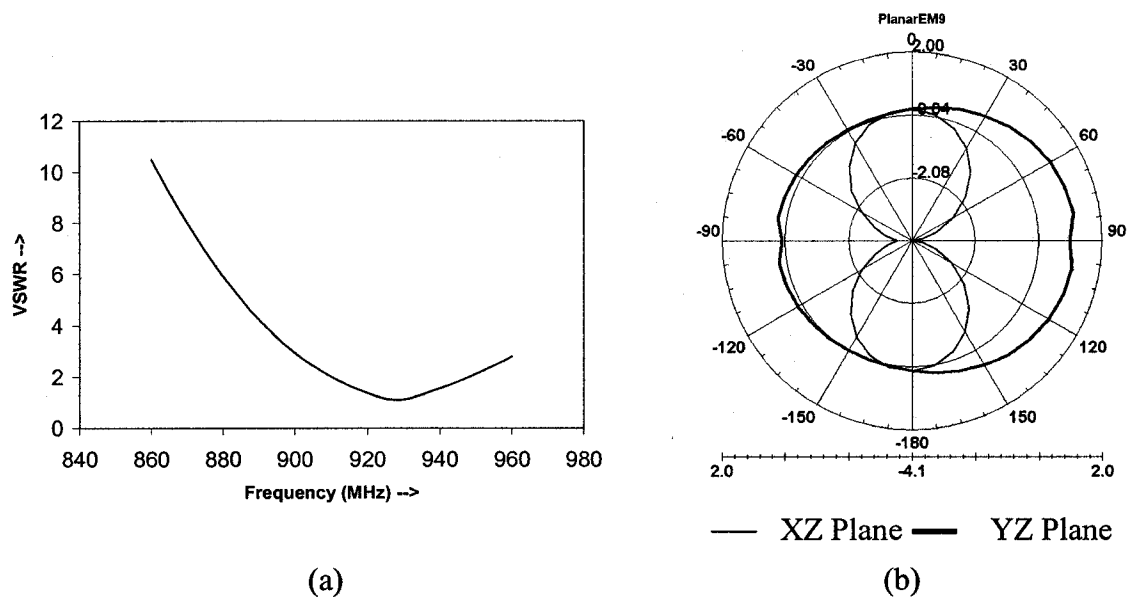


Fig. 2.39 (a) VSWR plot and (c) radiation pattern of triangular patch antenna.

### 2.3.5. Spiral Patch Antenna

The spiral antenna is considered to be a fast, leaky/traveling wave structure that radiates and receives a circularly polarized wave over a broad frequency range. The bandwidth is determined by a number of parameters, such as antenna size, geometry near the feeding port, feeding circuit, mounting configuration, etc. The spiral antenna can be studied in different configurations. One is the number of arms. It can be a single arm, double arm, or multiple arm spiral antenna. Another configuration is the layout. It could be in the form of a microstrip or a slot form. The prominent spiral antennas are the Archimedean, logarithmic and rectangular counterpart of the Archimedean spiral. The different parameters of the spiral antenna are (i) cavity diameter, (ii) cavity depth, (iii) spiral rate of growth (iv) dielectric base material, (v) conductor width and spacing, (vi) antenna feed and (vii) square versus round spiral [57]

The general accepted theory for operation of the spiral antenna is the “current band” theory [57], which indicates that the spiral radiates principally from a band on the

spiral surface where the currents in adjacent elements are most nearly in phase. From geometric analysis, we can see that the currents in adjacent conductors will reach an in-phase condition where the circumference of the ring is equal to one wavelength. Now, let us discuss how different parameters of a spiral antenna affect its performance:

(i) Cavity diameter: The cavity diameter should be chosen equal to the spiral diameter. A very small cavity diameter results in reduced gain, increased VSWR, and increased ellipticity ratio. Too large a cavity diameter results in pattern distortion due to higher order mode excitation of the cavity and/or the third radiating band.

(ii) Cavity depth: the gain gradually increases to a maximum at a spacing of  $\lambda/4$  and thereafter decreases to a minimum at a spacing of  $\lambda/2$ , corresponding to a split beam pattern with a null on-axis.

(iii) Spiral rate of growth: For an annular ring of given width and mean diameter equal to  $\lambda/\pi$ , the greater the number of turns, i.e. a small rate of growth, implies increased radiation of input power, less power available at the output turns, and hence a reduction of the axial ratio when the spiral is wound more tightly. The reduced axial ratio could also be attributed to the losses due to the increased electrical length. With respect to the effect of the spiral rate of growth on the gain, it was seen that the gain was not affected. Since more energy is associated with a tightly wound spiral, there is no corresponding decrease in gain with a decrease of axial ratio.

(iv) Dielectric base material: For a given aperture size and number of turns, lower axial ratios are obtained using materials having higher loss tangents. An increased loss tangent is generally associated with an increased dielectric constant due to which the phase velocity of the surface wave could be reduced, thereby effectively enlarging the electrical size of the antenna.

(v) Conductor width and spacing: The spirals are generally constructed so that the ratio of conductor width to conductor spacing is unity; i.e. the antenna is self-complementary. The input impedance of this class of antennas has been calculated to be about 180 ohms. As the antenna is generally fed from a 50-ohm line, a ratio other than unity would be more desirable.

(vi) Antenna Feed: If the feed radiates as a monopole, the far field pattern will consist of the feed radiation (linear polarization) and the spiral radiation (circular polarization); the resultant pattern will be elliptically polarized, asymmetrical with respect to the spiral axis, and with appreciable boresight errors. Improper excitation of the spiral antenna can give rise to pattern dissymmetry and pattern squint. Squint occurs if the feed lines themselves radiate or if the two-wire feed line is not balanced.

(vii) Square Vs Round Spiral: Square spirals exhibit a lag in the circular configuration when compared to the round spiral. This is due to the change in the continuous profile to the apparent discontinuities in the square configuration. Within the radiating band, the discontinuities are spaced near one-quarter wavelength apart so that the reflected components cancel.

The spiral patch antenna is developed first using the Ansoft HFSS simulation method and is then fine tuned for integration with the system (transmission line and circulator device) using Ansoft Designer.

#### **2.3.5.1 Design**

The widths of the spiral arm segments were varied to study the effect on the VSWR and the gain of the spiral antenna. The cases of uniform width, decreasing width, decrease-increase, increase-decrease and increasing width of the spiral arm were studied to obtain a design with good impedance match. Fig. 2.40 shows the simulation layout and

the VSWR plot for the 2 mm uniform width case. Fig. 2.41 shows the plots of the simulated radiation pattern. It was observed that “increase-decrease” and “increase” configurations had poor VSWR ( $<10$ ) with respect to other configurations. However, the gain performance was the same for all configurations. A parametric sweep of the widths of the spiral antenna, in the range of 0.04 cm to 0.3 cm for all the segments was run to obtain the least VSWR. The segments of the spiral antenna are numbered, as seen in Fig. 2.42.  $W_1$ ,  $W_2$ , etc. are the width of the first segment, second segment, etc.

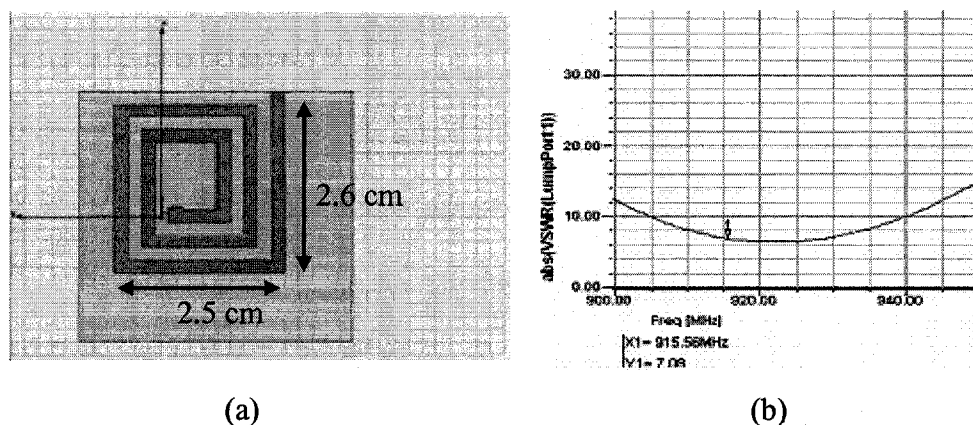


Fig. 2.40 (a) Simulation layout, (b) VSWR plot and (c) radiation pattern of uniform width spiral antenna.

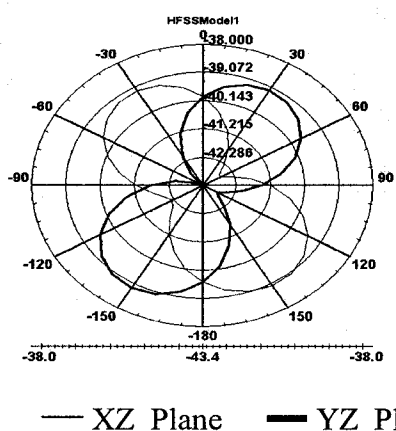


Fig. 2.41 Radiation pattern of uniform width spiral antenna.

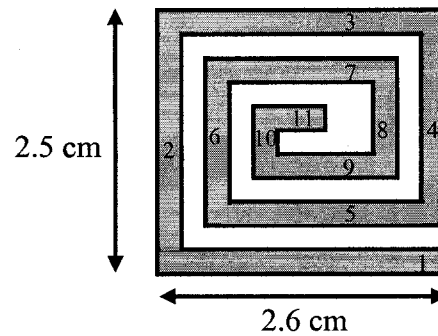


Fig. 2.42 Spiral arm of different segments.

The parametric sweep results, for the widths of all eleven segments of the spiral arm are tabulated in Table 2.2. Fig. 2.43 reveals the VSWR plot and the radiation pattern of the spiral antenna. The VSWR of the developed spiral antenna is found to be 1.25 and the radiation pattern was found to be bi-directional and slightly tilted to the left in the XZ-plane.

Table 2.2 Widths of the segments of the single arm spiral antenna.

Arm	Width (cm)	Arm	Width (cm)
W <sub>1</sub>	0.24	W <sub>7</sub>	0.22
W <sub>2</sub>	0.28	W <sub>8</sub>	0.2
W <sub>3</sub>	0.04	W <sub>9</sub>	0.24
W <sub>4</sub>	0.04	W <sub>10</sub>	0.28
W <sub>5</sub>	0.2	W <sub>11</sub>	0.2
W <sub>6</sub>	0.3		

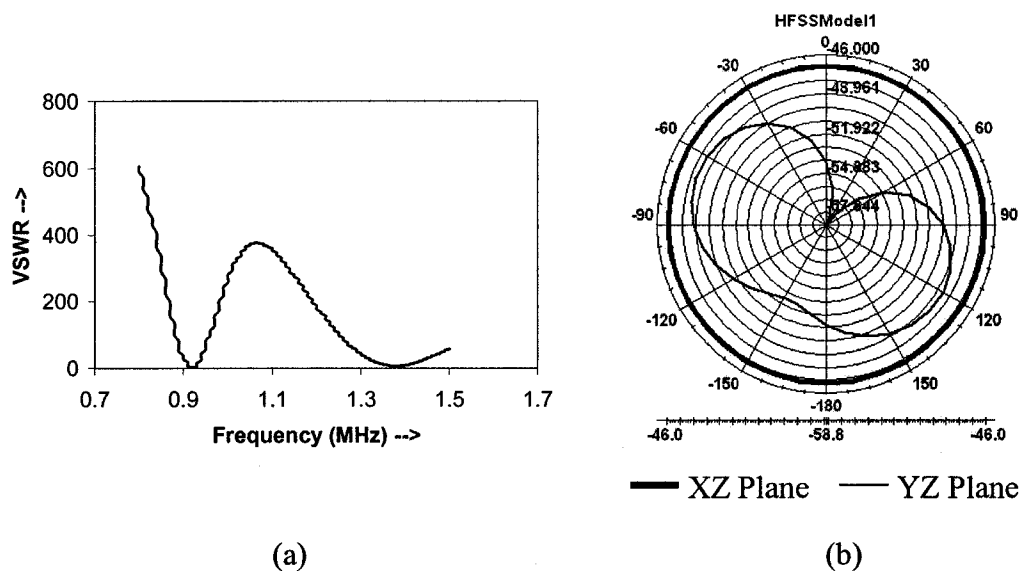


Fig. 2.43 (a) VSWR versus Frequency plot, and (b) radiation pattern of the spiral antenna.

### 2.3.5.2 Tuning

The layout of the spiral patch antenna generated using Ansoft Designer is then imported to the Ansoft Designer. On performing analysis of the antenna, imported from the HFSS, it was found that there was a slight increase of VSWR. The VSWR plot and plots of real and imaginary impedance is shown in Fig. 2.44.

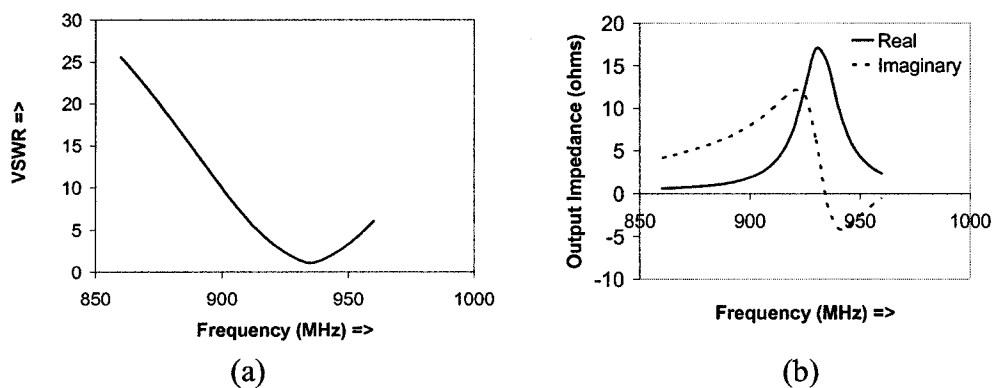


Fig. 2.44 (a) VSWR plot and (b) Real and imaginary impedance plots of the spiral patch antenna.

Using the tuning tool, the length of the stub and its location (the distance of the stub from the feed point) are determined. The length of the stub is found to be 83.17 cm and the distance of the stub from the feed point is found to be 60.23 cm. Upon adding the stub, the VSWR obtained was found to be 1.41 and the gain of the tuned spiral patch antenna was found to be about -45 dB, as seen in Fig. 2.45. Now, the spiral patch antenna is ready for integration with the system.

### **2.3.5.3 Gain improvement**

In order to develop the spiral patch antenna for commercial RFID applications, it was found necessary to increase the gain of the antenna over 0 dB or over 2.15 dBi. Two procedures have been followed to increase the gain of the spiral antenna. One is to increase the size of the spiral antenna and the other is a modification of the ground plane. Ansoft Designer was used to perform this simulation. The size of the spiral antenna was increased to 5.6 cm<sup>2</sup>. A parametric sweep of the widths of the spiral antenna, in the range of 0.1 cm to 0.8cm for all segments of the spiral antenna was run to obtain minimum VSWR. The number of segments considered for this larger spiral antenna is less than the earlier spiral antenna (Fig. 2.42). The segments of the spiral antenna are numbered, as seen in Fig. 2.46.  $W_1$ ,  $W_2$ , etc. are the width of the first segment, second segment, etc. The results of the parametric sweep of the widths of all nine segments of the spiral arm has given the values of the individual segments, which are tabulated in Table 2.3. The VSWR of the developed spiral antenna is found to be 1.23 and the gain was found to increase to -22 dB. The radiation pattern was found to be bi-directional and slightly tilted to the left. Fig. 2.47 reveals the VSWR plot and the radiation pattern of the higher gain spiral antenna.

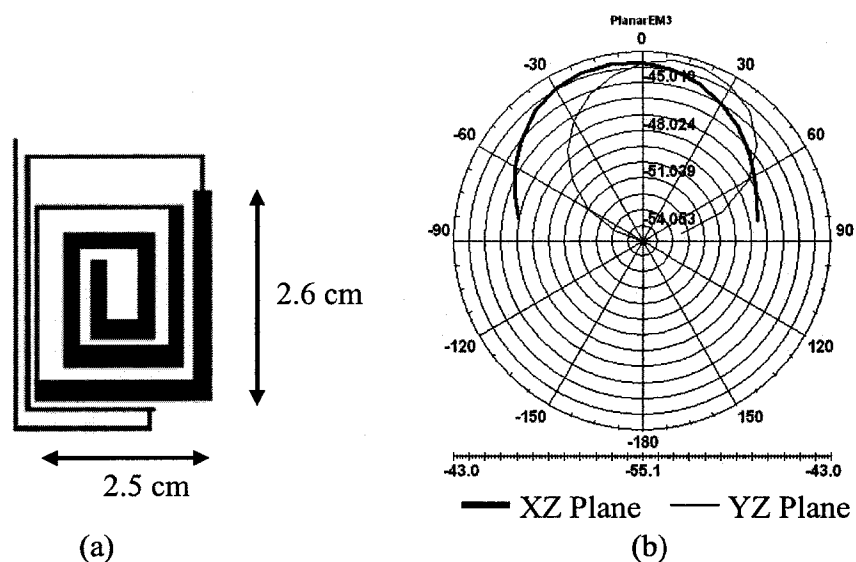


Fig. 2.45 (a) Layout and (b) gain of tuned spiral patch antenna.

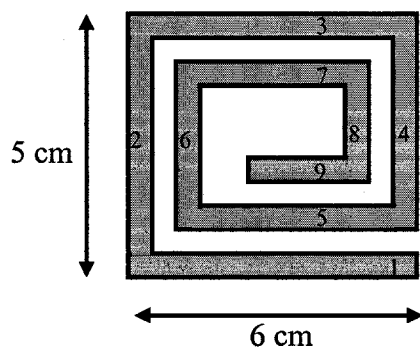


Fig. 2.46 Large spiral arm with different segments.

Table 2.3 Widths of the segments of the high gain single arm spiral antenna.

Arm	Width (cm)	Arm	Width (cm)
$W_1$	0.1	$W_6$	0.2
$W_2$	0.8	$W_7$	0.7
$W_3$	0.2	$W_8$	0.8
$W_4$	0.8	$W_9$	0.8
$W_5$	0.8		

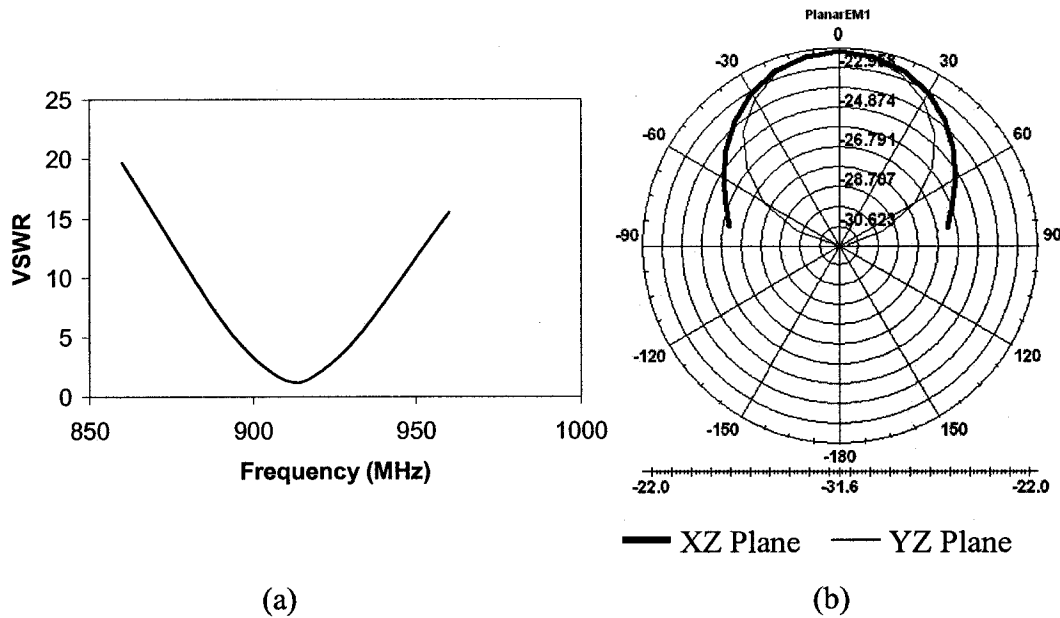


Fig. 2.47 (a) VSWR versus Frequency plot and (b) radiation pattern of the high-gain spiral antenna.

In order to further increase the gain of the spiral antenna, the ground plane was modified by introducing a slot. A rectangular slot is made in the ground plane of the triangular patch antenna. The length and the width of the ground plane slot are defined as parameters and a parametric sweep is run to obtain the required values of gain and VSWR. The relative position of the slot in the ground plane is tabulated in Table 2.4. The layout of the spiral patch antenna and the ground layout are shown in Fig. 2.48. The gain of the spiral patch antenna is found to be 0.05 dB and the VSWR is 1.87, which satisfies the impedance matching requirement. The simulation values of the radiation pattern in the XZ and YZ planes are shown in Fig. 2.49.

Table 2.4 Calculated slot edge location values with respect to the corresponding spiral antenna's outermost edges.

Slot location	Distance away from the antenna
Top edge	3 mm
Bottom edge	1 mm
Left side edge	2 mm
Right side edge	-1 mm*

\* A negative value implies that the edge of the slot is into the antenna

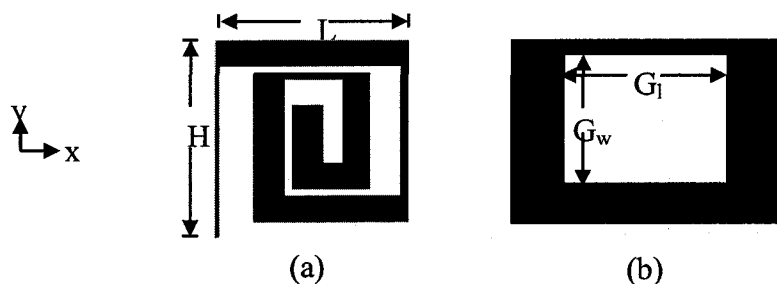


Fig. 2.48 (a) Patch and (b) ground layouts of the spiral antenna with the widths of the spiral arms (inward from outermost) 0.1 cm, 0.8 cm, 0.2 cm, 0.8 cm, 0.8 cm, 0.2 cm, 0.7 cm, 0.8 cm and 0.8 cm;  $H=6.0$  cm,  $L=5.0$  cm,  $G_1=5.4$  cm,  $G_w=5.7$  cm.

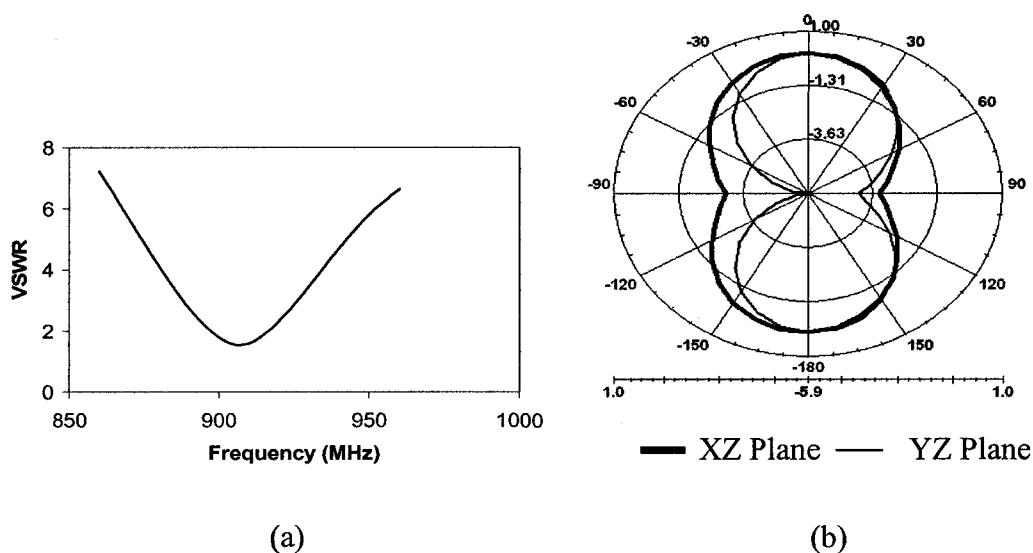


Fig. 2.49 (a) VSWR versus Frequency plot and, (b) radiation pattern plot of the spiral patch antenna.

### **2.3.6. Half-Sierpinski Fractal Antenna**

The word fractal means broken or irregular fragments, and was first coined by Mandelbrot [58] to describe a family of complex shapes that possess an inherent self-similarity of self-affinity in their geometrical structure. Fractals have been successfully used to model complex natural objects such as galaxies, cloud boundaries, mountain ranges, coastlines, snowflakes, trees, leaves and ferns, and much more. A wide variety of applications for fractals are found in many branches of science and engineering. Fractal electrodynamics is one such area, in which fractal geometry is combined with electromagnetic theory for the purpose of investigating a new class of radiation, propagation, and scattering problems [59]. One of the unique geometrical properties of fractal objects is the possibility to enclose, in a finite area, an infinitely long curve. The self-similarity property of fractals makes them especially suitable to design multi-frequency antennas. A few fractal shapes have complex, convoluted shapes that can enhance radiation when used as antennas [60]. For example, some fractal loops can be designed to enclose a finite surface with an arbitrarily large perimeter. A few monopoles can be designed to have an arbitrarily large length, although they can be constrained to fit a given volume. Hence, it is possible to design small antennas that occupy the same volume as their Euclidean counterparts.

An antenna becomes highly inefficient when the size of an antenna is made smaller than the operating wavelength. Its radiation resistance decreases and increases in the reactive energy stored in the neighborhood of the antenna. These two phenomena make small antennas difficult to match to the feeding circuit, and when matched, they display a high Q, i.e. a very narrow bandwidth. The fractal shapes were found to be more efficient. The advantages of the fractal antennas over their counterparts can be

summarized as follows: (i) compact size, (ii) low profile, (iii) conformal and (iv) multi-band or broadband [60].

One of the common fractal antennas is the Sierpinski gasket antenna. It is constructed as follows: Initially an equilateral triangle is contained in the plane, as seen in Stage 0 of Fig. 2.50. The next step in the construction process (see Stage 1 of Fig. 2.50) is to remove the central triangle with vertices that are located at the midpoints of the sides of the original triangle, as shown in Stage 0. Then, this process is repeated for the three remaining triangles, as illustrated in Stage 2 of Fig. 2.50. The next stage, Stage 3 is also shown in Fig. 2.50. Having an antenna engineering point of view, the black triangular areas represent a metallic conductor, whereas the white triangular areas represent regions where the metal has been removed.

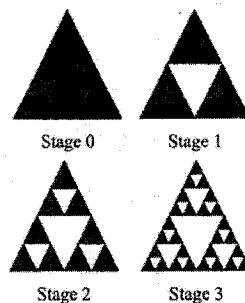


Fig. 2.50 Several stages in the construction of the sierpinski gasket-fractal.

When the Sierpinski gasket-fractal is split vertically into exactly two parts, we obtain the half-Sierpinski fractal antenna. Such a procedure is followed in order to decrease the size of the antenna and, at the same time, retain the multi-band properties of the Half-Sierpinski fractal antenna. The Half-Sierpinski patch antenna is developed first using the Ansoft HFSS simulation method and is then fine tuned for integration with the system (transmission line and circulator device) using Ansoft Designer.

### 2.3.6.1 Design

Simulation studies were performed to primarily obtain the smallest fractal for resonance at 915 MHz. The length of the Half-Sierpinski fractal antenna was gradually increased from 2.7 cm (Fig. 2.51) to 5.7 cm (Fig. 2.52) to obtain the resonant frequency of 915 MHz.

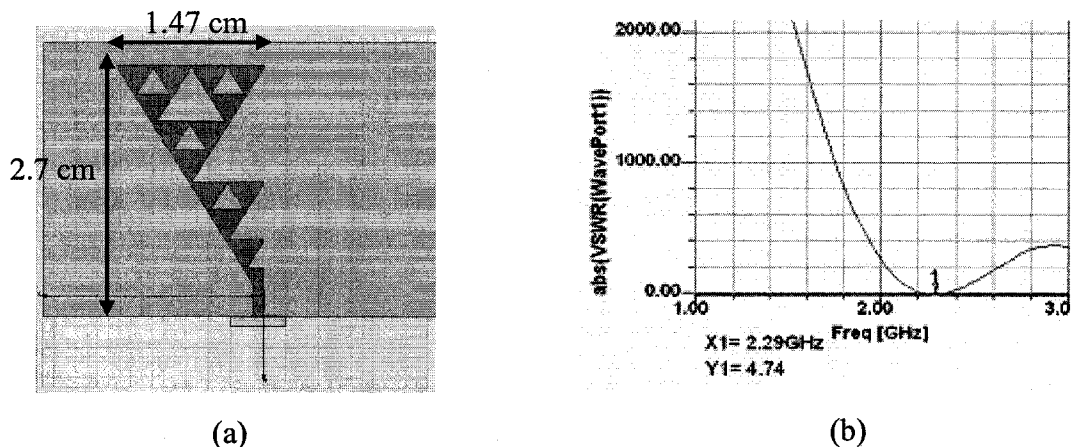


Fig. 2.51 Half-Sierpinski fractal (a) layout, and (b) VSWR versus Frequency plot.

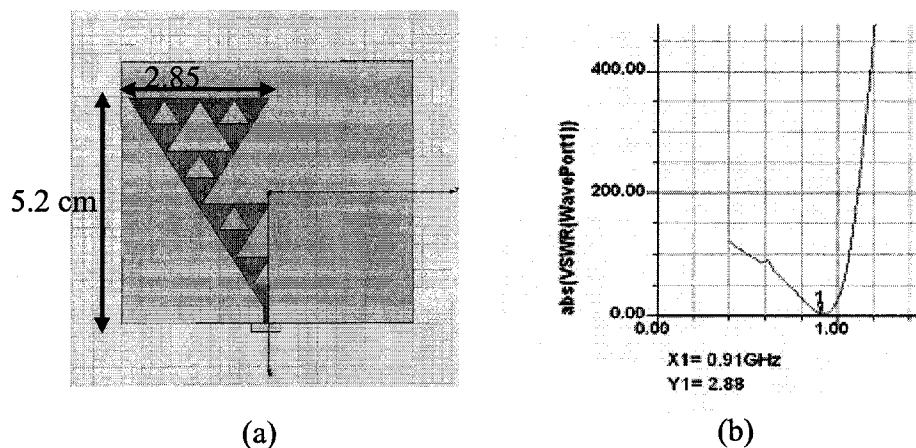


Fig. 2.52 Half-Sierpinski fractal (a) layout, and (b) VSWR versus Frequency plot.

At a broadside length of 5.2 cm, the resonant frequency of 915 MHz was obtained and the VSWR was 2.8. The width of the antenna feed was varied to improve the

matching to 50 ohms (Fig. 2.53). The feed width is divided into three partitions and their widths were varied individually to obtain the lowest VSWR and highest gain. The  $w_1$ ,  $w_2$  and  $w_3$  are the widths of section 1, section 2 and section 3, respectively. The width  $w_1$  is varied from 0.2 to 0.65 in steps of 0.05.  $w_2$  is varied from 0.2 to 0.5 in steps of 0.05.  $w_3$  is varied from 0.1 to 0.3 in steps of 0.05. The parametric analysis of the widths gives the output response for a fixed combination of the widths. The values of  $w_1$ ,  $w_2$  and  $w_3$  are found to be 0.25 cm, 0.35 cm and 0.15 cm. VSWR and gain are found to be 1.43 and -26 dB. Fig. 2.54 reveals the VSWR plot and the radiation pattern of the Half-Sierpinski fractal antenna.

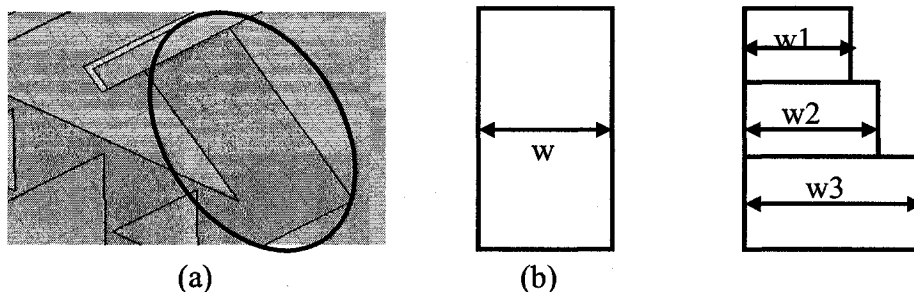


Fig. 2.53 Feed-width (a) simulation layout, and (b) cross-section having three partitions of widths,  $w_1 = 0.25$  cm,  $w_2 = 0.35$  cm, and  $w_3 = 0.15$  cm.

### 2.3.6.2 Tuning

The layout of the Half-Sierpinski patch antenna generated using Ansoft Designer is imported to the Ansoft Designer in which the antenna analysis is carried out. On performing analysis of the antenna design imported from the HFSS, it was found that there was a slight increase of VSWR, which can be seen in Fig. 2.55. The plots of real and imaginary impedance are shown in Fig. 2.55. Using the tuning tool, the length of the stub and its location (the distance of the stub from the feed point) is determined. The length of the stub is found to be 5.5 cm and the value of the distance of the stub from the

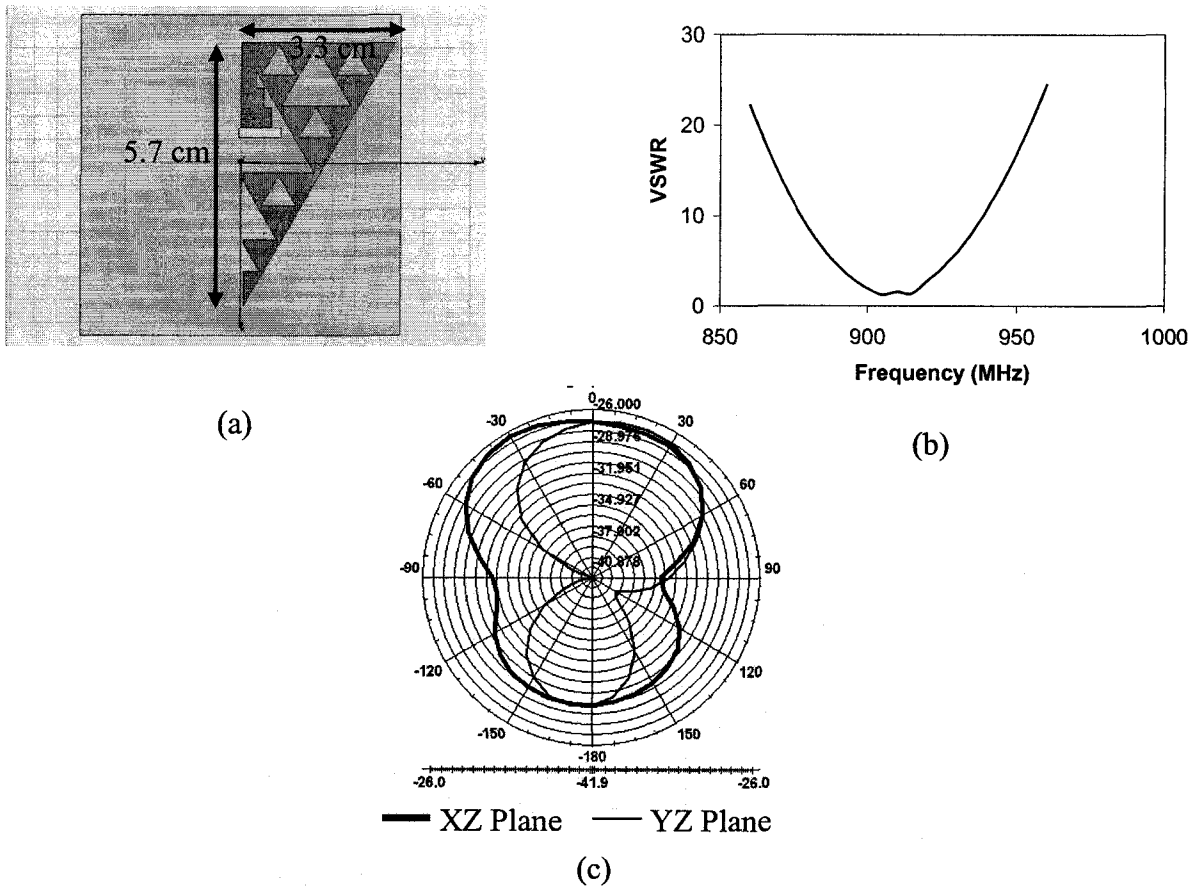


Fig. 2.54 (a) Simulation layout, (b) VSWR plot and (c) radiation pattern of the fractal antenna.

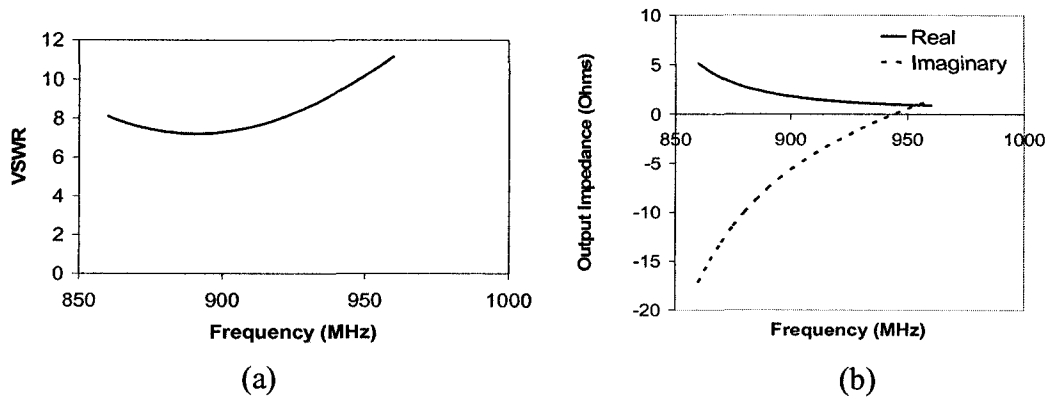


Fig. 2.55 (a) VSWR plot, (b) real and imaginary impedance plots of untuned Half-Sierpinski patch antenna.

feed point was about 0 cm, implying that the location is at the tip of the antenna feed. The shorting technique is used to decrease the length of the stub. After applying the shorting

technique, the length of the stub is found to be about 2 mm and located at the very tip of the feed-point. Upon adding the stub, the VSWR obtained was found to be 1.08. The real and imaginary impedance plots of the tuned Half-Sierpinski patch antenna are shown in Fig. 2.56. In Fig. 2.56, we see the gain of the tuned Half-Sierpinski patch antenna. Now, the Half-Sierpinski patch antenna is ready for integration with the system. In the frequency range of 0 to 4 GHz in Fig. 2.57, the VSWR plot of the Half-Sierpinski fractal antenna is found to resonate at the ISM band of 2.4 GHz, which implies that the Half-Sierpinski fractal antenna can be used for both 2.4 GHz and 915 MHz RFID technologies.

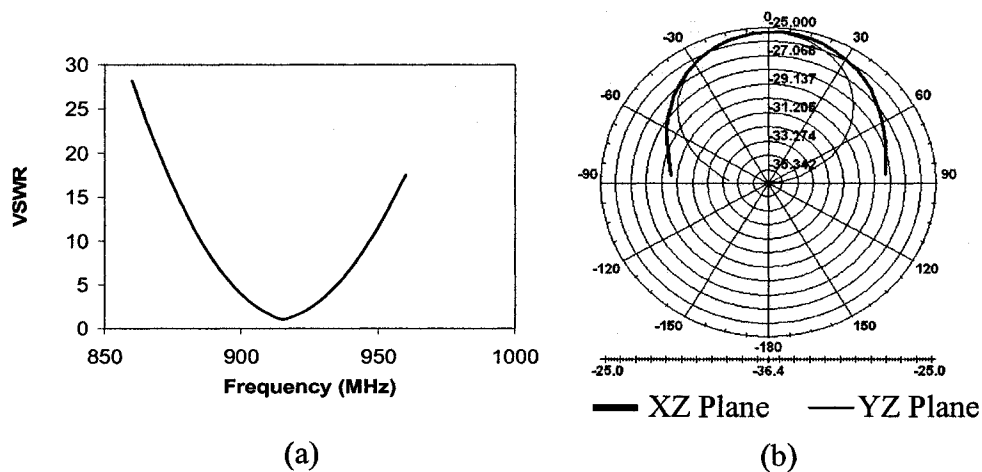


Fig. 2.56 (a) VSWR plot and (b) gain of tuned Half-sierpinski fractal patch antenna.

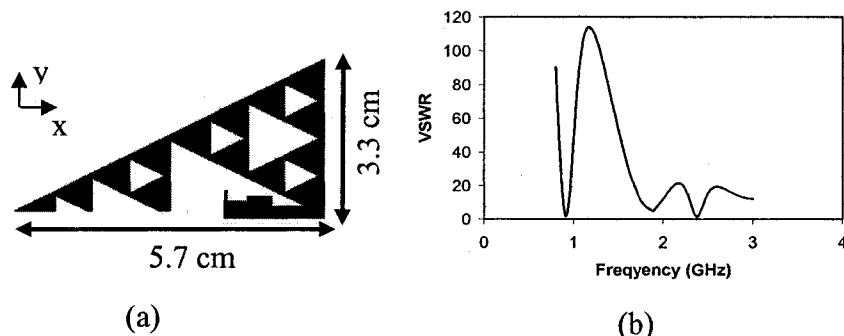


Fig. 2.57. (a) Layout and (b) VSWR versus frequency plot of tuned Half-Sierpinski fractal antenna.

### 2.3.6.3 Gain improvement

In order to develop the triangular patch antenna for commercial RFID applications, it was found necessary to increase the gain of the antenna over 0 dB or over 2.15 dBi. Modification of the ground plane was employed to increase the gain of the Half-Sierpinski patch antenna. Ansoft Designer was used to perform this simulation. Owing to the shape of the Half-Sierpinski fractal antenna and also to facilitate the grounding of the stub, a slot shape resembling the Half-Sierpinski fractal patch shape, instead of the regular rectangular slot, was chosen to be introduced in the ground. The gain of the antenna is increased by modifying the slot shape, such as the removal of the top inner copper triangle in the ground slot and modifying the shape of the slot below the antenna feed (Fig. 2.58). Introduction of the triangular slot is found to increase the gain of the half-Sierpinski antenna to -2.68 dB. The corners occupied by the slot in the ground plane perfectly align with the corners of the overlying Half-Sierpinski fractal antenna.

Fig. 2.58 shows the layout of the half-Sierpinski patch and the ground layer. The simulation results of the radiation pattern in the XZ and the YZ are shown in Fig. 2.59.

Table 2.5 gives the summary of the different design modifications that were utilized and had an effect on the antenna characteristics.

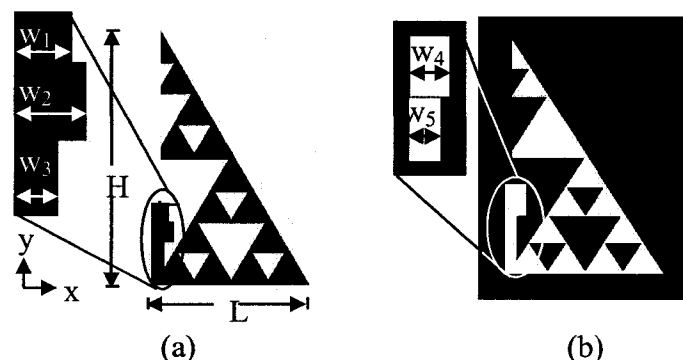


Fig. 2.58. (a) Patch and (b) ground layouts of Half-Sierpinski fractal antenna with  $H= 5.7$  cm,  $L= 3.3$  cm,  $w_1= 0.25$  cm,  $w_2= 0.35$  cm,  $w_3= 0.15$  cm,  $w_4= 0.35$  cm,  $w_5= 0.15$  cm.

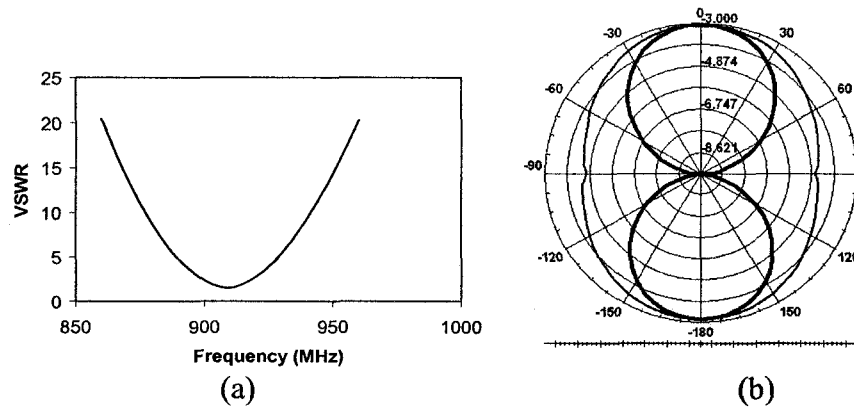


Fig. 2.59 (a) VSWR plot, and (b) and radiation pattern plot of the Half-Sierpinski fractal antenna.

Table 2.5 The Seven S Microstrip Antenna Design tool.

	Gain	VSWR	Bandwidth	Radiation pattern
Size	✓	✗	✗	✗
Shape	✗	✗	✓	✓
Slot	✗	✓	✓	✓
Slit	✗	✓	✓	✓
Stub	✗	✓	✗	✗
Skew	✓	✓	✗	✓
Short	✓	✓	✗	✓

✓ --- Employed for varying.

✗ --- Not-employed for varying.

## 2.4 Comparison of Antennas

All the designed antennas, namely the inset-fed triangular patch antenna, the spiral antenna and the half-Sierpinski fractal antenna, have a resonant frequency at 915 MHz. However, their behavior varies from each other at other frequencies, especially at higher than 1 GHz frequency. The VSWR plots of the three antennas can be seen in Fig. 2.60. It is seen that the triangular patch antenna has no resonances in the frequency range from 1 -10 GHz. The spiral antenna has a wide-band characteristic beyond 8 GHz and the fractal antenna has multiple resonances occurring in the 1-10 GHz frequency range.

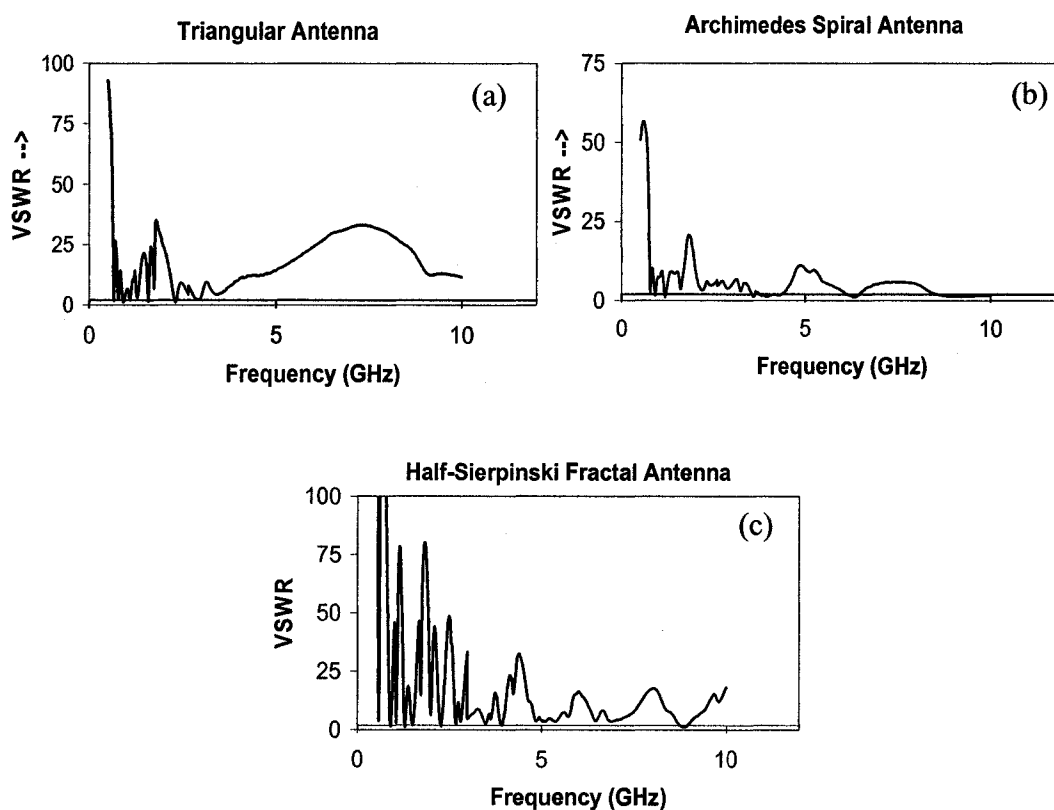


Fig. 2.60 VSWR versus frequency plots of (a) triangular, (b) spiral and (c) fractal antennas.

Table 2.6 summarizes the physical and electrical parameters of the designed antennas and the antennas that have already been designed by others [57-60]. All the designed antennas are found to be small and compact and also having desirable characteristics. It can be seen that omni-directionality, which is the desired characteristic of RFID antennas, is displayed by all the developed antennas. The VSWR of all the antennas developed is less than two, and being smaller and more compact than the other antennas, these antennas have a band-width and gain comparable to the other antennas.

Table 2.6 Comparison of the triangular, spiral and fractal antennas with other antennas (italicized).

Antenna	Size (cm <sup>2</sup> )	Gain (dBi)	VSWR	Bandwidth	Radiation pattern
<i>Meander tag 1 [61]</i>	<i>9.6 x 1.4</i>	<i>1.5</i>			<i>Omni-directional</i>
<i>Meander tag 2 [10]</i>	<i>8x 1.72</i>		<i>1.5</i>	<i>100 MHz</i>	
<i>Square patch (non-flexible) [17]</i>	<i>7 x 7</i>	<i>2.33</i>	<i>&lt;2</i>	<i>30 MHz</i>	
<i>PIFA (non-flexible)[62]</i>	<i>10 x 8</i>	<i>2.5</i>	<i>2</i>	<i>20 MHz</i>	<i>Bi-directional</i>
Triangular	5.6 x 5.6	3.35	1.6	32 MHz	Omni-directional
Spiral	5.6 x 5.6	2.2	1.3	18 MHz	Omni-directional
Fractal	3.2 x 5.5	-0.64	1.75	13 MHz	Omni-directional & Near Omni-directional

## CHAPTER 3

### FABRICATION AND CHARACTERIZATION

The triangular, spiral and fractal antenna designs having the highest gain and a VSWR less than two have been chosen for fabrication and subsequent characterization. During the fabrication process, it was necessary to obtain copper patterns free of any discontinuities or scratches in order to realize antennas exhibiting the desired resonance (i.e. at a frequency of 915 MHz). It was also observed that the alignment of the copper patterns with respect to the bottom ground slot is critical for achieving the expected performance of the antenna.

#### **3.1 Fabrication of Antennas**

The final versions of the triangular, spiral and fractal antennas with the highest gains are considered for fabrication (Figs. 2.38, 2.48 and 2.58 of the previous chapter). Since all the antennas are designed in simulation with an infinite ground plane, the size of the ground plane is taken to be more than six times the substrate thickness ( $177 \mu\text{m}$ ) in all directions (with respect to the patch dimensions, in order to reduce the effect of the finite ground plane) [63]. Two procedures have been considered for the fabrication of the antennas. The first one is the conventional procedure that includes photolithography and the second is a low-cost patterning method using a desk-top printer and a low-cost

electroless copper deposition method. The fabrication of the antennas using these two procedures is discussed below.

### **3.1.1 Photolithographic Method**

The photolithographic method involves basically two steps, namely the preparation of the mask for the lithography process and the lithography process itself in order to fabricate the copper pattern representing the antenna on the substrate.

#### **3.1.1.1 Mask preparation**

The Ansoft Designer has an import feature by which the layout of the antenna can be converted into a required file format. After selecting the layout for import of the file as a “drawing interchange format (dxf)” file, an option is given as to what layers are to be transported. Only the signal layer, which constitutes the pattern of the antenna is selected for transport. The final layout of the antenna in the Ansoft Designer is then converted into a dxf format. The dxf file is then converted into a post-script file using LinkCad software. The “postscript (ps)” file is then converted into a “portable document format (pdf)” file using a ps to pdf converter available online. The same procedure is to be followed for transferring the ground pattern. It is to be remembered, that in the Ansoft Designer, the visible object in the ground layer is indeed a slot and a negative image of the slot is to be created using Boolean subtraction between the slot and an 8 cm<sup>2</sup> square patch. Alignment marks are placed on the antenna and ground images far away from the patterns in order to align both the antenna and the ground layer masks above and below the polyimide sheet in the subsequent fabrication step. The pdf file for the layouts of the antenna and the ground layers is then fed into a mask making instrument. The mask of the antenna and the ground layers is then prepared using the Linotronix mask-maker

instrument. Now we have a positive mask with the emulsion coating containing the antenna pattern.

### 3.1.1.2 Lithography process

The substrate employed is a Kapton polyimide dielectric substrate, sandwiched between thin layers of adhesive (for the promotion of adhesion between the dielectric and copper films) and copper which is obtained from Pyralux Inc. (Fig. 3.1).

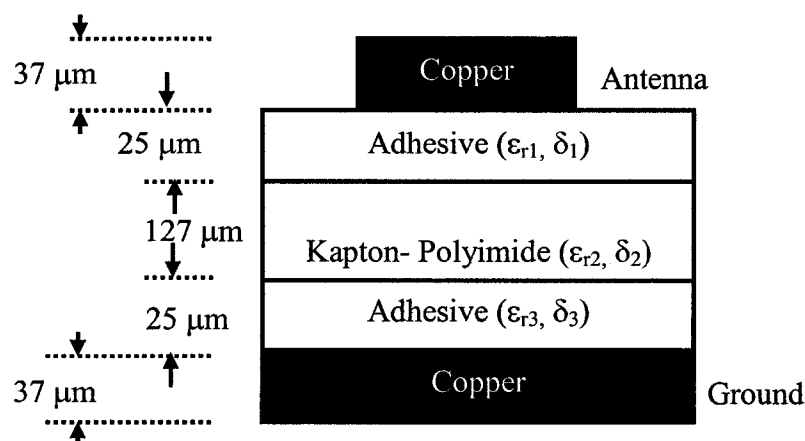


Fig. 3.1 Cross-section of the antenna substrate with  $\epsilon_{r1} = \epsilon_{r3} = 3.3$ ,  $\epsilon_{r2} = 3.5$ ;  $\delta_1 = \delta_3 = 0.027$ ,  $\delta_2 = 0.008$ .

An 8 cm<sup>2</sup> area of flexible polyimide sheet is cut from a large sheet without bending the sheet on the sides. Such care must be taken so that the mask, when placed on the substrate for contact lithography, would not have any air gaps in between the mask and substrate. The lithography process involves the following procedures:

(i) Cleaning of the substrate: The substrate is rinsed with acetone and de-ionized (DI) water to remove any impurities or dust-particles present on the substrate. The cleaned substrate is then placed on a hot-plate at 100 °C for 2 minutes to dry the samples.

- (ii) Coating with photo-resist: The cleaned substrate is then placed on a photoresist spinner. The photo-resist used is PR 1813. Care is taken to avoid any air-bubble formation during coating.
- (iii) Soft-bake: The coated substrate is then soft-baked for 2 minutes at 100 °C. The soft-bake step removes any moisture present in the photo-resist and makes it non-sticky.
- (iv) Exposure: The soft- baked substrate is then placed above the UV light. Care is taken so that the emulsion side of the mask is in full contact with the copper surface so that scattering of the UV-light is minimized and the line-width of the copper line is efficiently transferred from the mask.
- (v) Develop: The exposed resist is then placed in a MF-321 developer solution for 2 minutes until the exposed photo-resist is removed from the substrate. The unexposed photo-resist masking the antenna is left behind. The substrate is then rinsed with D.I. Water. Care is taken to ensure that all the exposed photo-resist is removed. This can be done either by visual examination based on technical experience or by checking for electrical continuity on the copper surface which should show  $\sim 0$  ohms, if all the exposed resist is removed.
- (vi) Hard-bake: The developed substrate is then placed on a hot-plate for 20 min at 100 °C to harden the photo-resist. The substrate is now ready for etching of the exposed copper with the antenna-patterned copper being protected by the hardened resist.
- (vii) Copper etching: The baked substrate is then placed in a ferric chloride solution which etches the copper. It takes approximately 20 minutes for the copper to be etched in a fresh ferric chloride solution. Ferric chloride being reactive with metal, care is to be taken to etch the substrate in a plastic container.

### **3.1.2 Low Cost Patterning Method**

A low cost patterning method was seriously considered for developing antennas. The patterning method is termed low-cost since it avoids the use of costly equipment such as the mask-making instrument, spinner and exposure tools. This patterning method involves two steps, namely the preparation of the mask and the patterning method itself.

#### **3.1.2.1 Mask preparation**

For the low cost patterning method, a negative mask is to be created. This can be done by employing the Boolean subtraction tool available in the Ansoft designer and creating the required negative pattern of the image by creating a 8 cm<sup>2</sup> square patch and subtracting the antenna pattern from it. Since the ground-plane is already in the negative-image, it can be directly transported. Alignment marks are placed on the antenna side and ground side, far away from the patterns in order to align both the mask above and below the polyimide sheet in the subsequent fabrication step. The import feature in Ansoft Designer is used to convert the layout of the antenna into the required file format. After selecting the layout for import of the file as a “graphic design system (gds)” file, and selecting the signal layer for transport, the final layout of the antenna in the Ansoft Designer is converted into a gds format. The gds file is then converted into a ps file using LinkCad software. The ps file is then converted into a pdf file using a ps to pdf converter available online. A negative pdf mask pattern is then ready for transfer onto the polyimide sheet.

#### **3.1.2.2 Patterning method**

The patterning of copper on the polyimide sheet involves the following steps:

- (i) Surface modification of the polyimide sheet [64]: The polyimide sheet is roughened mechanically using a dry cloth. Mechanical roughening initially helps to increase the

surface roughness, and therefore, increases the number of activation sites in order to enhance the deposition. This is followed by a sonication step in isopropyl alcohol. Adhesion of copper to the polyimide substrate can be increased by electroless deposition of a seed layer of copper on the polyimide substrate, heating at 400°C for 30 seconds, etching the copper away using HNO<sub>3</sub> and using the substrate for the final deposition of copper.

(ii) Pattern transfer: The surface treated standard size A4 polyimide sheet is then fed into a laser printer and the negative images of the antenna and the ground layers are printed on the polyimide sheet. The polyimide sheet employed for patterning and the cross-section of the toner-patterned polyimide is illustrated in Fig. 3.2.

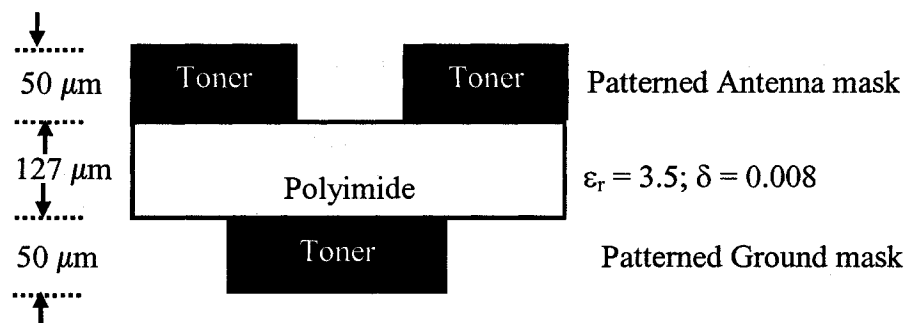


Fig. 3.2 Cross-section of the printed polyimide.

(iii) Activation and acceleration: The substrate is activated by immersing the sample in a solution of palladium chloride. After activation, the metallic palladium on the surface is surrounded by the hydrolyzed stannous hydroxide. The excess of stannous hydroxide is removed before the palladium can act as a catalyst. The accelerator solution consists of an organic or mineral acid which removes the excess tin from the part while leaving the palladium sites intact for the deposition of the electroless copper. Care should be taken that the calculated time for immersion is maintained to avoid skip-plating.

(iv) Electroless Copper Deposition: The activated polyimide sample is then placed in the electroless copper bath solution. Two electroless copper plating procedures have been considered, one for a thin (200nm) Cu deposit and the other for a thick ( $2\mu\text{m}$ ) Cu deposit. The compositions of these solutions and the operating temperatures are given in Table 3.1.

Though the low-cost patterning method has an advantage over the photolithography process in that it is a low-cost method and the fabrication procedure is simple, one of the main drawbacks is its instability. The films obtained through this process still have problems with surface-adhesion, and the cracking and trapping of air under the copper film resulting in a discontinuous layer. Moreover, the copper films were subject to rapid oxidation, if not protected by a surface coat of polyimide or epoxy. The thickness of the coated epoxy is also uncontrollable and would very much affect the resonant properties of the antenna, even if the antennas were designed for a definite amount of polyimide or epoxy thickness. All these factors have led to the use of the photo-lithography process to create tags that would sustain the fabrication effects. However, the low-cost patterning method is favored for the fabrication of RFID tags since the cost of the tag for commercial purposes should be only a few cents.

Table 3.1. Solution composition for low-build and high-build copper.

Low build copper-bath Operating Temperature = 50 <sup>0</sup> -55 <sup>0</sup> C	High-build copper-bath Operating Temperature = 36 <sup>0</sup> -38 <sup>0</sup> C
1000 ml Water	800 ml water
3g CuSO <sub>4</sub>	100 ml- Cuprothick 84 F
8g EDTA	40 ml- Cuprothick 84A
2-3ml of HCHO	30ml- Cuprothick 84 B
NaOH (till pH attained is 12.5 to 12.6)	30ml – Cuprothick Alkaline additive
100 mg – 2,2 di pyridyl	
0.05 ml Triton	

### 3.2. Characterization of Antennas

The fabricated antennas are characterized with respect to their impedance matching and gain values. Fig. 3.3 shows the optical images of the three antennas fabricated on a polyimide flexible substrate with the corresponding inset of the ground plane. The fabricated antennas are measured for their VSWR and radiation performance.

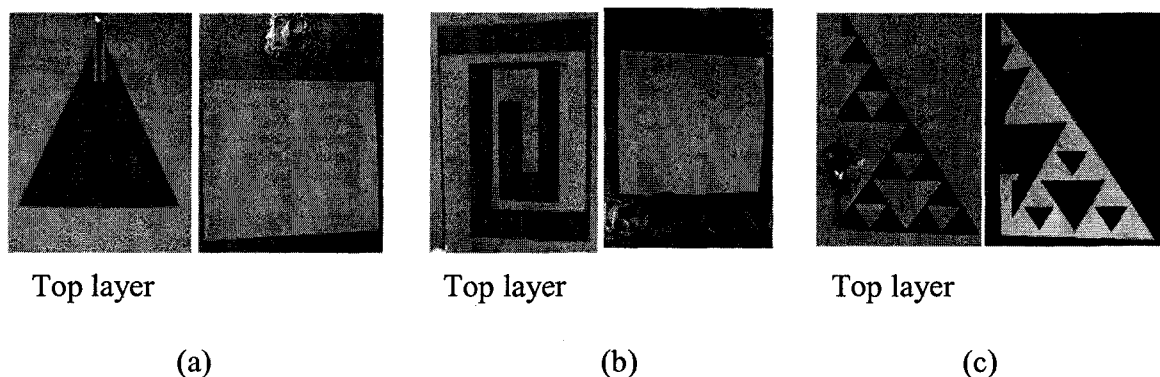


Fig. 3.3 Optical images of the top and ground layers of (a) triangular antenna (b) spiral antenna and (c) half-Sierpinski fractal antenna.

### **3.2.1. VSWR measurement**

The antennas are measured for their VSWR value using the Agilent 4396B Network Analyzer. Fig. 3.4 shows a picture of the Network Analyzer used for the measurement of the impedance of the antennas.

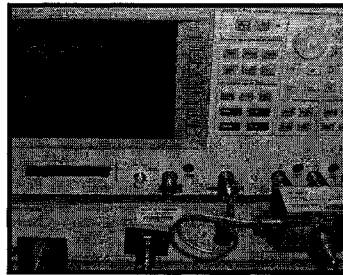


Fig. 3.4 Network Analyzer employed for measurement of antenna VSWR.

The measurement of the VSWR includes the following steps:

#### **3.2.1.1 Sample preparation**

Proper connection is to be provided to the antenna for measurement of the impedance. Since the calibration tool-kit employed is a SMA (Surface-Mount Adapter) type, an SMA connector is to be soldered to the feed of the antenna. The ground of the SMA is to be soldered to the ground of the antenna and the centre conductor to the microstrip feed. Care is to be taken to ensure a good connection is established between the microstrip copper and the SMA legs to prevent any unwanted parasitics.

#### **3.2.1.2 Network analyzer calibration**

The network analyzer has to be calibrated for making very accurate VSWR measurement. The standards used for calibration are to be employed. A 85033E 3.5mm test set is employed for calibration. The steps for calibration are as follows:

- (i) The machine is turned On after connecting the Test Set for reflection measurements.

- (ii) The measurement type “Network Analyzer” is selected and the mode A/R is selected.
- (iii) The Frequency sweep is selected by giving the start and the stop frequencies. The marker frequency, or the solution frequency, can be entered so that the cursor points to this specific frequency and the return loss, or the VSWR value, is displayed on the screen. Once the sweep is set-up, it should not be changed until the measurement is over. If the sweep is changed, the calibration procedure must be repeated again.
- (iv) The calibration button is then pressed. Now the device is ready to read the impedance values for open, short and load calibration standards.
- (v) First, the open standard is connected to the SMA end and the open button is pressed. This is followed by calibration using the short and the load standards. After completion of all the standards, “DONE” is pressed. Now the device is ready for measurement.

### **3.2.1.3 Measurement procedure**

The measure button is pressed to switch the device from the calibration to the measure mode. The sample with the SMA connector attached to it, is now connected to the SMA-end. Care should be taken that the SMA connector end at the Network Analyzer and the SMA connector attached to the antenna are of opposite polarity. After connecting the antenna, the VSWR-plot or the Return-Loss plot is readily displayed. By selecting the mode, the type of plot (VSWR-plot or Return-Loss plot) can be selected. The plot can then be saved as a “tagged image file format (tiff)” picture file or the solution data can be exported into a removable storage device, such as a floppy.

### 3.2.1.4 Results and discussion

The VSWR plot of the triangular, spiral and the half-Sierpinski fractal patch antennas can be viewed in Fig. 3.5. The VSWR plots of the three antennas were found to show that the VSWR value was less than 2 at 915 MHz (Fig. 3.5). The -10 dB bandwidth was found to be the least (13 MHz) for the Half-Sierpinski fractal antenna and the maximum (32 MHz) for the triangular antenna. The -10 dB bandwidth for the spiral antenna is 18 MHz. Higher bandwidth implies a greater ability to withstand fabrication anomalies and better performance under adverse operating conditions. The experimental results were found to match the simulation results for these antennas (Fig. 3.6.)

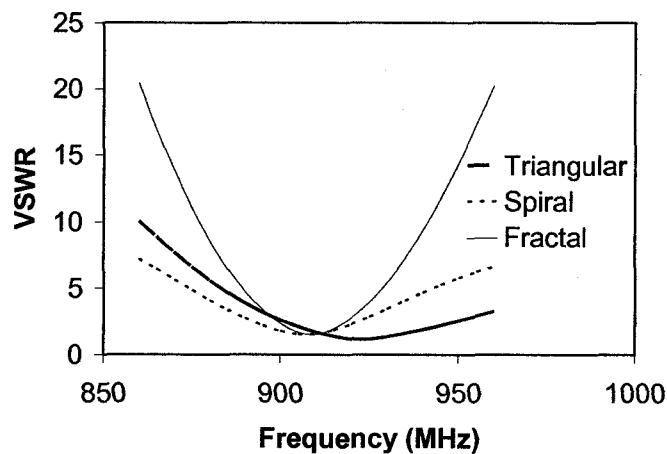


Fig. 3.5 VSWR versus Frequency plot for three different antennas.

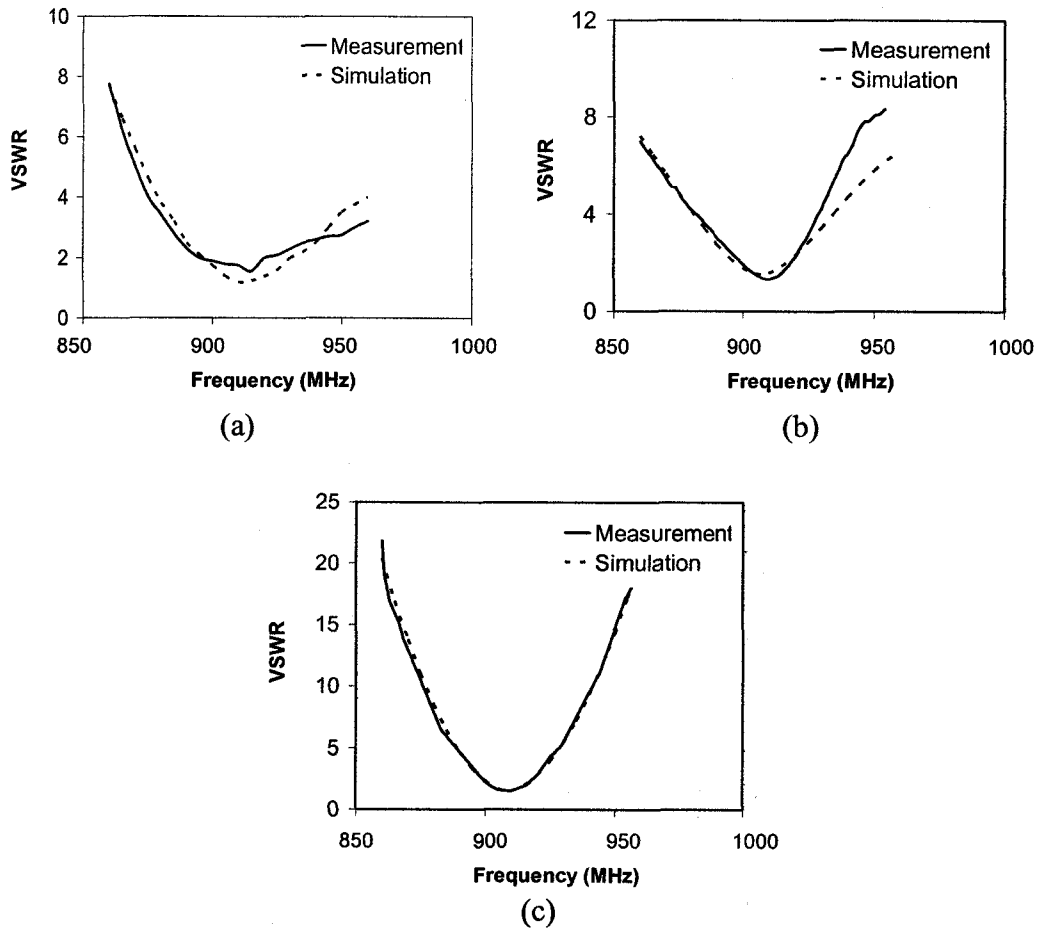


Fig. 3.6. Simulation and experimental VSWR plots of (a) triangular (b) spiral and (c) Half-Sierpinski fractal antennas.

### **3.2.2 Radiation Pattern Measurement**

The measurement of the radiation pattern, or the gain of the antenna, includes the following steps:

#### **3.2.2.1 Sample preparation**

The samples prepared for the VSWR measurement can be used to measure the radiation pattern of the antenna.

### 3.2.2.2 Experimental set-up

The radiation pattern of the antenna is to be ideally measured in an anechoic chamber that prevents any reflections from the ground or the surrounding walls. The measurement can also be made in open-air or a large room such as an auditorium, to minimize the effect of the reflections from the walls. A gymnasium was chosen whose walls were more than 30 feet away from the centre of the setup. Fig. 3.7 shows the picture of the test-site. Fig. 3.8 shows the transmitting and receiving junctions set-up at the test site.

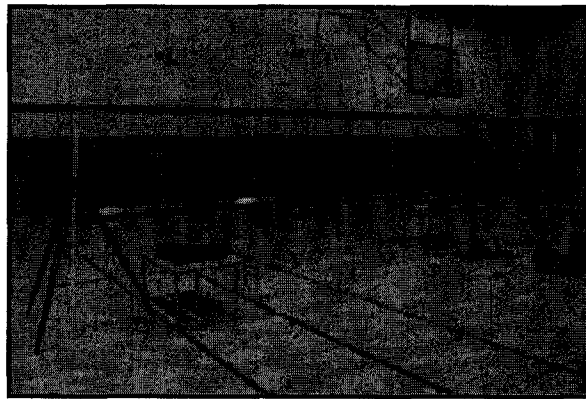
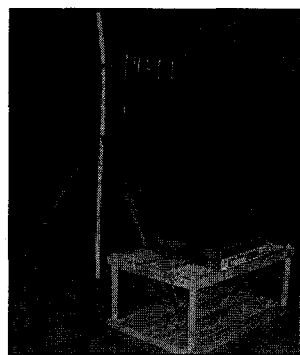
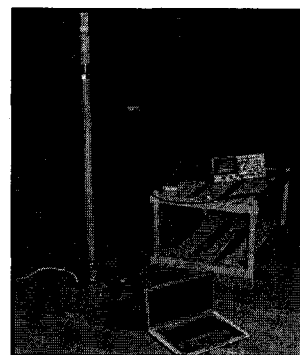


Fig. 3.7 Test site for antenna radiation pattern measurement.



(a)



(b)

Fig. 3.8 (a) Transmitting and (b) receiving junctions.

The transmitting and the receiving junctions are separated by a distance of 13 feet. At the transmitting junction we have a signal generator connected to a 915 MHz highly-directional Yagi antenna of gain 8.5 dBi. The Yagi antenna, as can be seen in Fig. 3.8 (a), is fixed to a mast more than 6 feet away from the ground to prevent reflection from the ground. At the receiving junction, we have a spectrum analyzer connected to the antenna that is to be tested, as seen in Fig 3.8 (b). The antenna that is to be measured for its radiation pattern is fixed on a card-board mast placed on a rotator. The rotator is moved in a clock-wise direction in steps of 11.25 degrees. The antenna is rotated through an entire 360 degrees with readings taken at every step of 11.25 degrees. The power output at the signal generator is chosen in such a way that the power captured by a test yagi antenna placed at the walls of the gymnasium is of the order of -55 dBm (or no signal at all). The power output selected in this way is -7 dBm.

### **3.2.2.3 Results and discussion**

The data points obtained from these experiments are then plotted using Microsoft Excel software to obtain the experimental radiation pattern measurements. Figs. 3.9-3.11 shows the experimental and the simulation plots of the antennas considered. The experimental results obtained closely match the simulation results. The radiation pattern of the triangular antenna (Fig. 3.9) was found to be omni-directional in the YZ-plane and near omni-directional in the XZ-plane. The highest gain of 3.35 dBi was observed for the triangular antenna in the YZ-plane. The spiral antenna was found to exhibit near omni-directionality in both the XZ and the YZ planes (Fig. 3.10). The highest gain observed for spiral antenna was about 2.2 dBi in both the XZ and the YZ planes. The Half-Sierpinski fractal antenna was found to be omni-directional in the YZ-plane and near omni-directional in the XZ plane (Fig. 3.11). The difference between the maximum and

minimum gain in the XZ-plane was 8 dB and that in the YZ-plane was only 2 dB. The maximum gain that was exhibited by the Half-Sierpinski fractal antenna was about 0 dBi in both the XZ and the YZ-planes.

It was observed that the radiation patterns in the YZ plane of the triangular antenna (variation of 1 dB over  $\theta = 0$  to  $360^\circ$ ) and in the YZ plane of the Half-Sierpinski fractal antenna (variation of 2 dB over  $\theta = 0$  to  $360^\circ$ ) are more omni directional compared to the radiation patterns in the XZ planes of the respective antennas. This could be

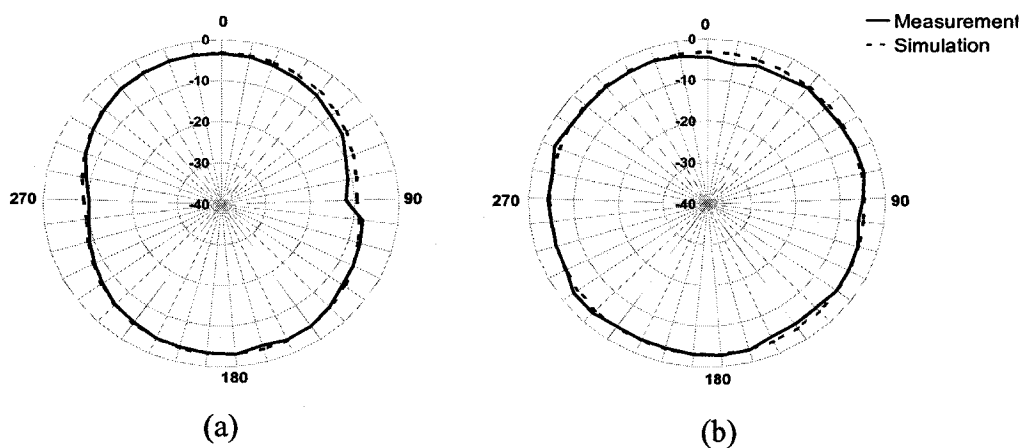


Fig. 3.9 Radiation plots of triangular antenna in (a) XZ-plane and (b) YZ-plane.

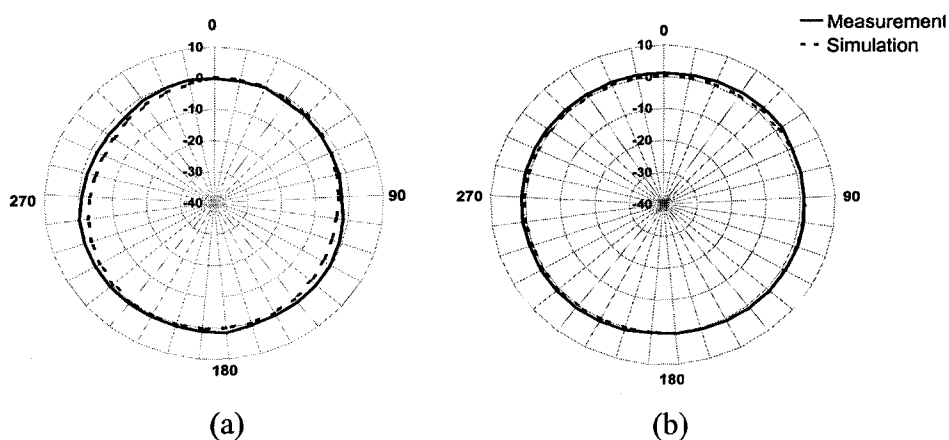


Fig. 3.10 Radiation plots of spiral antenna in (a) XZ-plane and (b) YZ-plane.

attributed to the reduced directionality of the flow of current in these antennas, in contrast to the circular directional flow of current in the spiral antenna (variation of 4 dB in the XZ plane and 6 dB in the YZ plane).

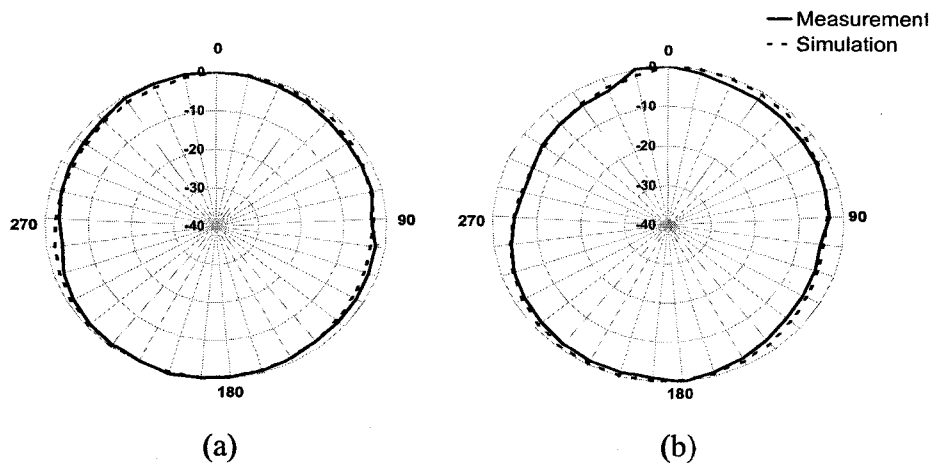


Fig. 3.11 Radiation plots of Half-Sierpinski fractal antenna in (a) XZ-plane and (b) YZ-plane.

## **CHAPTER 4**

### **ANTENNA INTEGRATION IN DELAY BASED RFID SYSTEM**

This chapter outlines a few simulation experiments related to the integration of the antenna with the transmission line, the modulation scheme employed and the fabrication and the characterization of RFID tags.

#### **4.1 Simulated Integrated System**

The antennas designed, fabricated and characterized are now to be integrated with the transmission line ID circuit. As explained in Chapter 3, the transmission line ID circuit is based on a delay scheme. The antennas have been matched to 50 ohms and the transmission ID is designed for a characteristic impedance of 50 ohms. This ensures that there will be an absence of any reflections on integration with the transmission line. However, a few questions arise as to what is the effect of the transmission line, the relative location of the antenna with respect to the tag and the grounding of the transmission line on the radiation pattern of the antenna. In an effort to answer these questions, a few simulation experiments have been run. The Half-Sierpinski fractal antenna has been chosen for these simulation experiments.

#### 4.1.1. Transmission Line Influence on the Antenna Radiation Pattern

In order to examine the effect of the transmission line on the radiation pattern of the antenna, the gains of the transmission line ID and the half-sierpinski fractal are found separately. The gain of the fractal antenna was found to be -25 dB (Fig. 4.1) and that of the transmission line, -49 dB (Fig. 4.2)

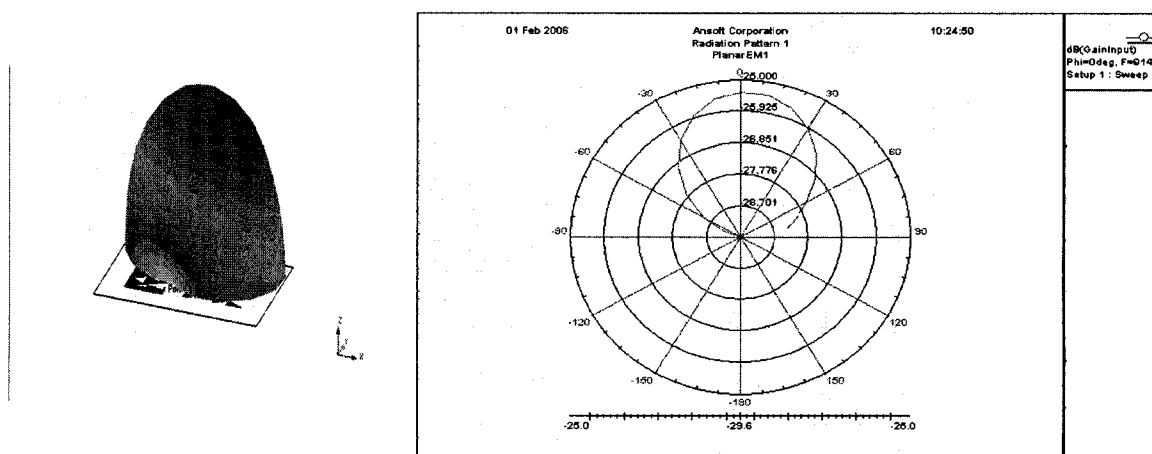


Fig. 4.1 (a) 3-dimensional radiation plot and (b) radiation pattern of gain ( $\phi = 0, \theta = 0$  i.e. normal to the plane of the antenna) for the half-Sierpinski fractal antenna.

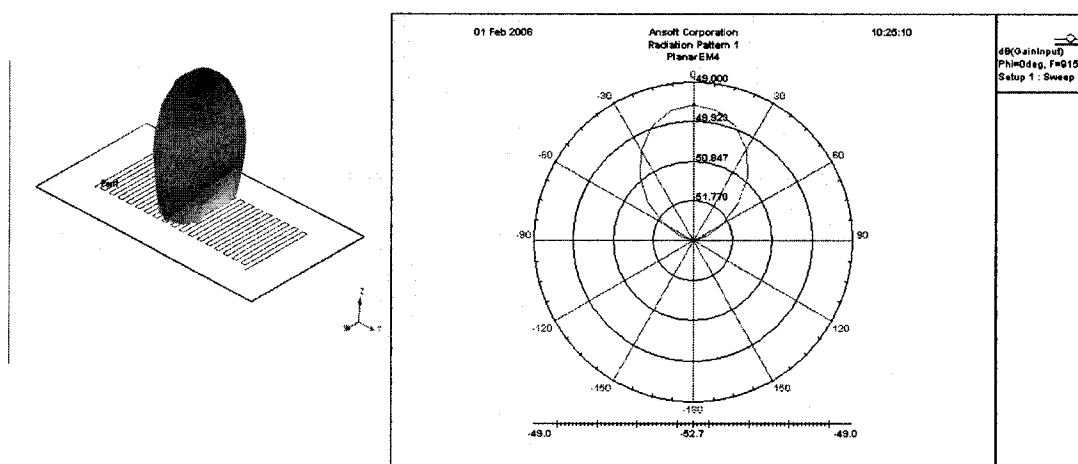


Fig. 4.2 (a) 3 dimensional radiation plot and (b) radiation pattern of gain ( $\phi = 0, \theta = 0$  i.e. normal to the plane of the antenna) of the open-ended transmission line.

The low radiation emitted by the transmission line, and hence the high isolation (25 dB) between the antenna and the transmission line, should help in maintaining the non-interference of the transmission line with the radiation performance of the antenna. This was further proven when the radiation pattern analysis is done with the antenna integrated with the transmission line (Fig. 4.3). We see here that the radiation pattern aligns itself to the pointing direction of the Sierpinski fractal antenna. Hence, one can state that the Sierpinski antenna is the principal radiator in the planar integration of the transmission line with the Sierpinski antenna. The radiation characteristics of the antenna are preserved on integration with the transmission line.

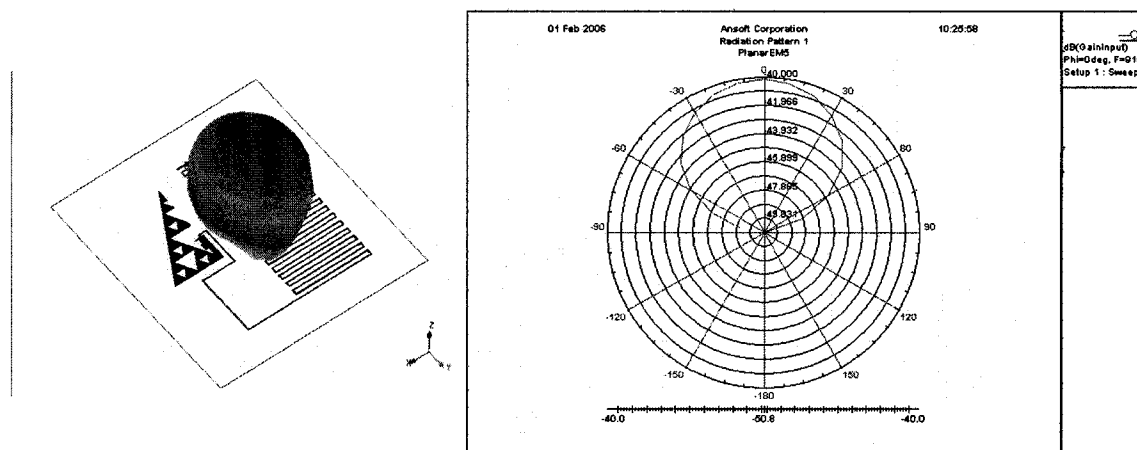


Fig. 4.3 (a) 3 dimensional radiation plot and (b) radiation pattern of the integrated sierpinski fractal.

#### **4.1.2. Line Grounding Influence on the Antenna Radiation Pattern**

The effect of the grounding of the finite substrate is attempted in the simulation to see if there is any increase in gain that can be attributed to the decrease of the surface wave losses. The transmission line is grounded at various locations on the microstrip feed line moving away from the feed-junction. From Fig. 4.4, it can be seen that there is an

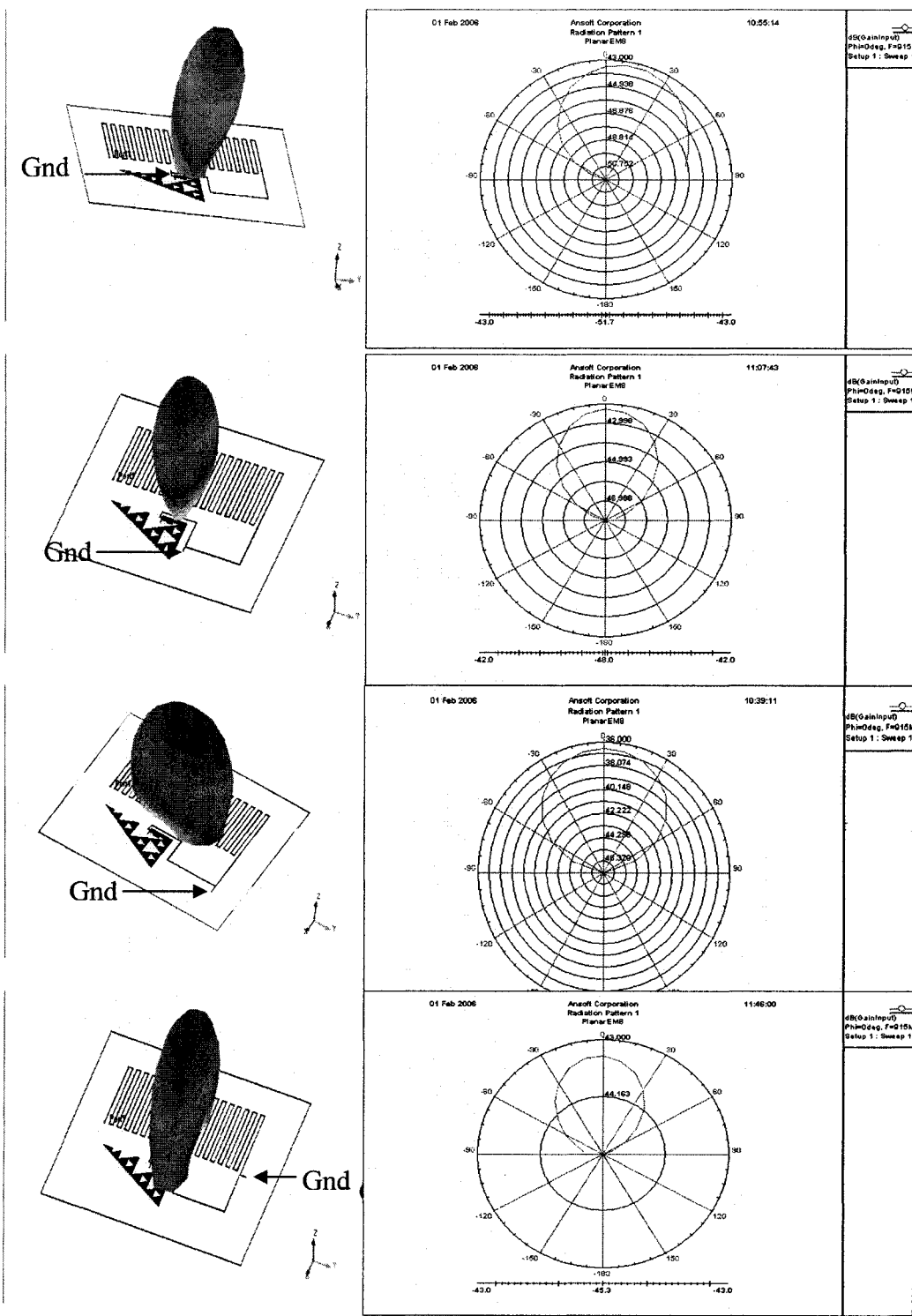


Fig. 4.4 Effect of ground location at a distance of (a).25" (b) 2.5" (c) 5" and (d) 7.5"from the feed-junction.

increase of gain only at a specific distance away from the feed-junction. Also it is found that the radiation pattern is altered with the deterioration of gain, when the transmission line is grounded at other locations.

#### 4.1.3. Transmission Line Layout Influence on the Antenna Radiation Pattern

In order to make the tag compact, the longer side of the Half-Sierpinski was placed parallel to the longer side of the transmission line (Fig. 4.5). This placement gave an antenna gain of -40 dB. When the shorter side of the antenna was placed parallel to the longer side of the tag, it was found that a greater gain is obtained and also the gain varies with respect to the relative location of the tag.

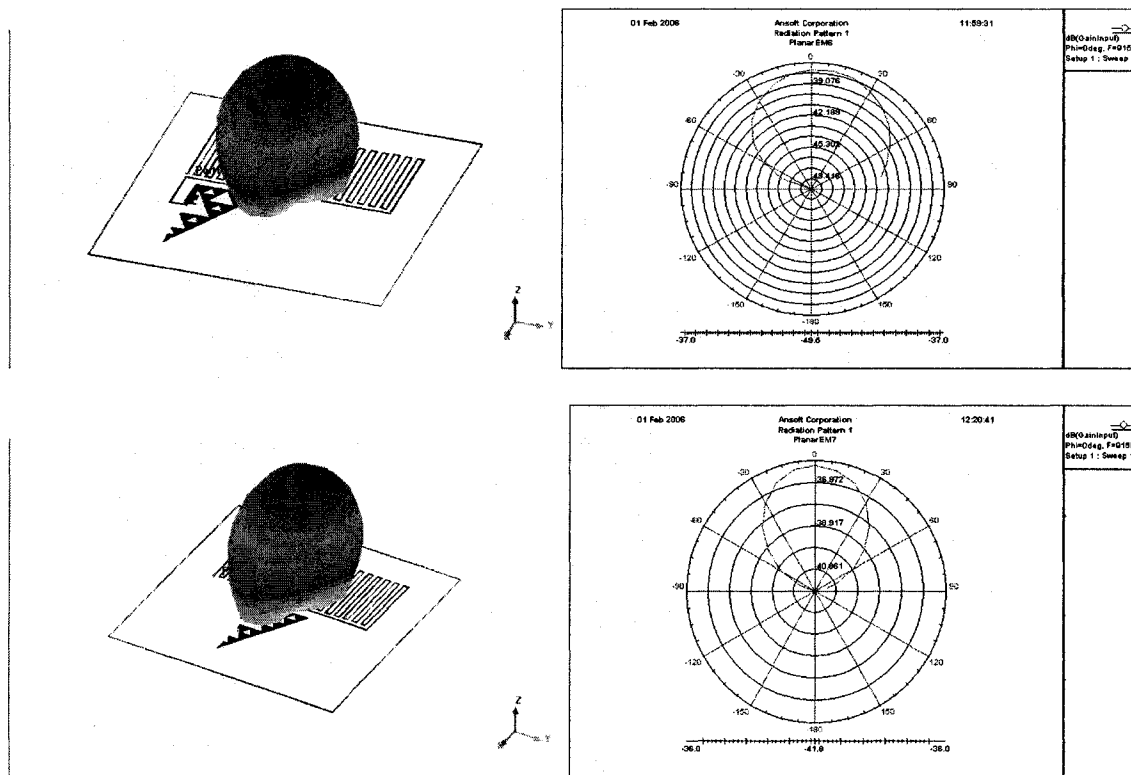


Fig. 4.5 Effect of antenna location at the (a) corner and (b) middle of the transmission line.

## 4.2 Modulation Scheme

The modulation procedure used is the On-Off Keying (OOK). To achieve this modulation, we require a sinusoidal signal generator to produce a 915 MHz signal and an RF switch which shuts the sinusoidal wave on and off for the desired On/Off time. The RF switch can be switched On and Off by means of a pulse signal. By controlling the pulse-width and the pulse repetitive frequency (PRF) of the pulse, the On time and off time can be controlled. Fig. 4.6 shows the picture of the RF switch and the pulse-generator employed for the generation of an On-Off pulse-modulated sinusoidal signal. A DC supply of 1.6-2.3V is required for the operation of the RF switch. The switch has a rise time ( $t_r$ ) of 3 nsec and a fall time ( $t_f$ ) of 6 nsec. Thus, the minimum width of the pulse that can be obtained without losing amplitude of the signal is 9 nsec.

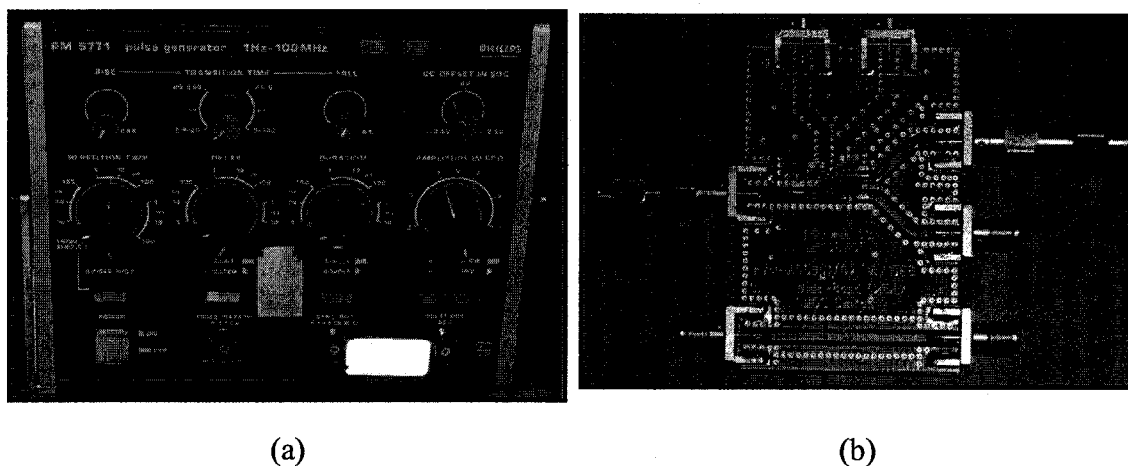


Fig. 4.6 Picture of the (a) Pulse-Generator and (b) the RF switch.

Let us now discuss the concept of the generation of ID with this modulation scheme applied to the delay-based transmission line. The delay obtained by the transmission line, that is designed for a characteristic impedance of 50 ohms (line-width = 406.25  $\mu\text{m}$ ) is 0.13 nsec/ inch. In order to create a delay that can be observed with the

type of modulation scheme and the intrinsic limitation posed by the switch, a delay greater than 9 nsec has to be generated for the delayed signal in order to be observed without mixing with the direct signal. A 72 inch meandered transmission line, as shown in Fig. 4.7, has been designed, as explained in Chapter 2, to produce a delay of 9.36 nsec.

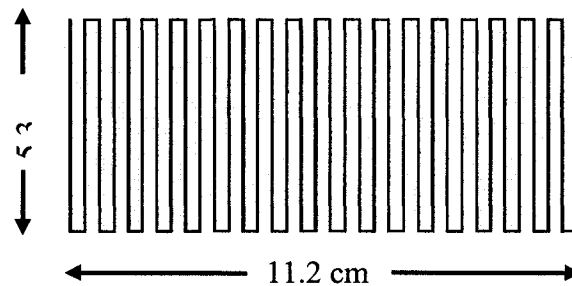


Fig. 4.7 Schematic of meandered transmission line.

A pulse width of 10 nsec implies a bit-rate of 100 Mbps and a bandwidth of 200 MHz. In order to transmit such a high band-width signal, it was required to design a wide band-width source antenna to replace the narrow band-width Yagi antenna.

### **4.3. Fabrication of Integrated System**

The simulation layouts of the antenna and the transmission line are integrated in the layout such that the ends of the microstrip feed of the antenna and the two ends of the transmission line are aligned with respect to the three contacts of the circulator device. Fig. 4.8 shows pictures of the tags. The photolithography method, as explained in Chapter 3, is employed to realize the tag with the antenna pattern and transmission line. A surface-mount circulator is then soldered to the tip of the antenna's microstrip feed and the two ends of the transmission line to complete the tag which is capable of delivering a delay-based ID code, the number of bits dependent upon the pulse width, and the delay

chosen. The delay should be greater than the pulse-width in order to obtain a readable ID code.

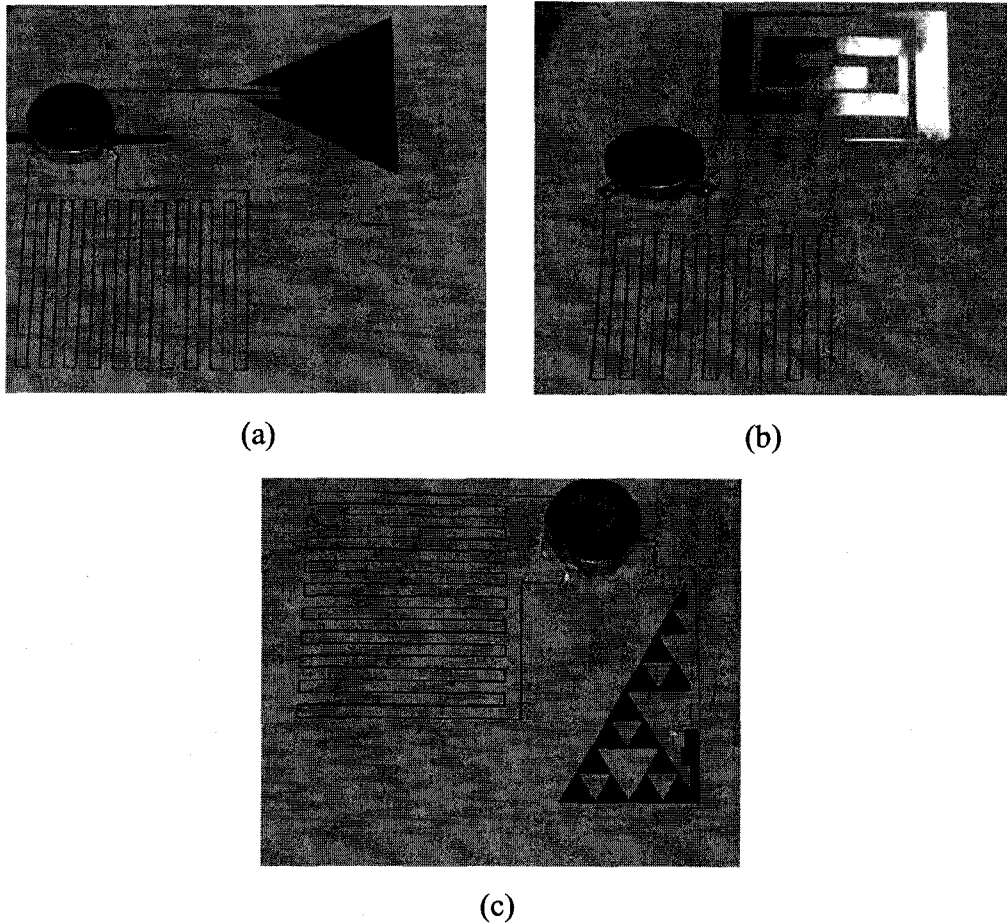


Fig. 4.8 Pictures of the fabricated (a) triangular, (b) spiral, and (c) Half-Sierpinski fractal tags.

#### **4.4. Characterization of Integrated System**

The fabricated tag is now to be tested in an anechoic environment so that the external reflections off the walls and any noise will be eliminated. In order to simulate such an environment a 2 ft<sup>3</sup> closed anechoic housing is constructed (Fig. 4.9). The material used is polyurethane foam capable of absorbing the 915 MHz signal. The antennas and the tag to be tested are supported by triangular polyurethane posts.

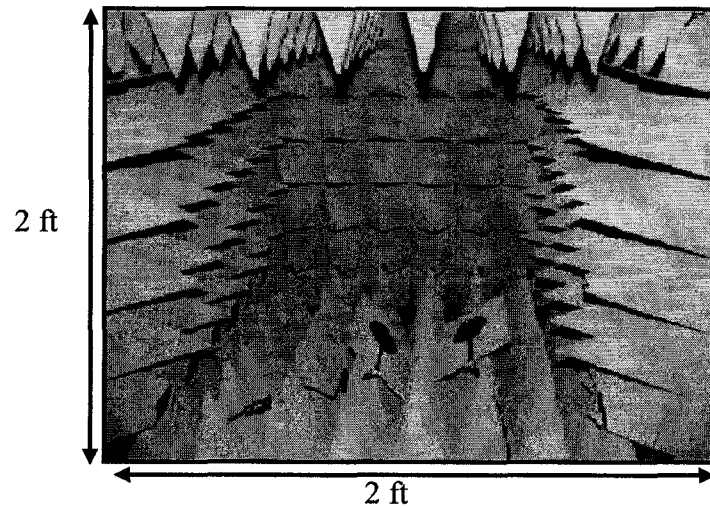


Fig. 4.9 Optical picture of anechoic housing for tag testing.

The distance of separation between the transmitting circular disc monopole (CDM) antenna and the tag and the receiving circular disc monopole and the tag is 10 inches. All three components, the tag and the two CDM antennas are placed in a triangular configuration with each facing the other at an angle of  $60^\circ$  to maximize the signal capture of the antennas. The tag and the two circular disc monopoles are placed inside the chamber at a distance of 10 inches from each other in a triangular pattern. The transmitting and the receiving circular disc monopoles are connected by a coaxial cable, which runs through a small opening in the corners of the housing. This type of housing was found to increase the amplitude of the signal absorbed. Fig. 4.10 shows the amplitude of the signal inside and outside the anechoic chamber.

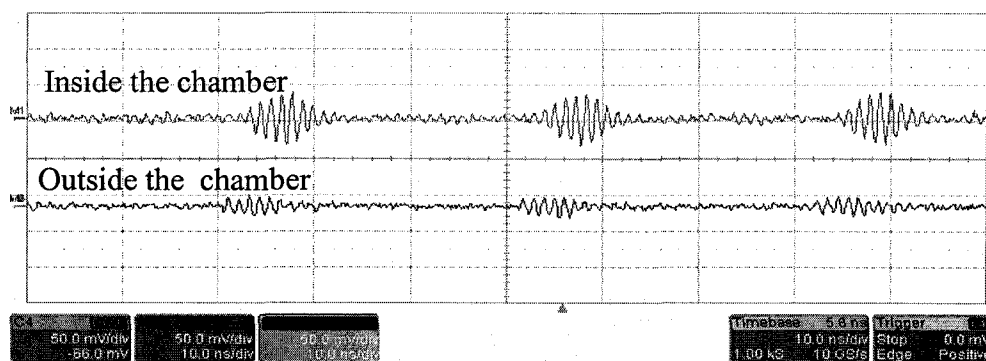


Fig. 4.10 Effect of anechoic housing.

The schematic and the picture of the experimental set-up for the tag is shown in Figs. 4.11 and Fig. 4.12.

#### 4.4.1 Pulse Spreading Effect

In order to test the tags, narrow-band Yagi antennas, having a bandwidth from 902-928 MHz were employed.

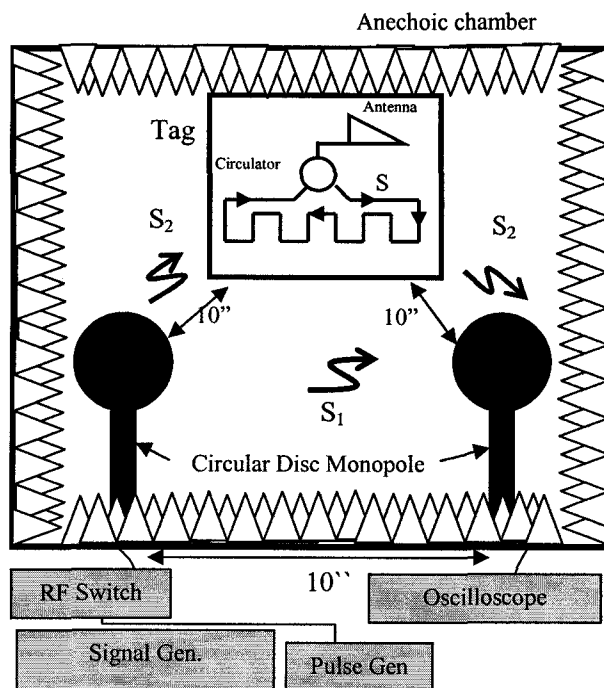


Fig. 4.11 Schematic of experimental set-up.

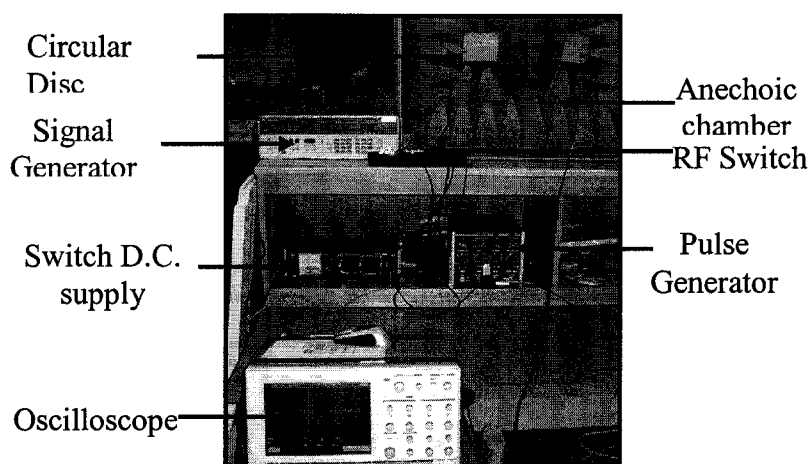


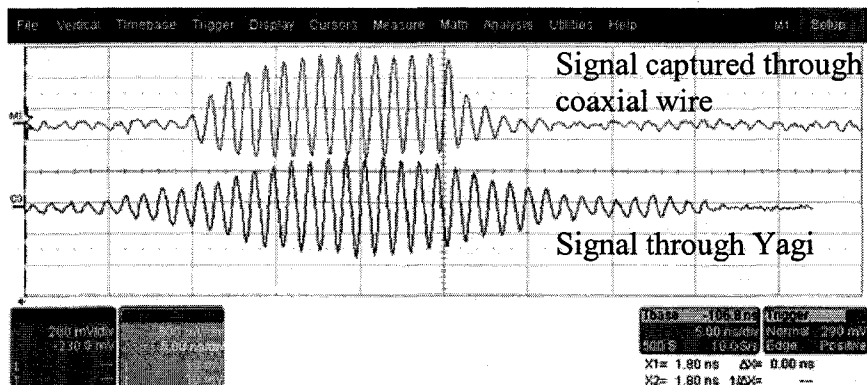
Fig. 4.12 Experimental set-up for tag characterization.

The narrow-band nature of these antennas caused the pulse to spread at the edges of the pulse. This is a phenomenon that can result when a wide-band pulse is made to pass through a narrow-band antenna. In order to circumvent the problem, a wide bandwidth circular disc monopole antenna having a -10 dB bandwidth at greater than 300 MHz, was designed. This antenna was found to faithfully transfer the pulse signal without any pulse spreading. Fig. 4.13 depicts the pulse spreading effect of the Yagi antennas and the faithful transfer of the pulse signal through the circular disc monopole antennas.

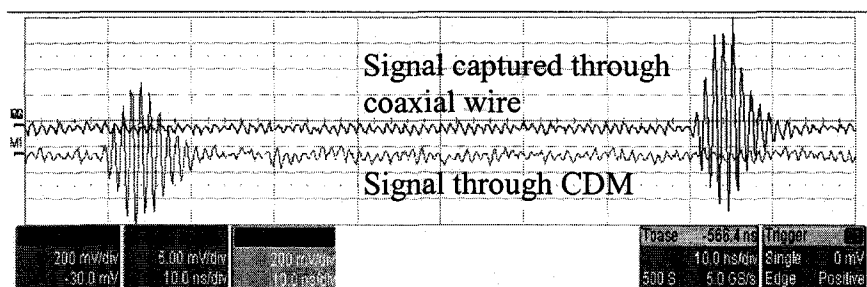
#### **4.4.2 Design, Fabrication and Testing of a Circular Disc Monopole**

A circular disc monopole is known to exhibit wide-band behavior [65]. Ansoft HFSS simulation software was employed to develop a wide-band circular disc monopole antenna centered around a frequency of 915 MHz. A  $11.34 \times 13.5 \text{ cm}^2$  PCB substrate is chosen for the simulation (Fig. 4.14). A circular disc of radius 2.7 cm, feed width of 7 mm, and ground-plane of dimensions  $11.34 \text{ cm} \times 5.4 \text{ cm}$ , is initially chosen. In order to decrease the transmitted power of the antenna, the width of the ground plane and the

width of the feed (Fig. 4.15) are labeled as parameters in a parametric sweep to obtain a very low VSWR of 1.04, as can be seen in Table 4.1.



(a)



(b)

Fig. 4.13 Pulse spreading through (a) Yagi and (b) Circular Disc Monopole antennas at 915 MHz.

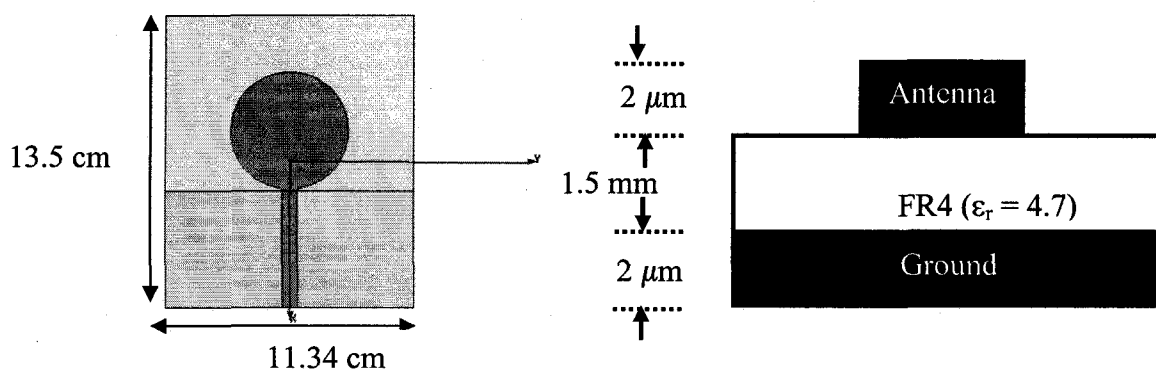
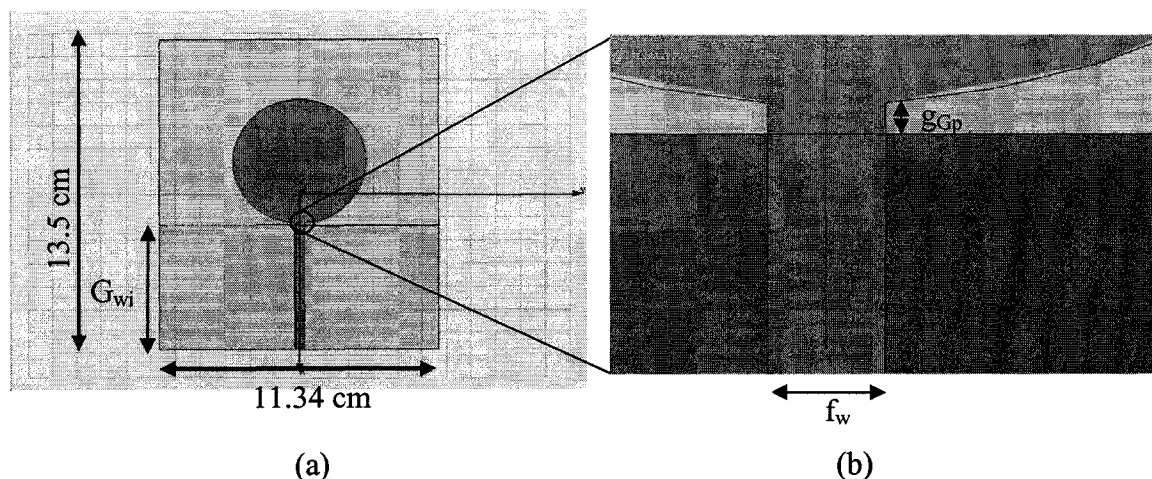


Fig. 4.14 (a) Simulation Layout and (b) cross-section of the Circular Disc Monopole.



$G_{wid}$ : The width of the ground plane  
 $g_{Gp}$ : The distance in the x-direction between the ground plane and the circular patch  
 $f_w$ : Width of the feed

Fig. 4.15 Simulation layout of the (a) 2.7cm radius microstrip fed CDM and (b) enlarged view of gap between ground point and the feed location.

Hence, a feed width of 0.378 cm and a ground plane width of 5.382 cm is chosen because of low VSWR. In order to increase the gain of the CDM antenna, a skewing technique is followed by which the dimensions of the antenna are scaled differently in the x and y-axis (Fig. 4.16). It was found that a scaling factor of 2.05 in the x-axis and a scaling factor of 2.1 in the y-axis gives rise to a high gain of about 6 dB and a VSWR of 2.4 (Table 4.2). An increase in power, for the improved circular disc monopole, of 3.13 times more than the older version is observed (Table 4.3). The circular disc monopole is fabricated using the photolithography procedure explained in Chapter 4 and the Return Loss plot is measured, as explained in Chapter 5. Fig. 4.17 (a) shows the fabricated circular disc monopole. Fig. 4.17 (b) shows the return-loss plot for the circular disc monopole. The wide-band nature of the antenna can be clearly observed from the graph. The discrepancy in the return-loss plot between the experimental and simulation results at higher frequencies could be attributed to the soldering method used to connect the SMA

connector, because the connector junction inductance effects become dominant at higher frequencies.

Table 4.1 Obtained values of VSWR and gain for different values of ground plane width and ground-plane gap.

Gwid (cm)	Fw (cm)	VSWR	Gain (dB)
5.400	0.702	1.91	1.70
4.980	0.360	1.52	1.89
5.130	0.414	1.42	1.87
5.328	0.378	1.32	1.77
4.986	0.396	1.22	1.74
<b>5.382</b>	<b>0.378</b>	<b>1.04</b>	<b>1.73</b>

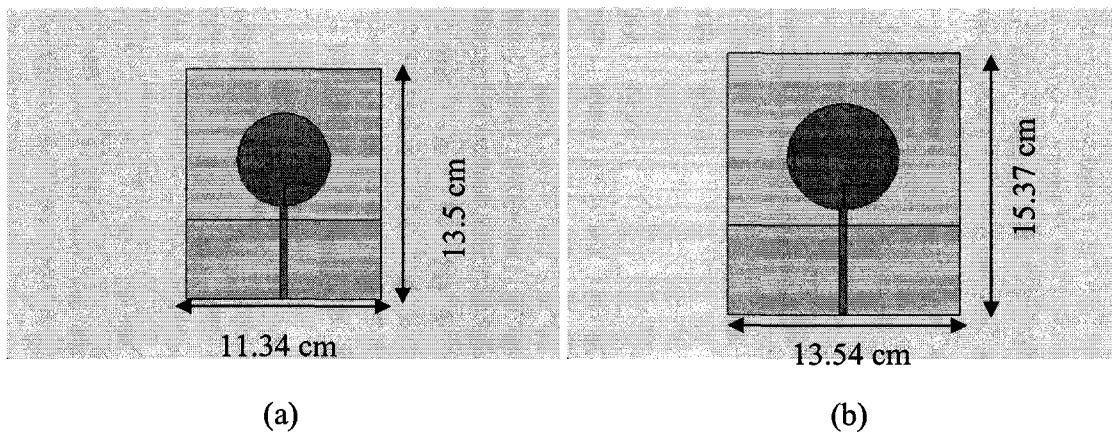


Fig. 4.16 Simulation layouts of (a) old and (b) new versions of Circular Disc Monopole. The antenna is found to be resonant ( $S_{11} > -10$  dB) from 780 MHz to 1.8 GHz.

Table 4.2 Values of gain of CDM as a function of the dimensions of the CDM.

Scaling factor in the x direction (s)*	Scaling factor in the y-direction (s <sub>1</sub> )*	Gain (dB)
1.8	1.8	1.73
1.8	2.25	2.06
1.85	2.3	2.13
1.95	2.4	2.9
<b>2.05</b>	<b>2.15</b>	<b>6.73</b>
2.15	2.2	3.73
2.2	2.4	2.25
2.4	2.35	2.46

\* A "s" value of 1.8 = 13.5 cm; A "s<sub>1</sub>" value of 1.8 = 11.34 cm

Table 4.3 Comparison table of old and improved versions of Circular Disc Monopole.

Feature	Older Version	Improved Version
Size	11.34 x 13.5 cm <sup>2</sup>	13.54 x 15.37 cm <sup>2</sup>
VSWR	1.04	1.11
Power Transmitted	100%	99.7%
Gain	1.75	6.73
Power captured/received (normalized)	1	3.83

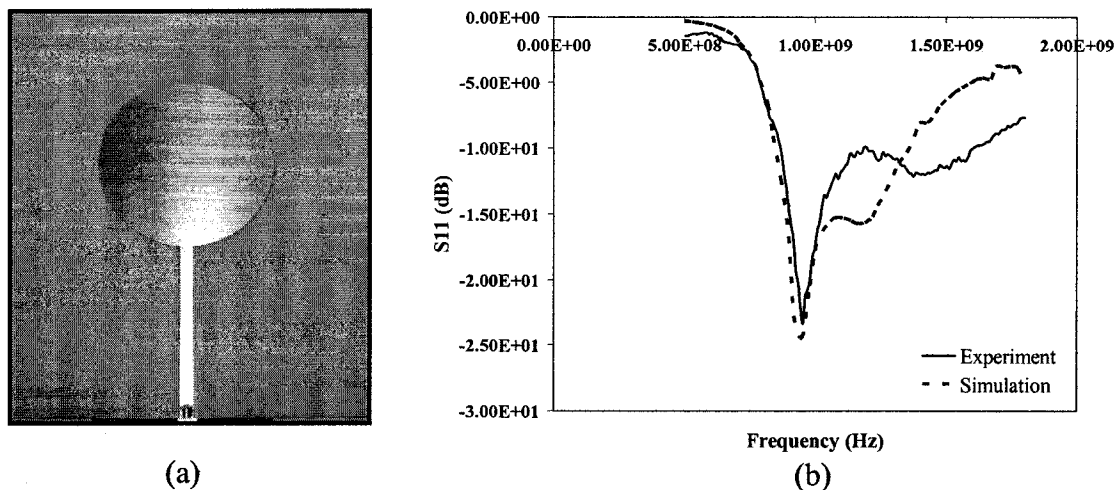


Fig. 4.17 (a) Picture and (b) return-loss plot of circular disc monopole.

#### 4.4.3 System Testing

The 10 nsec delay deliverable tag was characterized for the power back-scattered by the tag. The method outlined in [61] was followed to measure the back-scattered power. The schematic for the back-scattered power measurement is shown in Fig. 4.18.

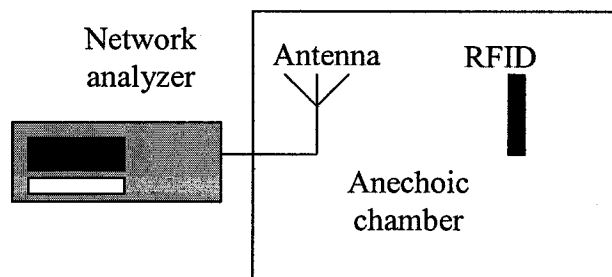


Fig. 4.18 Measurement set for determining back-scattered power.

The HP4396B network analyzer was used to make the measurements. Calibration is made with the network analyzer connected to the transmitting antenna and with no RFID tag present. The reference level, after subtracting the effects of transmitting antenna mismatch and anechoic chamber multipath, is found to be about -50 dB. The tag is then

introduced into the chamber and the measurements are made. The transmitted power was 1 mW. The antenna return loss measured in the anechoic chamber with the RFID tag present is shown in Fig. 4.19. By using the measured value of the return loss at 915 MHz, which can be approximated as the ratio of power back-scattered to transmitted power, the power back-scattered is found to be 0.169 uW. Using the classical radar equation [66],

$$P_{\text{backscattered}} = \frac{P_t G_t \lambda^2 \sigma}{(4\pi)^3 r^4} \quad (4.1)$$

where  $G_t$  is the gain of the transmitting antenna, the radar cross-section ( $\sigma$ ) is found to be  $0.16 \times 10^{-3}$  sq.m. The circular disc monopole discussed earlier was used as the transmitting antenna.

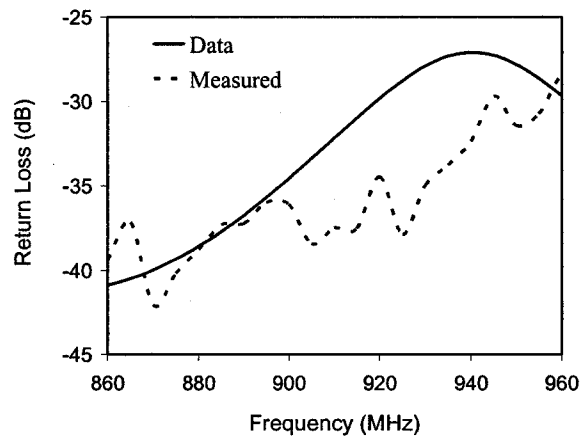


Fig. 4.19 Antenna return loss measured in anechoic chamber with RFID tag present.

The fabricated tag was then tested at a very small distance of 6 cm (just above the near-field limit of 5cm for the CDM microstrip antenna at 915 MHz) using the circular disc monopole (CDM) antenna. The amplitude of the delayed 10 nsec width signal is found to be dependent on the distance of the separation. Fig. 4.20 shows the waveforms observed on the oscilloscope with and without the tag. S1 is the signal passing directly

from one CDM antenna to another. S2 is the delayed signal from the tag. The tag that was tested was that of the Half-Sierpinski antenna. In order to determine the limit of the reading range, the antennas were kept at a greater distance, at about 10 inches, and the planes of the antenna were placed at an angle of  $60^\circ$  relative to each other to maximize signal capture. Future experiments were carried out using this set-up.

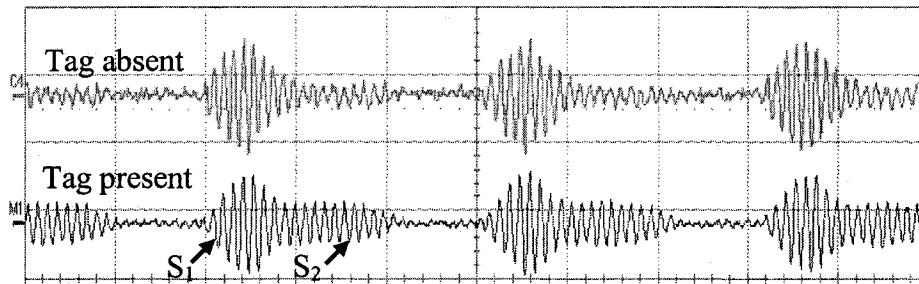


Fig. 4.20 Signals with and without tag.

#### 4.4.3.1 System with triangular patch

The tags with 5 nsec and 10 nsec delay were fabricated and tested for their output. Fig. 4.21 displays the output waveforms for the triangular tags with different delays. One can observe from the waveform, that for the 5 nsec delay tag, an extension of 5 nsec is observed in the output waveform and for the 10 nsec delay tag an extension of 10 nsec is seen. The dotted lines show the limits of the noise signal and the continuous line, the limits of the delayed signal. The high rise and fall times of the pulse is attributed to the slow switching of the RF switch. The lowest amplitude of the delayed signal is found to be 26 mV and the amplitude of the noise is found to be 16.67 mV. Thus, a threshold of 20 mV can be set for reading a 1110 or 1111 bit.

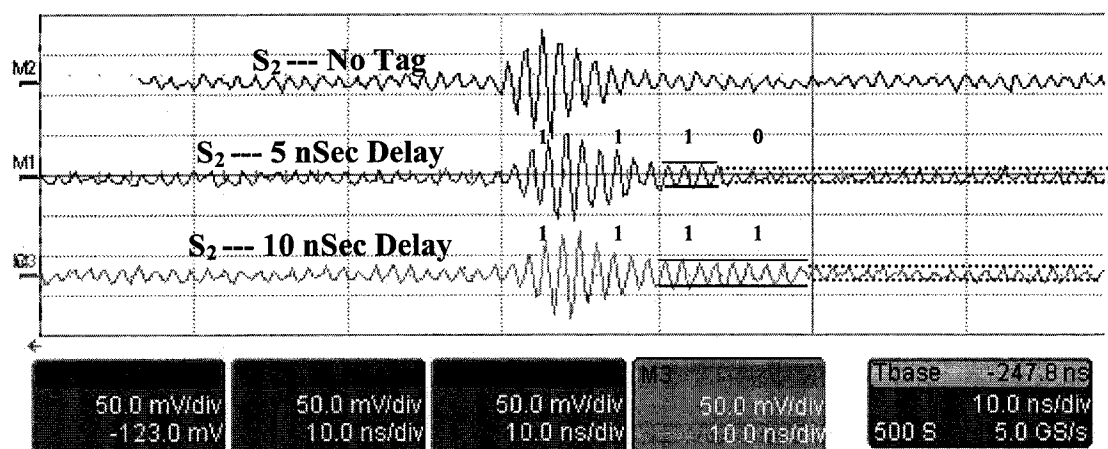


Fig. 4.21 5 nsec and 10 nsec delay deliverable triangular antenna RFID tag.

#### 4.4.3.2 System with spiral patch

The spiral antenna, with a gain less than that of the triangular antenna, is found to exhibit the same behavior (Fig. 4.22). However, for the 5 nSec delay measurements, the noise level was found to be high, which can be attributed to the solder connections in the tag. Also, the low amplitude of the delayed signal can be attributed to the bandwidth of the spiral antenna, which is lower than that of the triangular antenna. The dotted lines show the limits of the noise signal and the continuous line, the limits of the delayed signal.

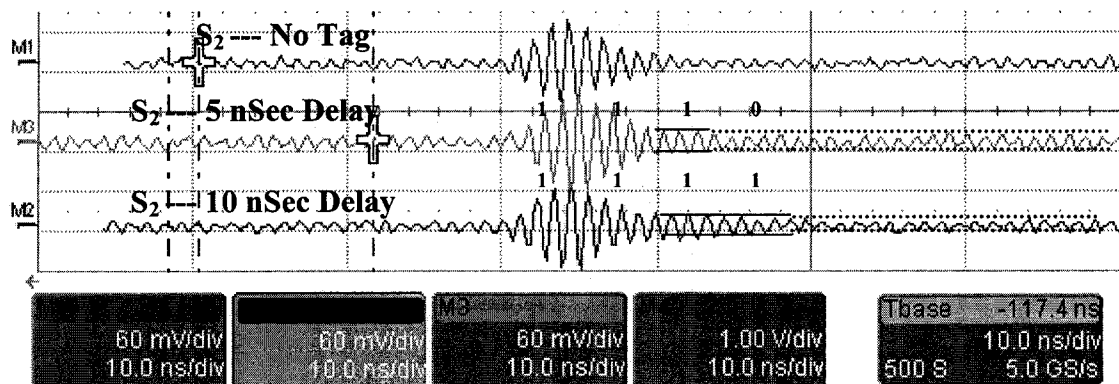


Fig. 4.22 5 nsec and 10 nsec delay deliverable spiral antenna RFID tag.

For the 10 nsec delay measurement, the amplitude of the noise is found to be 15 mV and the lowest amplitude of the delayed signal, 21 mV. Thus, the threshold for bit reading could be placed in between the above two values at 18 mV. For the 5 nsec delay measurement, the amplitude of the noise is found to be 24 mV and the lowest amplitude of the delayed signal is found to be 30 mV. Thus, the threshold for bit reading could be placed in between the above values, at 27 mV.

#### **4.4.3.3 System with Half-Sierpinski patch**

Due to the gain of the Half-Sierpinski patch antenna being too low, the delayed signal could not be seen for the realization of an ID. Also, the low bandwidth (13MHz) of the fractal antenna could result in reduced amplitude for delayed signal. The antenna can be utilized for RFID purposes, with a switch with higher isolation. It is to be noted that the Half-Sierpinski antenna was successfully tested at lower read ranges.

The pulse-widths used in the characterization of the tags are 10 nSec and 5 nsec which would require high band width antennas for the transfer of the signals without pulse-spreading, which is a phenomena observed when large band-width signals are made to pass through a narrow band-width antennas. The bandwidth of the antennas affects the amplitude of the delayed signal. A higher bandwidth (32 MHz) triangular antenna would allow for less pulse spreading of the signal than the lower bandwidth (18 MHz) spiral antenna. However, it is to be noted that the lowest bandwidth observed, (13 MHz) which is for the Half-Sierpinski fractal antenna, is quite sufficient for commercial RFID applications, wherein higher width pulses of the order of 100 nsec are utilized for data communication.

## CHAPTER 5

### CONCLUSION AND FUTURE WORK

#### 5.1 Conclusions

This work comprises the development of a small-size antenna which will be extremely useful for the tagging of small-size objects in the future. A compact triangular antenna, (a type of single band resonant antenna), a spiral antenna (a type of wide-band resonant antenna) and a half-Sierpinski fractal antenna (a type of small size multi-band resonant antenna) were developed on a flexible polyimide platform. The introduction of slots in the ground has been used to increase the gain. These antennas have been designed for an output impedance of 50 ohms and a frequency of 915 MHz. Two of these antennas (the triangular and the spiral antenna) display peak gains of over 2 dBi and the third one (Half-Sierpinski fractal antenna) has a gain close to 0 dBi. The triangular and spiral antenna, owing to their high gain, have successfully been integrated with the transmission line RFID tag for the generation of bits. The Half-Sierpinski fractal tag can still be used in the presence of an efficient reader that can detect the presence of a weak back-scattered signal.

The primary constraints for the integration of a patch antenna are both small size and high gain. Both of these constraints have been seriously considered in this work and considerable lot of effort was put into developing small resonant antennas at 915 MHz.

Several reasons for this approach is the application of power-efficient tags to be attached onto small objects. Large retailers, such as Wal-Mart Inc., are welcoming RFID as its security mode and also to minimize the cross-coupling effects between two nearby tags.

The triangular antenna has been designed to perform with a gain of 3.35 dBi and the Half-Sierpinski antenna with a gain of -0.64 dBi. Though having low gain, the Half-Sierpinski antenna still qualifies for UHF RFID application due to its near omnidirectionality. The gain is a parameter of the antenna which can be best decided when the details of the application are known, such as the location of the tag, surrounding objects, their proximity to the tagged object and the dielectric of the surrounding objects. High gain implies increased directionality of the radiation and a higher concentration of power in one direction. Low gain implies that the power spreads out more. High gain antennas, are no doubt, the only type preferred for a “fixed point-fixed point communication” application. However, when one of the points is not-fixed, as in the case of a RFID system, a sound judgment is to be based upon intuition and testing as to whether a high gain antenna is still preferred over a lower gain antenna. On the other hand, a very high gain or very directional antenna implies a higher reading distance and less interference. However, a omni-directional or a low gain antenna offers the advantage of more reading space, which is a direct advantage for the case of reading multiple tags that are not very close. Also, it is a better design for a transceiver – tag system wherein the directionality of the transceiver antenna can be further improved to decrease the interference between the other readers and still be able to read multiple tags. In the report by Foster et. al. “Antenna Problems in RFID systems” *Microwave and Antenna Systems, 1999 IEE*, it is inferred that omni-directional is favored but pure omni directionality however, is to be avoided because of interference issues. Hence, a balance is to be sought in the designing

of antennas for RFID systems whereby neither omni directionality nor directionality is sacrificed.

In order to enhance the functionality of the RFID tag, a sensing mechanism can be incorporated within the tag, wherein the tag not only conveys information written on it, but also conveys the status of the environment or the object on which it is placed such as temperature, pressure or humidity or if the object has been tampered with or not. Initial work has been done on modifying the tag to be a temperature sensor, which will be discussed in section 5.2 of this chapter. The antenna sensor behavior can be altered and thus, a faulty performance can be exhibited under special circumstances. One particular situation is when the sensor is close to the human skin. Simulation experiments were performed to study the effect of the proximity of human skin on the performance of the antenna. Fig. 5.1(a) shows that there is a change in the resonant frequency of the antenna when it is close to the skin. This can be corrected by scaling of the antenna. A scale factor of 1.05 is chosen, as can be seen in Fig. 5.1 (b) to correct the error.

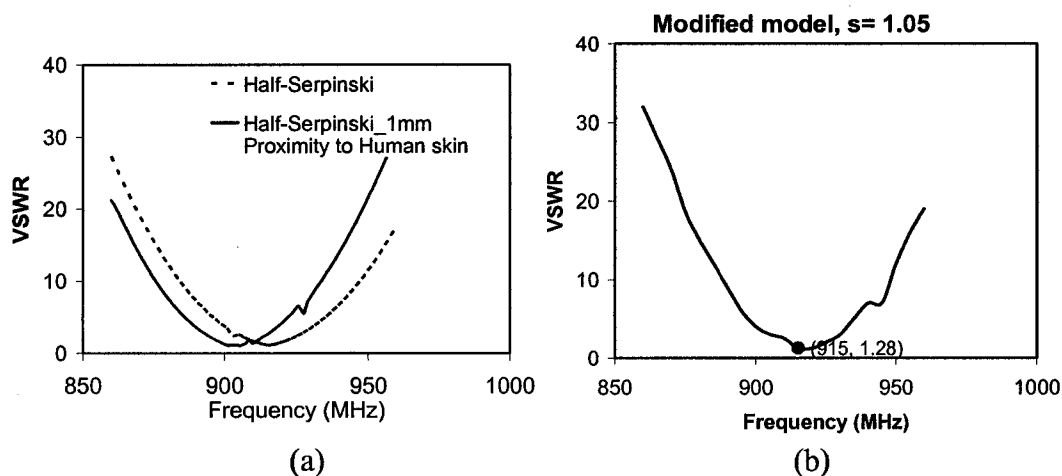


Fig. 5.1 (a) Effect due to proximity of human skin on the resonant frequency and (b) correction of the error through scaling.

Thus, the designer of the patch antenna must take the environmental conditions in consideration and incorporate the details into his design for that particular application.

### 5.2 Preliminary Results for Antenna Temperature Sensor

The dielectric constant of the epoxy varies when subjected to a temperature change at a fixed pressure, as shown in Fig. 5.2. The higher temperature plots are towards the right. The change in dielectric constant depends on the temperature and pressure of the ambient and also on the frequency [67].

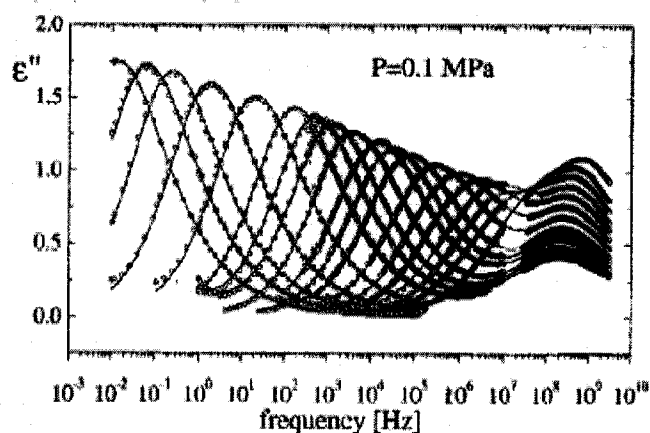


Fig. 5.2 Loss tangent plots at different temperatures [67].

The antenna is designed for 915 MHz frequency and with the dielectric constant of the superstrate corresponding to the temperature to be sensed (threshold temperature). When the temperature of the ambient, or the surface on which the tag is placed, reaches the threshold temperature, the antenna resonates and allows the incident signal to pass through it.

The dielectric material was initially tested for its change in dielectric characteristics with respect to temperature. The dielectric material was sandwiched

between two copper strips and the change in the capacitance was measured with respect to the change in temperature. The temperature effect was brought about by placing a hot-plate close (a few centimeters away) to the capacitor element for an increase of temperature and moving it away for a decrease in temperature to normal conditions.

The value of the capacitance was found to be 3.5 pF and 4.7 pF when the temperature of the plate was 460 °C. Applying the relation  $C = \epsilon A/d$ , we can obtain the dielectric constants corresponding to the room-temperature and at a temperature of 460 °C as 5.07 and 6.8 respectively.

Hence, if the temperature is increased, the dielectric constant is increased which, when used as the substrate or superstrate of the antenna, would change its performance characteristics and thus enable it to act as a sensor.

A few simulation experiments were performed to study the variation of the resonant frequency of the antenna with a temperature sensitive dielectric as the substrate and superstrate. Fig. 5.3 reveals that the sensing element when used as the substrate for the antenna, is found to have more sensitivity. A material, which exhibits a change in the dielectric constant with respect to temperature, is Poly (phenyl glycidyl co-ether formamide). Since it is highly viscous at room- temperature, it is cured using the curing agent, 2,2- Dimethylcyclohexane at 80 degrees Celsius for 8 hours. The materials were drop-cast over the substrate. Different deposition procedures were employed to deposit the temperature sensitive material. Fig. 5.4 depicts the various procedures that were followed. The motivation for preparing samples using procedures 1 and 2, with more than one sensitive layer, is to increase the sensitivity of the device. The motivation for preparing samples using procedure 3, with a reduced amount of curing agent, is to

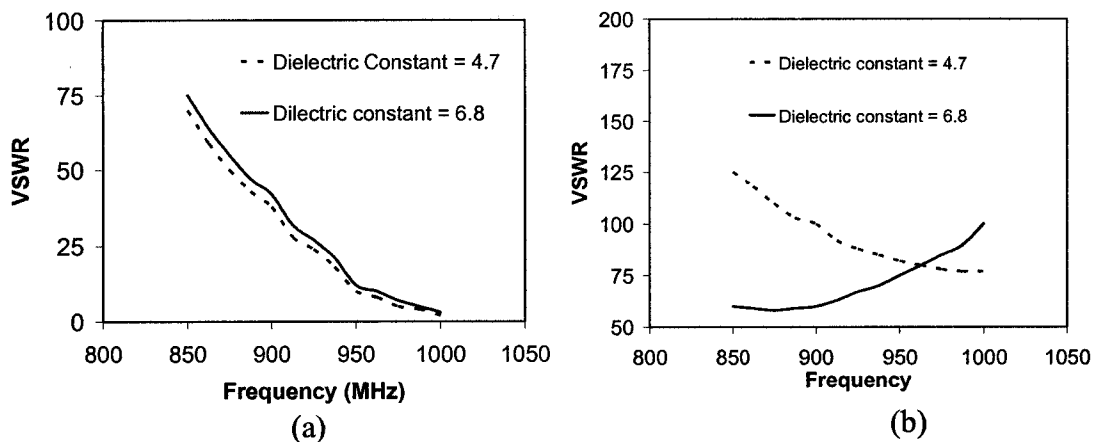
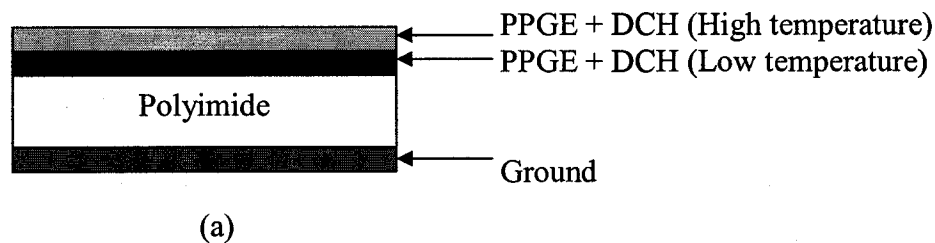
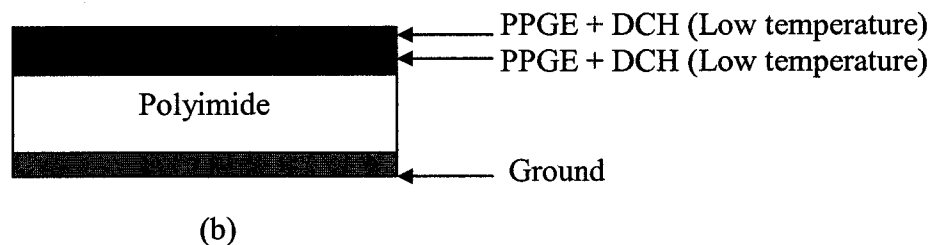


Fig. 5.3 VSWR versus frequency plots of the antenna with temperature sensitive material (a) over the antenna, (b) over the polyimide, as the substrate for the antenna.

Procedure 1:



Procedure 2:



Procedure 3:

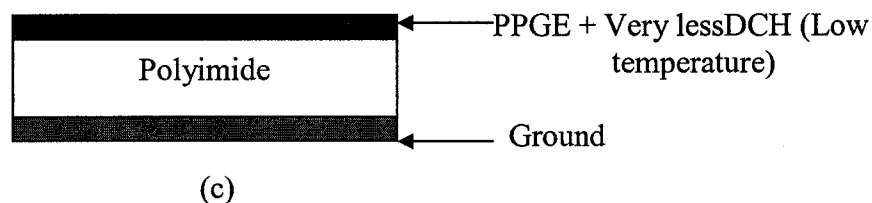


Fig. 5.4 Polyimide with (a) a differential deposited PPGE and DCH in two coatings (b) a uniform deposited PPGE and DCH in two coatings and (c) a single coating of PPGE and minute quantity of DCH.

attempt to obtain a purer epoxy film and thus a better transfer of the temperature-dielectric loss characteristics. Two observations were made from the above experiment:

- (i) Samples prepared with procedures 1 and 2 cured properly. The sample prepared using procedure 3 did not cure properly and was sticky.
- (ii) The sample prepared with procedure 1 was found to show a steady signal strength difference of 15 dBm and the sample prepared with procedure 2 was found to show less than 5 dBm and was not steady.

A Half-Sierpinski fractal was fabricated on a 0.2 mm thick epoxy. A 915 MHz Yagi antenna connected to a 13 dBm power transmitting signal generator, is placed 4 feet away from the microstrip patch antenna. Table 5.1 shows the signal difference captured by the RF receiver as a function of temperature. The resonant frequency was found to be observed at 1.1 GHz in Fig. 5.5. A shift of 25 MHz towards the left from 1100 MHz (2.27%) was observed. The shift magnitude is similar to that observed in simulations. Also, referring to Fig. 5.2 we see that the higher the temperature, the higher the loss tangent and the higher the dielectric constant. From the relation [68],

$$\frac{\delta f}{f_0} = -\frac{1}{2} \frac{\delta \epsilon_r}{\epsilon_r} \quad (5.1)$$

one can infer that there would be a decrease in the resonant frequency, which is the behavior observed in Fig. 5.5.

Table 5.1. Magnitude of measured signal with respect to the temperature sensed by the tag.

Temperature (Deg C)	Response Time (sec)	Re-setting Time (sec)	Meas. Signal (dBm)	Signal (Room Temp) (dBm)
68	9	11	-34	-40
88	5	10	-35	-40
158	4	30	-36	-40
230	4	35	-37	-40

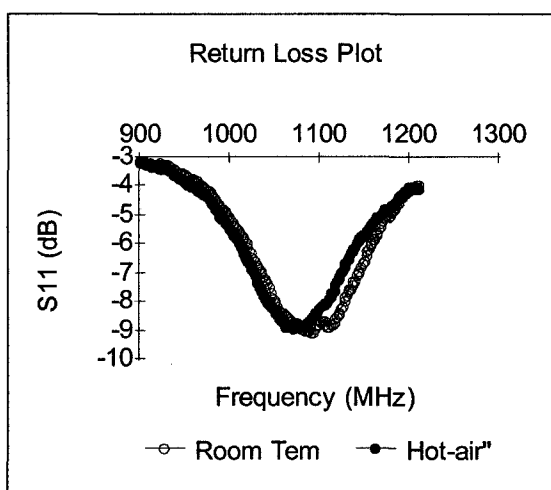


Fig. 5.5 Variation of resonant frequency when subject to temperature.

## **APPENDIX**

### **FULL-WAVE METHODS FOR ANTENNA ANALYSIS**

The Method of Moments procedure is followed in Ansoft Designer. In the Method of Moments, the field sources are attacked. The equations are integral. The general format of these equations is [47]:

$$L(f) = g, \quad (1)$$

Where L is an integral operator, g is the source or excitation, which is assumed to be a known function, and f is the field or response, which is the unknown function to be determined. The linearity of the operator follows from the linearity of Maxwell's equations and the constitutive equations. In Method of Moments, the unknown quantity (f) is expanded in terms of a set of linearly independent known functions,  $f_n$

$$f = \sum_{n=1}^N \alpha_n f_n \quad (2)$$

where  $\alpha_n$  are unknown coefficients yet to be determined. The expansion functions should be chosen, usually based on experience, so that a reasonable approximation of f is obtained with a small number of terms, N.

When Equation (1) is substituted into Equation (2), one obtains the approximate equation,

$$L\left(\sum_{n=1}^N \alpha_n f_n\right) \approx g \quad (3)$$

Since the operator is linear, we can write Equation (3) as

$$\sum_{n=1}^N \alpha_n L(f_n) \approx g \quad (4)$$

The unknown coefficients  $\langle \alpha_n \rangle$  should now be determined such that Equation (4) is satisfied. A measure is needed describing the degree of accuracy to which the left side and the right side of Equation (4) match.

In the MoM, this measure is obtained in the following way. Both sides of Equation (4) are multiplied by a known, properly selected function, referred to as the weighting function,  $w_m$  and the results integrated over a spatial region. The choice of the weighting functions and the inner product is based on experience. Now, we have

$$\sum_{n=1}^N \alpha_n \langle w_m, L(f_n) \rangle = \langle w_m, g \rangle \quad (5)$$

The inner products in Equation (5) are definite numbers, because they can be evaluated analytically or, more frequently, numerically. For this reason, Equation (6) represents a linear equation in coefficients  $\alpha_n$ . To obtain a determined system of linear equations for these coefficients, the weighting procedure is done for a linearly independent set of  $N$  functions, yielding

$$\sum_{n=1}^N \alpha_n \langle w_m, L(f_n) \rangle = \langle w_m, g \rangle \quad (6)$$

$$m=1, \dots, N$$

Equation (6) represents a system of  $N$  ordinary linear equations in  $N$  unknowns, and it can be solved using various techniques. The methods based on differential equations result in huge, but sparse systems of linear equations, which are solved using specific techniques. The Method of Moment, which is based on integral equations, results in more compact, but full systems, which are usually solved using Gaussian elimination or similar techniques [85], such as the LU decomposition.

Ansoft HFSS is based on the Finite Element method (FEM). The FEM is a technique that can be used to efficiently analyze electromagnetic structures that include homogeneous and anisotropic materials [86a]. The FEM is based on solving for the field distribution, or equivalently, solving for the potentials. The equation that is to be solved

numerically is usually derived from the differential form of Maxwell's equations following the so-called variational approach. The region where the fields exist is divided into a large number of subdomains, which are of a finite size. Within each subdomain, the field or potential distribution is approximated by a basis function, which is most often a linear or a quadratic function.

Because of the finite size of the subdomains, the basic FEM is most suitable for the analysis of fields within an electromagnetically shielded region, such as a microwave cavity or a shielded microwave circuit. However for antenna problems, the space occupied by the fields is infinite. So, in order to analyze antennas, it is necessary to bypass the limitation of the finite-size subdomains, which can be done following two distinct approaches. One approach is to construct special basis functions on subdomains that extend to infinity, which has not been suitable enough for antenna applications. The second approach is to assume that the region where the finite elements are distributed is bounded by a finite closed surface,  $S$ . This surface, then encompasses all material inhomogeneities making an efficient use of the FEM. In antenna radiation problems, the surface simulates an infinite open space into which the antenna radiates. This simulation is performed in the following way.

A local boundary condition on  $S$  is imposed. A simple approach is to assume  $S$  to be a sphere located in the far-field region. In this case, the electric and magnetic field vectors are practically tangential to the sphere, are mutually orthogonal, and are related by the so-called radiation boundary condition, which is

$$\mathbf{H} = \frac{\mu_r \times \mathbf{E}}{\zeta_0} \quad (7)$$

where  $H$  is the radiated magnetic field,  $E$  is the electric field and  $\zeta_0 = \sqrt{\mu_0 / \epsilon_0}$  is the wave impedance (intrinsic impedance) of vacuum. The basic problem is to have  $S$  really far away, in the far-field zone, to be sure Equation (7) is valid and provides sufficient accuracy.

## REFERENCES

- [1] M. Keskilammi, L. Sydanheimo and M. Kivikoski, "Radio Frequency Technology for Automated Manufacturing and Logistics Control. Part 1: Passive RFID Systems and the Effects of Antenna Parameters on Operational Distance", *Int. J. Adv. Manuf. Technology* 2003 vol. 21, pp. 769-774.
- [2] <https://ewhdbks.mugu.navy.mil/iff.htm>, Date accessed: February 14, 2006.
- [3] H. Stockman, "Communication by means of reflected Power," *Proc. Of the IRE*, October 1948, pp. 1196-1204
- [4] [www.rfidjournal.com](http://www.rfidjournal.com), Date accessed: February 16, 2006.
- [5] R. Bansal, "Coming soon to a Wal-Mart near you," *IEEE Antennas Prop. Mag.*, vol. 45, December 2003, pp. 105-106.
- [6] <http://en.wikipedia.org/wiki/Rfid>, Date accessed: February 18, 2006.
- [7] <http://www.newscientist.com/article.ns?id=dn7209>, Date accessed: February 18, 2006.
- [8] <http://www.roadbeacon.com/>, Date accessed: February 18, 2006.
- [9] V. Patrick, C. Bour, E. Dallard, D. Lattard, J. De Pontcharra, G. Robert and S. Roux, "A low-voltage mixed-mode CMOS/SOI integrated circuit for 13.56 MHz RFID applications" "*IEEE International SOI Conference*", 2002, pp. 163-164
- [10] H. W. Son and C. S. Pyo, "Design of RFID tag antennas using an inductively coupled Feed," *Electronics Letters*, vol. 41, no. 18, September 1, 2005, pp. 994-996.
- [11] H. Huang and C. Liu, "Design of combined voltage reference and temperature sensor for RFID applications," *Sensor Review*, vol. 26, no. 2 2006, pp. 106-107.
- [12] M. Taketoshi, S. Yoshiko, N. Hiroshi, S. Tomomasa, "Multiple people tracking by integrating distributed floor pressure sensors and RFID system", *IEEE International Conference on Systems, Man and Cybernetics*, SMC 2004, pp. 5271-5278.
- [13] J. Row, "Planar Inverted-F antenna with slotted ground plane," *Microwave and Optical Technology Letters*, vol. 39, no. 1, October 2 2003, pp. 72-75.

- [14] Gaetano and Marrocco, "Gain-Optimized Self-Resonant Meander Line Antennas for RFID Applications," *IEEE Antennas and Wireless Propagation Letters*, vol. 2, 2003, pp. 302-305.
- [15] Y. S. Na, J. S. Kim, Y.C. Kang, S. G. Byeon, and K. H. Rha, "Design of a 2.45 GHz passive transponder using printed dipole rectenna for RFID application," *IEEE TENCON 2004 - 2004 IEEE Region 10 Conference Proceedings: Analog and Digital Techniques in Electrical Engineering*, 2004, pp. C547-C549.
- [16] X. Qing, and N. Yang, "A folded dipole antenna for RFID," *AP-S International Symposium (Digest)*, vol. 1, 2004, pp. 97-100.
- [17] C. A. Diugwu, J. C. Batchelor, R. J. Langley, and M. Fogg, "Planar antenna for passive radio frequency identification [RFID] tags," *IEEE AFRICON Conference*, vol. 1, 2004, pp. 21-24.
- [18] L. Ukkonen, L. Sydanheimo, and M. Kivikoski, "Patch antenna with EBG ground plane and two-layer substrate for passive RFID of metallic objects," *AP-S International Symposium (Digest)*, vol. 1, 2004, pp. 93-96.
- [19] Y. R. Samii and H. Mosallaei, "Electromagnetic Band-Gap Structures: Classification, Characterization, and Applications," *International Conference on Antennas and Propagation*, vol. 2, IEE 2001, pp. 560-564.
- [20] S. K. Padhi, N. C. Karmakar, C. L. Law, and S. Aditya, "A dual polarized aperture coupled microstrip patch antenna with high isolation for RFID applications," *IEEE Antennas and Propagation Society, AP-S International Symposium (Digest)*, vol. 2, 2001, pp. 2-5.
- [21] M. Keskilammi and M. Kivikoski, "Using Text as a Meander Line for RFID Transponder Antennas," *IEEE Antennas and Wireless Propagation Letters*, vol. 3, no. 1, December 2004, pp. 372-374.
- [22] P. R. Foster and R. A. Burberry, "Antenna Problems in RFID Systems," The Institution of Electrical Engineers, 1999.
- [23] S. Lee, J. Woo, M. Ryu, and H. Shin., "Corrugated circular microstrip patch antennas for miniaturization," *Electrons Letters*, vol. 38, March 2002, pp. 262-263.
- [24] T. K. Lo, C. O. Ho, Y. Hwang, E. K.W. Lam, and B. Lee, "Miniature aperture-coupled microstrip antenna of very high permittivity," *Electrons Letters*, vol. 33, January 1997, pp. 9-10.
- [25] J. W. Chien and D. F. Hsu, "A frequency-reduction scheme for spiral slot Antenna," *IEEE Trans. Wireless Prop. Letters*, vol. 1, 2002, pp. 161-164.

- [26] S. A. Bokharri, J. F. Zurcher, J. R. Mosig, and F. E. Gardiol, "A small microstrip patch antenna with a convenient tuning option," *IEEE Trans. Antennas Prop.*, vol. 44, November 1996, pp. 1521-1528.
- [27] J. George, C. K. Aanandan, P. Mohanan, and K. G. Nair, "Analysis of a New Compact Microstrip Antenna," *IEEE Trans. Antennas Prop.*, vol. 46, November 1998, pp. 1712-1717.
- [28] J. P. Gianvittorio and Y. R. Samii, "Fractal Antennas: A Novel Antenna Miniaturization Technique, and Applications," *IEEE Antennas and Propagation Magazine*, vol. 44, no. 1, Feb. 2002, pp. 20-36.
- [29] G. Leon, R. R. Boix, and F. Medina, "A comparison among different reduced-size resonant microstrip patch," *Microwave and Optical Tech. Letters*, vol. 29, no. 3, 2001, pp. 143-146.
- [30] H. Nakano, Y. Shinma, and J. Yamauchi, "A monofilar spiral antenna and its array above a ground plane-Formation of a circularly polarized tilted fan beam," *IEEE Trans. Antennas Prop.*, vol. 45, October 1997, pp. 1506-1511.
- [31] T. E. Morgan, "Spiral Antennas for ESM," *IEE Proceedings, Part F: Communications, Radar and Signal Processing*, vol. 132, no. 4, July 1985, pp. 245-251.
- [32] S. K. Khmas and G. G. Cook, "Moment Method Analysis of Printed Eccentric Spiral Antennas using Curved Segmentation," *IEE Proc. Microwaves, Antennas, and Propagation*, vol. 146, no. 6, December 1999, pp. 407-410.
- [33] R. L. Li and H. Nakano, "Numerical Analysis of Probe-Excited Multiple-Arm Printed Wire Antenna," *IEE Proc. Microwaves, Antennas, and Propagation*, vol. 146, no. 1, February 1999, pp. 70-76.
- [34] T. Iwasaki, A. P. Freundorfer, and K. Iizuka, "A Unidirectional Semicircular Spiral Antenna for Subsurface Radar," *IEEE Transactions on Electromagnetic Compatibility*, EMC-36, February 1994, pp. 1-6.
- [35] J. A. Kaiser, "The Archimedean Two-Wire Spiral Antenna," *IRE Transactions on Antennas and Propagation*, AP-8, May 1960, pp. 312-323.
- [36] C. A. Balanis, *Antenna Theory, Analysis and Design*, 2nd Edition, New York, Harper & Row, 1982.
- [37] H. Nakano, S. R. Kerner, and N. G. Alexopoulos, "The Moment Method Solution for Printed Wire Antennas of Arbitrary Configuration," *IEEE Transactions on Antennas and Propagation*, vol. 36, no. 12, December 1988, pp. 1667-1673.

- [38] H. Nakano, J. Eto, Y. Okabe, and J. Yamuchi, "Tilted-and Axial-Beam Formation by a Single-Arm Rectangular Spiral Antenna with Compact Dielectric Substrate and Conducting Plane," *IEEE Transactions on Antennas and Propagation*, AP-50, no. 1, January 2002, pp. 17-24.
- [39] T. Ozdemir, J. L. Volakis, and M. W. Nurnberger, "Analysis of Thin Multioctave Cavity-Backed Slot Spiral Antennas," *IEE Proc. Microwaves, Antennas, and Propagation*, vol. 146, no. 6, December 1999, pp. 457- 454.
- [40] J. L. Volakis, M. W. Numberger, and D. S. Filipovic, "A Broadband Cavity-Backed Slot Spiral Antenna," *IEEE Antennas and Propagation Magazine*, vol. 43, no. 6, December 2001, pp. 15-26.
- [41] M. N. Afsar, Y. Wang, and R. Cheung, "Analysis and Measurement of a Broadband Spiral Antenna," *IEEE Antennas and Propagation Magazine*, vol. 46, no.1, February 2004, pp. 59-64.
- [42] W. Chen and K. F. Lee, "Input Imdepance of Coaxially Fed Rectangular Microstrip Antenna on Electrically Thick Substrate," *Microwave Opt. Technol. Lett.*, 6, 1993, pp. 387-390.
- [43] R. Q. Lee, K. F. Lee, and J. Bobinchak, "Characteristics of a Two-Layer Electromagnetically Coupled Rectangular Patch Antenna," *Electron. Lett.*, 23, 1987, pp. 1070-1072.
- [44] P. S. Hall, "Probe Compensation in Thick Microstrip Patches," *Electrons Letters*, 23, 1987, pp. 606-607.
- [45] Ramisetti, S. "Design and development of an ID generation circuit for low- cost passive RFID-based applications," Master of Science Thesis, Louisiana Tech University, 2006
- [46] Aravind Chamarti, "Delay line based passive radio frequency identification tags," Ph.D. Dissertation, Lousiana Tech University, 2006.
- [47] L. C. Godara, *Handbook of Antennas in Wireless Communications*, 2002 CRC Press.
- [48] J. Helszajin and D. S. James, "Planar triangular resonators with magnetic walls," *IEEE Trans. Microwave Theory Tech.*, vol. 26, February 1978, pp. 95-100.
- [49] D. Karaboga, K. Guney, N. Karaboga, and A. Kaplan, "Simple and accurate effective sidelength expression obtained by using a modified genetic algorithm for the resonant frequency of an equilateral triangular microstrip antenna," *Int. J. Electronics*, vol. 83, January 1997, pp. 99-108.
- [50] H. Nakano, *Helical and spiral antennas*, Research Studies Press, England, 1987.

- [51] H. O. Peitgen, H. Jurgens, and D. Saupe, *Chaos and Fractals*. New York: Springer-Verlag, 1990.
- [52] W. Sierpinski, "Su rune courbe dont tout point est un point de ramification," *C. R. Acad.*, Paris 160 302, 1915 Ansoft Designer, Edition 1.1, Software Version 1.1, 8 September 2003.
- [53] C. P. Baliarda, J. Romeu, R. Pous and A. Cardama, "On the Behavior of the Sierpinski Multiband Fractal Antenna," *IEEE Transactions on Antennas and Propagation*, vol. 46, no. 4, April 1998.
- [54] Ansoft Designer, Edition 1.1, Software Version 1.1, 8 September 2003.
- [55] Ansoft HFSS, Edition 2, Optimetrics 3 HFSS 9, January 2004.
- [56] R. Garg, P. Bhartia, I. Bahl, and A. Ittipiboon, *Microstrip Antenna Design Handbook*, Artech House, Inc 2001.
- [57] J.A. Kaiser, "The Archimedean two-wire spiral antenna," *IRE Trans. On Antennas and Propagation*, vol. 8, May, pp. 312-323, 1960.
- [58] B.B. Mandelbrot, *The Fractal Geometry of Nature*, New York, W.H. Freeman, 1983.
- [59] C.P. Baliards, Jordi Romeu, Angel Cardama, "The Koch Monopole: A Small Fractal Antenna," *IEEE Trans. On Antennas and Prop.*, Vol 48, No. 11, November 2000, pp 1773-1781.
- [60] D. H. Werner and S. Ganguly, "An Overview of Fractal Antenna Engineering Research," *IEEE Antennas and Prop. Mag.*, vol. 45, no. 1, February 2003.
- [61] K. V. Seshagiri Rao, Pavel V. Nikitin, and Sander F. Lam, "Antenna Design for UHF RFID Tags: A Review and a Practical Application," *IEEE Trans. Antennas Propag.*, vol. 53, no. 12, December 2005, pp. 3870-3876.
- [62] U. Leena ; Engels, Daniel; Sydanheimo, Lauri; Kivikoski, Markku, "Planar wire-type inverted-f RFID tag antenna mountable on metallic objects," *IEEE Antennas and Propagation Society, AP-S International Symposium (Digest)*, v 1, 2004, pp101-104.
- [63] G. Kumar and K.P. Ray, *Broadband microstrip antennas*, Artech House, Boston, 2003.
- [64] Faster Caustic Etching of Kapton H, E, and KN types, Dupont Kapton Technical Bulletin, <http://www.dupont.com/kapton/general/caustic-etching.pdf>, Date accessed: March 16, 2006.

- [65] J.Liang, C.C. Chiau, X.Chen and C.G. Parini, "Study of a Printed Circular Disc Monopole Antenna for UWB Systems," *IEEE Trans. On Anten. And Propag.*, Vol. 53, No. 11, Nov 2005.
- [66] White, M.O., "Radar Cross-Section: Measurement, Prediction, Control," *Electronics and Communication Enineering Journal*, vol. 10, no. 4, pp. 169-180, August 1998.
- [67] Casalini, R. ; Capaccioli, S.; Presto, S.; Lucchesi, M.; Rolla, P.A.; Corezzi, S.; Paluch, M., "Influence of temperature and pressure on the dynamics of glass formers explored by dielectric spectroscopy," *IEEE Transactions on Dielectrics and Electrical Insulation*, v 8, n 3, June, 2001, pp 395-400.
- [68] K. R. Carver and J.W. Mink, "Microstrip Antenna Technology," *IEEE Transactions on Antennas and Propagation*, vol. AP-29, no. 1, pp. 2-24, Jan. 1981.